

Lund and Cambridge multiplicities for precision physics

Rok Medves,^a Alba Soto-Ontoso,^b Gregory Soyez^b

^a*Rudolf Peierls Centre for Theoretical Physics, Clarendon Laboratory, Parks Road, University of Oxford, Oxford OX1 3PU, UK*

^b*Université Paris-Saclay, CNRS, CEA, Institut de physique théorique, 91191, Gif-sur-Yvette, France*

E-mail: rok.medves@physics.ox.ac.uk, alba.soto@ipht.fr,
gregory.soyez@ipht.fr

ABSTRACT: We revisit the calculation of the average jet multiplicity in high-energy collisions. First, we introduce a new definition of (sub)jet multiplicity based on Lund declusterings obtained using the Cambridge jet algorithm. We develop a new systematic resummation approach. This allows us to compute both the Lund and the Cambridge average multiplicities to next-to-next-to-double (NNDL) logarithmic accuracy in electron-positron annihilation, an order higher in accuracy than previous works in the literature. We match our resummed calculation to the exact NLO ($\mathcal{O}(\alpha_s^2)$) result, showing predictions for the Lund multiplicity at LEP energies with theoretical uncertainties up to 50% smaller than the previous state-of-the-art. Adding hadronisation corrections obtained by Monte Carlo simulations, we also show a good agreement with existing Cambridge multiplicity data. Finally, to highlight the flexibility of our method, we extend the Lund multiplicity calculation to hadronic collisions where we reach next-to-double logarithmic accuracy for colour singlet production.

Contents

1	Introduction	1
2	Lund-based multiplicity	3
3	Revisiting DL and NDL results	5
3.1	Double-logarithmic (DL) accuracy	6
3.2	Next-to-double-logarithmic (NDL) accuracy	9
3.2.1	Running coupling effects	12
3.2.2	Hard-collinear correction	13
4	Calculation at NNDL accuracy	14
4.1	Contributions and master formula	14
4.2	Corrections involving a pure α_s contribution	19
4.2.1	Hard-collinear endpoint	19
4.2.2	Hard matrix-element corrections (top of the Lund plane)	20
4.2.3	Soft-and-collinear emissions at commensurate angles and k_t	22
4.2.4	Clustering corrections	25
4.2.5	A primary large-angle emission with $k_t \sim k_{t,\text{cut}}$: the Cambridge multiplicity	27
4.3	Corrections involving two $\alpha_s L$ factors	27
4.3.1	Energy loss	27
4.3.2	Squared hard-collinear correction	28
4.3.3	A hard-collinear emission with a soft emission at commensurate angle	30
4.3.4	A primary large-angle emission	31
4.3.5	Three emissions at commensurate angles	32
4.4	Corrections involving the running of the strong coupling	33
4.4.1	Squared running-coupling correction	33
4.4.2	Running-coupling and hard-collinear correction	34
4.5	Final result	35
5	Validation and phenomenology	39
5.1	Fixed-order validation	39
5.2	Matching with fixed-order	41
5.3	Comparison to LEP data	43
6	A byproduct: multiplicity in hadron collisions at NDL accuracy	44
7	Conclusions and outlook	50

A	Subjet multiplicity definition and logarithmic accuracy	52
A.1	Angular ordered vs k_t -based clustering algorithms	52
A.2	Recombination scheme independence	52
A.3	Lund and Cambridge multiplicities	53
B	$1 \rightarrow 3$ splitting functions in the soft limit	56

1 Introduction

Multiplicities, e.g. of (charged) particles or jets, are amongst the most fundamental observables studied in collider physics. Since they probe the full multiple branching structure of QCD, they have been used in various forms to probe the dynamics of the strong interaction. This has been the case, historically, when assessing Quantum Chromodynamics (QCD) as the fundamental theory of strong interactions at e^+e^- colliders (see e.g. [1–4]). Besides this, multiplicities have been relied upon in several contexts, including for instance the tuning of Monte Carlo event generators (see e.g. [5–7]) or the tagging of quark and gluon jets (e.g. [8–10]). Experimentally, charged-particle multiplicity is one of the simplest and cleanest observables, and its importance stretches from calibration to advanced tagging techniques. In fact, the first experimental paper using LHC data reported the measurement of charged hadron multiplicity in proton-proton collisions [11].

From the theoretical viewpoint, the definition of multiplicity can be rather subtle. Early work considered the total hadronic multiplicity within a jet. This is equivalent to the first moment of the jet fragmentation function and was studied in perturbative QCD in several works [12–21]. These calculations played a pivotal role in understanding the singularity structure of QCD, see Ref. [22] for a review. Since the total hadronic multiplicity is obviously infrared-and-collinear unsafe, the calculations introduced an infrared regulator $Q_0 \sim \Lambda_{\text{QCD}}$ that was fitted to the data. The probability distribution of hadronic multiplicity in QCD jets was measured in e^+e^- annihilation [23] and shown to be well reproduced by the aforementioned analytic calculations.

A theoretically more favourable way of determining the multiplicity of an event was established with the advent of jet clustering algorithms, basing it on the number of reconstructed jets. In Ref. [24], the average jet multiplicity, $\langle N \rangle$, was defined as the average number of reconstructed jets that pass a certain resolution cut, typically a transverse momentum cut $k_{t,\text{cut}}$, guaranteeing infrared-and-collinear safety. As $k_{t,\text{cut}}$ is reduced from the hard scale Q down, more jets are resolved and $\langle N \rangle$ increases. A step further was considered in Ref. [25], where the concept of ‘subjet multiplicity’ was introduced. In this case, a jet finder is run twice with two different resolution scales. The jets are defined with $k_{t0,\text{cut}}$ and the subjets with a finer scale $k_{t1,\text{cut}} < k_{t0,\text{cut}}$. The first step is thus to classify the event as an n -jet event and then, for each individual jet, to count the number of subjets above $k_{t1,\text{cut}}$.

Let us now discuss the basic structure of the average jet multiplicity in perturbative QCD. The presence of two disparate scales in the problem, either $k_{t,\text{cut}}$ and the hard scattering scale Q in the case of jet multiplicity or $k_{t0,\text{cut}}$ and $k_{t1,\text{cut}}$ for subjet multiplicity, splits the phase-space into three different regimes. If $k_{t,\text{cut}} \sim Q$, fixed-order perturbation theory applies. Otherwise,

when $\Lambda_{\text{QCD}} \ll k_{t,\text{cut}} \ll Q$ the logarithm $L \equiv \ln(Q/k_{t,\text{cut}})$ becomes large and must be resummed to all orders in order to guarantee the convergence of the perturbative expansion. In such a case the resummation structure of jet multiplicity can be organised as follows

$$\langle N(\alpha_s, L) \rangle = \langle N(\alpha_s, 0) \rangle \left[\underbrace{h_1(\alpha_s L^2)}_{\text{DL}} + \underbrace{\sqrt{\alpha_s} h_2(\alpha_s L^2)}_{\text{NDL}} + \underbrace{\alpha_s h_3(\alpha_s L^2)}_{\text{NNDL}} + \dots \right] + \mathcal{O}\left(e^{-|L|}\right), \quad (1.1)$$

where α_s is the strong coupling constant and the $N^k\text{DL}$ function $\alpha_s^{k/2} h_{k+1}(\alpha_s L^2)$ resums terms of order $\alpha_s^n L^{2n-k}$. That is, the function h_1 captures the double logarithmic (DL) contribution, h_2 the next-to-double-logarithmic (NDL) enhancements, h_3 the next-to-next-to-double-logarithmic (NNDL) enhancements and so on. Typical values of $\alpha_s L^2$ at high-energy colliders are approximately $\alpha_s L^2 \leq 5$ (see e.g. Ref. [26]). Finally, whenever $k_{t,\text{cut}} \approx \Lambda_{\text{QCD}}$ the jet multiplicity calculation enters the domain of non-perturbative QCD.

Previous calculations of Eq. (1.1) date back to the early 90's. In Ref. [24], the average jet multiplicity in e^+e^- collisions was computed at NDL accuracy using the Durham clustering algorithm [25, 27] (see also Ref. [28] for a calculation of the average jet multiplicities using different jet algorithms). This resummed calculation was then used by the OPAL Collaboration to extract the value of the strong coupling constant at the Z -boson mass [29]. In both theory and experimental papers it was realised through general-purpose Monte Carlo event generators that non-perturbative corrections affected the jet multiplicity for $k_{t,\text{cut}}$ values well above Λ_{QCD} , i.e. $k_{t,\text{cut}} \approx 4$ GeV [24]. This was among the motivations to develop a new jet clustering algorithm that uses angular distance as its metric, the so-called Cambridge algorithm [30]. To demonstrate the benefits of the novel algorithm, the authors of Ref. [30] computed the average jet multiplicity using the Cambridge algorithm at NDL accuracy and showed the reduction of non-perturbative effects with respect to the k_t prescription, i.e. the value of $k_{t,\text{cut}}$ at which parton-level and hadron-level Monte Carlo results start to differ significantly is reduced from $k_{t,\text{cut}} \sim 4$ GeV to $k_{t,\text{cut}} \sim 1.5$ GeV (see Ref. [30] as well as Fig. 9a below) when using the Cambridge algorithm instead of Durham.

Concerning other collision systems, the extension of both the k_t -clustering algorithm and the multiplicity calculation to deep-inelastic scattering was presented shortly after the e^+e^- case in Refs. [31, 32], respectively. The first subjet multiplicity calculation in a hadron collider jet was reported in Refs. [33, 34] and used to extract the multiplicity ratio between quark and gluon jets at Tevatron energies [35]. So far, average subjet multiplicity has neither been predicted nor measured at LHC energies.

More recently, a rising interest in jet substructure has prompted a family of analysis based on the Lund jet plane, originally introduced in Ref. [36] for proton-proton (pp) collisions. In such an approach, a full clustering tree, based on the Cambridge/Aachen (C/A) clustering algorithm [30, 37], is constructed for an event, tracking its properties at each clustering vertex. Traversing backwards the C/A clustering sequence one constructs a tree structure, the Lund planes, where the kinematic properties of the C/A pairwise recombinations are tuples called *Lund declusterings*. This construction provides an angular-ordered picture similar to that of Lund diagrams [38] used in resummation and Monte Carlo developments. This provides a useful tool both theoretically and experimentally. For example, a precise calculation of the primary Lund plane density in

perturbative QCD [39] has been successfully compared to the ATLAS experimental measurement in Ref. [40]. The Lund jet plane has also been successfully utilised to inform machine-learning-based studies for jet tagging [41, 42] and quark/gluon jet discrimination [43].

The goal of this paper is to extend the programme of Lund plane physics to the concept of (sub)jet multiplicity. To do so, we propose an alternative definition of subjet multiplicity based on Lund declustering that we dub ‘Lund multiplicity’. We compute Lund multiplicity at NNDL accuracy — i.e. up to and including the h_3 term in Eq. (1.1) — in $\ell^+\ell^- \rightarrow Z \rightarrow q\bar{q}$ and $\ell^+\ell^- \rightarrow H \rightarrow gg$ collisions, an order higher in logarithmic accuracy than previous works in the literature. We derive this result from a novel resummation approach that does not rely on the generating functional approach. As a byproduct, we also obtain the resummed average Cambridge multiplicity at NNDL accuracy. Our full results are summarised in Sec. 4.5. We further provide a compact analytic expression for the subjet multiplicity at NDL accuracy for colour singlet production in hadronic collisions, i.e. Drell-Yan ($pp \rightarrow q\bar{q} \rightarrow Z$) and Higgs production via gluon fusion ($pp \rightarrow gg \rightarrow H$). This would, for example, be directly useful to test the logarithmic accuracy of new hadron-collider showers, as was done for e^+e^- collisions in Ref. [44].

The potential impact of our result is two-fold. First, our NNDL result for the Cambridge multiplicity could be matched with recent progress to compute next-to-next-to leading order (NNLO, α_s^3) fixed-order distributions. This would yield to interesting phenomenological studies either at LEP (e.g. compared to measurements from the OPAL collaboration [45]) or at future circular colliders. Besides the potential phenomenological impact of this calculation, an analytic formula for NNDL subjet multiplicity is fundamental for testing the logarithmic accuracy of parton showers beyond NLL accuracy, along the lines of Ref. [44].

This paper is organised as follows. We begin by providing the algorithmic definition of Lund multiplicity in Sec. 2. In Sec. 3, we introduce the building blocks of the new resummation approach for subjet multiplicity and, as a warm-up exercise, use it to re-derive previous results in the literature at DL and NDL accuracy. Sec. 4 is the core of this paper since it contains all the steps of the NNDL calculation, with ready-to-use formulæ for both the Lund and Cambridge multiplicities given in Sec. 4.5. We cross-check the $\mathcal{O}(\alpha_s^2)$ expansion of our resummation against **Event2** [46, 47] simulations in Sec. 5.1. In Sec. 5.2, we match our resummed result to exact next-to-leading order (NLO, $\mathcal{O}(\alpha_s^2)$) distributions and briefly discuss Lund multiplicity at LEP energies. In Sec. 5.3 we provide a short comparison to the Cambridge multiplicity measured by the OPAL collaboration [45], including hadronisation effects from Monte Carlo simulations. The extension of our calculation to initial-state radiation is presented in Sec. 6, where we compute the Lund multiplicity at NDL accuracy in colour singlet production. Finally, we conclude and outline some potential extensions of this work in Sec. 7. The impact of choosing a different jet clustering algorithm and/or recombination scheme is presented in Appendix A.

2 Lund-based multiplicity

We begin by introducing a novel algorithm for evaluating the multiplicity of jets with a relative k_t above a given $k_{t,\text{cut}}$ in e^+e^- collisions. The algorithm draws from the Lund diagram representation of the phase-space where the emission kinematics is visualised in the $(\eta, \ln k_t)$ plane [36, 38, 48], where η is the rapidity of the emission, and Q the centre of mass energy.

The procedure to compute the Lund multiplicity, $N^{(\text{Lund})}$, is the following. The starting point is to cluster the full event with the Cambridge algorithm [30] with resolution parameter $y_{\text{cut}} = 1$,¹ so as to generate a single jet with an angular-ordered clustering sequence. We first undo the last step of the clustering i.e. get the two exclusive Cambridge jets. We work in the centre-of-mass of the collision, where this yields a pair of back-to-back jets, splitting the event in two hemispheres. For each jet, we proceed as follows (still working in the centre-of-mass of the collision)

1. Set $N^{(\text{Lund})} = 1$.
2. Undo the last clustering step to generate two subjets j_1 and j_2 , with j_1 the most energetic, i.e. $E_1 > E_2$.
3. Calculate the relative transverse momentum of the splitting as

$$k_t \equiv \min(E_1, E_2) \sin \theta = E_2 \sin \theta, \quad (2.1)$$

with θ the opening angle between the pair of subjets.

4. If $k_t \geq k_{t,\text{cut}}$ the splitting contributes to the Lund multiplicity, i.e. $N^{(\text{Lund})}$ is incremented by one, and we go back to step 2 for *each* of the two subjets.
5. Otherwise, if $k_t < k_{t,\text{cut}}$, repeat from step 2 following only the hardest subjet j_1 .

The procedure terminates when there is nothing left to decluster. The event-wide Lund multiplicity would then be the sum of the results obtained for each of the two exclusive jets.

Naturally, the Lund multiplicity fluctuates on an event-by-event basis. In this work, we compute the average $\langle N^{(\text{Lund})} \rangle$, up to NNDL accuracy, and leave the calculation of the full distribution (or of its moments) for future work.

For the case of pp collisions we introduce an analogous procedure where (a) instead of using the Cambridge algorithm we cluster the event with Cambridge/Aachen [30, 37] with a finite radius R of order 1 (in practice, we use $R = 1$), (b) the ordering measure in step 2 is taken by the (sub)jet transverse momentum relative to the beam, p_t , instead of its energy, and (c) the relative transverse momentum of a declustering in step 3 is defined as $k_t = \min(p_{t,i}, p_{t,j}) \Delta_{ij}$ with the distance $\Delta_{ij} = \sqrt{\Delta y_{ij}^2 + \Delta \phi_{ij}^2}$ computed in the rapidity-azimuth plane [36]. Roughly speaking, the pp procedure is an iteration of the e^+e^- recipe for each of the $R = 1$ jets found by the Cambridge/Aachen algorithm. These $R = 1$ jets can thus be viewed as the primary event radiation, associated with the incoming-incoming dipole, just like the primary radiation in e^+e^- stems from the leading $q\bar{q}$ pair, and the subjets as subsidiary radiation. Similarly, in deep-inelastic scattering one would follow the same steps but clustering in the Breit frame instead of in the event frame.

¹or, equivalently, the generalised e^+e^- k_t algorithm with $p = 0$ and $R > \pi$ [49]. Note that we use the standard convention whereby y_{cut} is normalised by the squared centre-of-mass energy Q^2 .

Relation to other multiplicities. The Lund-based definition of multiplicity shares some similarities with other multiplicities in the literature. Let us first discuss its relation with previous definitions of multiplicity using the Cambridge algorithm [30]. We show in Appendix A.3 that, in the e^+e^- case, the Lund procedure is equivalent to running the standard Cambridge algorithm with $y_{\text{cut}} = 1$ and counting the total number of clusterings for which $k_t > k_{t,\text{cut}}$, provided that the Lund k_t definition, Eq. (2.1), is used in both cases. If one uses instead the Cambridge definition for the relative transverse momentum of a clustering

$$k_t^{(\text{Cam})} = \min(E_i, E_j) \sqrt{2(1 - \cos \theta_{ij})}, \quad (2.2)$$

and imposes the condition $k_t^{(\text{Cam})} > k_{t,\text{cut}}$, one obtains a different average multiplicity. We show in Sec. 4 that it starts to differ from the Lund multiplicity at NNDL and we compute the difference. Furthermore, the *standard* definition of the Cambridge jet multiplicity would instead count the number of jets obtained when running the Cambridge algorithm with $y_{\text{cut}} = k_{t,\text{cut}}^2/Q^2$. We show in Appendix A.3 (and Sec. 4) that, at our targeted NNDL accuracy, this is also equivalent to counting the total number of clusterings in the Cambridge sequence with $y_{\text{cut}} = 1$ using the definition (2.2) for the relative transverse momentum.

Additionally, if, in the Lund declustering procedure, we only follow the hardest branch (in step 4 above) instead of iterating over both branches, we recover the primary Lund plane multiplicity. Note that beyond the soft-and-collinear approximation, the primary Lund-plane multiplicity has a more involved analytic structure than $\langle N^{(\text{Lund})} \rangle$ since, as we will see below, clustering logarithms only appear from NNDL onwards while they would start already at NDL for the primary case (see e.g. Ref. [39]). This is also reminiscent of the iterated Soft Drop multiplicity n_{SD} [10] defined as the number of splittings on the primary Lund plane that satisfy the Soft Drop condition [50] (for the Soft Drop parameter β set to -1).

An approach often used in the literature is to define the jet multiplicity using the Durham (k_t) algorithm (as done, for example in Ref. [24]). At NDL accuracy, one gets the same multiplicity whether one uses the Cambridge or Durham algorithm. However, the two definitions start to differ at NNDL. We argue in Appendix A.1 that the use of the Cambridge algorithm considerably simplifies the NNDL calculation, while reaching NNDL accuracy with the k_t algorithm would require semi-numerical ingredients.

Finally, we show in Appendix A.2 that using a different recombination scheme, such as the winner-takes-all [51], would only bring differences beyond our targeted NNDL accuracy.

3 Revisiting DL and NDL results

In this section, we derive the average Lund and Cambridge multiplicities at double (DL) and next-to-double (NDL) logarithmic accuracy. These agree with the NDL result of Ref. [24] based on the Durham algorithm, although they would start to differ at NNDL accuracy.

For the all-order NDL resummation, we introduce a new formalism compared to what was initially used in Refs. [24, 30, 32]. This new formalism is, we believe, considerably simpler and can almost straightforwardly be extended to NNDL accuracy as we will show in Sec. 4. The DL resummation is presented in Sec. 3.1, with the NDL resummation following in Sec. 3.2.

3.1 Double-logarithmic (DL) accuracy

To gain insight into the resummation structure of double logarithms, we start by discussing the first orders in the strong coupling. For simplicity, we calculate the multiplicity in one of the two hemispheres, $\langle N_i^{(\text{Lund})} \rangle \equiv \langle N^{(\text{Lund})} \rangle / 2$, with $i = q, g$, which depends only on the flavour of the hard partons produced in the underlying Born-level process (at least at the accuracy we are interested in here). We denote by $h_{1,2,3}^{(i)}$ the corresponding DL, NDL and NNDL functions that appear in Eq. (1.1) (for a single hemisphere).

We consider two hard processes at Born-level: (i) a back-to-back $q\bar{q}$ pair produced by the decay of a Z boson and (ii) the equivalent situation but for gluons arising from a Higgs boson, i.e. $e^+e^- \rightarrow H \rightarrow gg$. In this way, we compute the multiplicity for both quark and gluon jets. The centre-of-mass energy of the e^+e^- system is denoted by Q .

Initially, at order α_s^0 we have a single parton in each hemisphere and thus $\langle N_i^{(\text{Lund})} \rangle = 1$. At $\mathcal{O}(\alpha_s)$, we can either have a real emission or a 1-loop virtual correction. We thus write

$$\langle N_i^{(\text{Lund})} \rangle_{\mathcal{O}(\alpha_s)} = \frac{1}{\sigma_0 + \sigma_1} \left\{ [1]\sigma_0 + \int d\Phi |\mathcal{M}_R|^2 [1 + \Theta(k_t > k_{t,\text{cut}})] + \int d\Phi |\mathcal{M}_V|^2 [1] \right\}, \quad (3.1)$$

where σ_0 is the Born-level cross-section, σ_1 the $\mathcal{O}(\alpha_s)$ correction to the inclusive cross-section, $d\Phi$ is the phase-space element and $|\mathcal{M}_{R(V)}|^2$ is the real (virtual) matrix element. Note that this $\mathcal{O}(\alpha_s)$ expression is completely general so as to facilitate future discussions at higher logarithmic accuracy.

In Eq. (3.1), the first term is the Born-level contribution with a single parton in the hemisphere, the second term is the real $\mathcal{O}(\alpha_s)$ correction which, in addition to the hard parton, can receive an additional contribution to the multiplicity if the emitted gluon has a k_t above $k_{t,\text{cut}}$, and the last term is the one-loop virtual correction where there is again a single parton in the hemisphere. The contribution from the hard parton in the real and virtual $\mathcal{O}(\alpha_s)$ terms gives (by definition) the correction σ_1 to the inclusive cross-section, therefore cancelling the overall normalisation. Furthermore, in the contribution from the new emission (proportional to $\Theta(k_t > k_{t,\text{cut}})$) the σ_1 correction in the normalisation can be neglected since it's beyond NDL accuracy,² leading to

$$\langle N_i^{(\text{Lund})} \rangle_{\mathcal{O}(\alpha_s)} = 1 + \int d\Phi \frac{|\mathcal{M}_R|^2}{\sigma_0} \Theta(k_t > k_{t,\text{cut}}). \quad (3.2)$$

At DL accuracy, it is sufficient to consider the emission of a soft-and-collinear gluon, in which case the Born-level kinematics factorises from the gluon emission and Eq. (3.2) becomes

$$\langle N_i^{(\text{Lund})} \rangle_{\mathcal{O}(\alpha_s)} = 1 + \int [dk] |\mathcal{M}(k)|^2 \Theta(k_t > k_{t,\text{cut}}), \quad (3.3)$$

with $[dk] \equiv d^4k \delta(k^2)/(2\pi)^3$. In the soft-and-collinear limit, we have

$$k_t \approx \frac{Q}{2} z \theta \approx Q z e^{-\eta}, \quad (3.4)$$

with z the energy fraction of the emitted gluon, i.e. $E_k = zQ/2$, θ its emission angle, and $\eta = -\ln \tan(\theta/2)$ its rapidity. Furthermore, the matrix element integration becomes

$$\int [dk] |\mathcal{M}(k)|^2 = \frac{2\alpha_s C_i}{\pi} \int_0^\infty d\eta \int_{e^{-\eta}}^1 \frac{dz}{z} = \frac{2\alpha_s C_i}{\pi} \int_0^\infty d\eta \int_0^{Qe^{-\eta}} \frac{dk_t}{k_t}, \quad (3.5)$$

²As we will see in Sec. 4.2.2, this also holds at NNDL accuracy, where σ_1 can also be neglected.

where C_i is the colour factor of the emission. Then, the integration in Eq. (3.3) yields

$$\langle N_i^{(\text{Lund})} \rangle_{\mathcal{O}(\alpha_s)} = 1 + \bar{\alpha} \frac{C_i}{C_A} \frac{L^2}{2}, \quad \text{with} \quad L = \ln \frac{Q}{k_{t,\text{cut}}}, \quad \bar{\alpha} = \frac{2\alpha_s C_A}{\pi}, \quad (3.6)$$

with $C_i = C_F$ for quarks and $C_i = C_A$ for gluons. As expected, we obtain the double-logarithmic enhancement characteristic of soft-and-collinear emissions.

Moving on to $\mathcal{O}(\alpha_s^2)$, we restrict the discussion to the configurations relevant in the double-logarithmic limit. That is, we need to account for two soft-and-collinear emissions each either real or virtual. The $\mathcal{O}(\alpha_s^2)$ contribution to the Lund multiplicity can be written as

$$\begin{aligned} \langle N_i^{(\text{Lund})} \rangle_{\mathcal{O}(\alpha_s^2)} = & \left(\frac{2\alpha_s}{\pi} \right)^2 \int_0^\infty d\eta_1 \int_0^1 \frac{dz_1}{z_1} \int_0^\infty d\eta_2 \int_0^1 \frac{dz_2}{z_2} \left\{ C_i^2 [1] - C_i^2 [1 + \Theta(k_{t,2} > k_{t,\text{cut}})] \right. \\ & - C_i^2 [1 + \Theta(k_{t,1} > k_{t,\text{cut}})] - C_i C_A [1 + \Theta(k_{t,1} > k_{t,\text{cut}})] \Theta(\eta_2 > \eta_1) \\ & + C_i^2 [1 + \Theta(k_{t,1} > k_{t,\text{cut}}) + \Theta(k_{t,2} > k_{t,\text{cut}})] \\ & \left. + C_i C_A [1 + \Theta(k_{t,1} > k_{t,\text{cut}}) + \Theta(k_{t,21} > k_{t,\text{cut}})] \Theta(\eta_2 > \eta_1) \right\}, \quad (3.7) \end{aligned}$$

where the first line includes the virtual-virtual (VV) and virtual-real (VR) cases, the second line corresponds to the real-virtual (RV) case and the last two lines contain the real-real case (RR). We have accounted for the fact that the second emission, when being real, can be either a *primary* emission (i.e. a radiation from the leading parton, with a colour factor C_i), or a *secondary* emission (i.e. a radiation from the first gluon, with a colour factor C_A). In writing Eq. (3.7), we have defined η_2 as the rapidity of emission 2 with respect to its emitter, i.e. with respect to the parent parton for primary emissions, $\eta_2 = -\ln \tan(\theta_{2q}/2)$, and with respect to the first emitted gluon for secondary emissions, $\eta_2 = -\ln \tan(\theta_{21}/2)$. With this in mind, we note the presence of the angular-ordering constrain ($\Theta(\eta_2 > \eta_1)$) for the (secondary) $C_i C_A$ contribution in both the RR and RV contributions.³ At DL accuracy where we have strong angular ordering, the relative transverse momentum is also measured with respect to the emitter. In the soft-and-collinear limit and with our convention for η_2 , we therefore have $k_{t,2} \approx E_2 \theta_{2q} \approx Q z_2 e^{-\eta_2}$ for primary emissions and $k_{t,21} \approx E_2 \theta_{21} \approx Q z_2 e^{-\eta_2}$ for secondary emissions. Finally, while in an exact $\mathcal{O}(\alpha_s^2)$ calculation the multiplicity should be normalised by the $\mathcal{O}(\alpha_s^2)$ inclusive cross-section, at DL accuracy it can safely be normalised by the Born-level condition for reasons equivalent to those discussed above at $\mathcal{O}(\alpha_s)$. Taking these facts into account, we find that the only terms that do not cancel in Eq. (3.7) are

$$\langle N_i^{(\text{Lund})} \rangle_{\mathcal{O}(\alpha_s^2)} = \bar{\alpha}^2 \frac{C_i}{C_A} \int_0^1 \frac{dz_1}{z_1} \int_0^\infty d\eta_1 \int_0^1 \frac{dz_2}{z_2} \int_{\eta_1}^\infty d\eta_2 \Theta(k_{t,21} > k_{t,\text{cut}}), \quad (3.8)$$

The key observation in Eq. (3.7) is that all the real contributions cancel against virtual corrections except the contribution from the second gluon emission in the real $C_i C_A$ term, i.e. the secondary gluon radiation. Physically, this comes from the fact that, in an angular-ordered picture, the leading parton carries on radiating independently of whether the first emitted gluon is real or virtual.

³Both these terms share the same soft matrix element (modulo an overall sign). Angular ordering arises after azimuthal averaging.

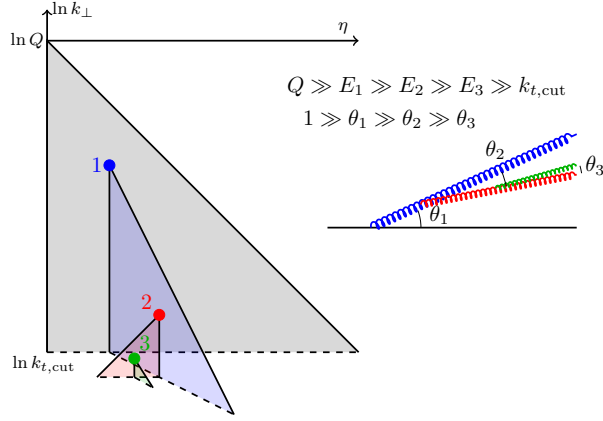


Figure 1: Representation of the nested gluon-emission pattern, strongly-ordered in both energies and angles, which constitutes the all-order DL contribution.

At DL accuracy, it is relatively straightforward to show that the above arguments at $\mathcal{O}(\alpha_s^2)$ generalise to all orders. More precisely, at order α_s^n , the only non-zero contribution comes from the kinematic configuration where the n soft gluon emissions are *nested*, i.e. where the second gluon is collinear to the first, the third is collinear to the second, ..., and the n^{th} gluon is collinear to the $(n-1)^{\text{th}}$. This is schematically represented in Fig. 1. To write down the all-orders expression, it is useful to introduce for a given emission i its energy fraction with respect to the initial hard parton x_i , i.e. $x_i = 2E_i/Q = \prod_{j \leq i} z_j$ with z_j the energy fraction of each emission with respect to the previous one, and the product running over all previous emissions. We do so since x_i is the strongly ordered variable. We can therefore write the all-orders expression for the Lund multiplicity at DL accuracy as:

$$\begin{aligned} \langle N_i^{(\text{Lund})} \rangle_{\text{DL}} &= 1 + \frac{C_i}{C_A} \sum_{n=1}^{\infty} \bar{\alpha}^n \int_0^{\infty} d\eta_1 \int_{\eta_1}^{\infty} d\eta_2 \cdots \int_{\eta_{n-1}}^{\infty} d\eta_n \\ &\quad \int_0^1 \frac{dx_1}{x_1} \int_0^{x_1} \frac{dx_2}{x_2} \cdots \int_0^{x_{n-1}} \frac{dx_n}{x_n} \Theta(x_n e^{-\eta_n} > e^{-L}) \quad (3.9) \\ &= 1 + \frac{C_i}{C_A} \sum_{n=1}^{\infty} \bar{\alpha}^n \int_0^L d\eta_n \frac{\eta_n^{n-1}}{(n-1)!} \frac{(L-\eta_n)^n}{n!} = 1 + \frac{C_i}{C_A} \sum_{n=1}^{\infty} \frac{(\bar{\alpha}L^2)^n}{(2n)!}. \end{aligned}$$

The series can easily be summed to get

$$N_i^{(\text{DL})} \equiv \langle N_i^{(\text{Lund})} \rangle_{\text{DL}} = 1 + \frac{C_i}{C_A} (\cosh \nu - 1), \quad (3.10)$$

where we introduce the following notations which will be helpful throughout this paper:

$$\nu = \sqrt{\bar{\alpha}L^2} = \sqrt{\frac{2C_A\xi}{\pi}} = \sqrt{\frac{2C_A\alpha_s L^2}{\pi}}. \quad (3.11)$$

Eq. (3.10) is in agreement with earlier results in the literature [24]. In this soft-and-collinear limit, both hard legs in a $Z \rightarrow q\bar{q}$ or $H \rightarrow gg$ process are independent of one another. Thus, the average Lund multiplicity is $\langle N_Z^{\text{DL}} \rangle = 2N_q^{(\text{DL})}$ and $\langle N_H^{\text{DL}} \rangle = 2N_g^{(\text{DL})}$, respectively.

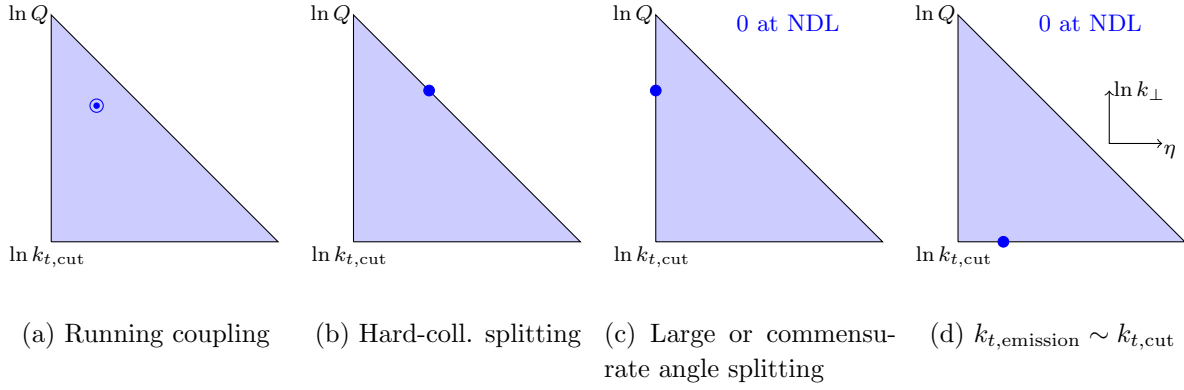


Figure 2: Lund representation of the configurations that potentially contribute to the multiplicity at NDL. The diagrams are drawn for the primary Lund plane but similar contributions exist for subsidiary planes as well.

$N_i^{(\text{DL})}$ is the total number of Lund declusterings above a fixed $k_{t,\text{cut}}$. In future discussions we also consider the *differential* distribution, i.e. the distribution of Lund declusterings at a given k_t , which can be trivially obtained from the cumulative result:

$$n_i^{(\text{DL})} = \frac{dN_i^{(\text{DL})}}{dL} = \frac{C_i}{C_A} \sqrt{\alpha} \sinh \nu. \quad (3.12)$$

3.2 Next-to-double-logarithmic (NDL) accuracy

We now move to the calculation of the NDL h_2 function in Eq. (1.1), where $\sqrt{\alpha_s} h_2$ resums terms of order $\alpha_s L (\alpha_s L^2)^n$. This result can be extracted from Ref. [24], but we here propose a more simple and explicit derivation of h_2 , thereby introducing a resummation procedure that will be helpful for the NNDL resummation as well.

The central observation is that contributions of the form $\alpha_s L (\alpha_s L^2)^n$ can only be obtained with n soft-collinear emissions, each contributing a factor $\alpha_s L^2$, and a single correction to one of the emissions in the full sequence giving the extra factor $\alpha_s L$. To find the potential configurations that can yield a factor $\alpha_s L$, it is sufficient to go back to the $\mathcal{O}(\alpha_s)$ expression discussed at DL accuracy and list all possible NDL corrections. From Eq. (3.3), we see that we can get corrections beyond DL from either the matrix element, or from the expression of the relative transverse momentum k_t . NDL, single-logarithmic, corrections to the matrix element, Eq. (3.5), can be of three origins: (i) one-loop running-coupling corrections to α_s , (ii) hard-collinear corrections where one would have to take into account the full Altarelli–Parisi [52] splitting functions at large z , and (iii) potential soft large-angle corrections away from the collinear limit. These three contributions are schematically represented in Figs. 2a-2c. Finally, potential corrections associated with the $k_t > k_{t,\text{cut}}$ condition are depicted in Fig. 2d.

The diagrams in Fig. 2b-2d clearly exhibit a single-logarithmic behaviour, where the logarithm stems from integrating over a line in the Lund plane, i.e. over a region which extends over a distance of order L in one direction and is limited to an extent of order 1 in the other direction.

Out of the 4 possibilities sketched in Fig. 2, neither the large-angle correction to the matrix element, Fig. 2c, nor the emission near the $k_{t,\text{cut}}$ boundary, Fig. 2d, contribute at NDL. The

case of corrections with $k_t \sim k_{t,\text{cut}}$, Fig. 2d, is particularly trivial: single-logarithmic emissions along the $k_{t,\text{cut}}$ boundary are soft and collinear; the DL relations in Eq. (3.4) as well as the DL simplification of the matrix-element, Eq. (3.5), are therefore still valid, yielding no NDL correction in Eq. (3.3).

Let us therefore discuss the case of emissions at large angle. The matrix element for a soft emission, p_k , off a dipole with legs (p_i, p_j) is given by the well-known eikonal factor:

$$\begin{aligned} \int [dk] |M(k)|^2 &= \frac{\alpha_s}{2\pi} (-2T_i \cdot T_j) \int \frac{dE_k}{E_k} \frac{d^2\theta_k}{2\pi} E_k^2 \frac{(p_i \cdot p_j)}{(p_i \cdot p_k)(p_j \cdot p_k)} \\ &\equiv \frac{\alpha_s}{2\pi} (-2T_i \cdot T_j) \int \frac{dE_k}{E_k} \frac{d^2\theta_k}{2\pi} (p_k | p_i p_j), \end{aligned} \quad (3.13)$$

with $T_{i,j}$ the colour matrices associated with the dipole legs, and $d^2\theta_k/2\pi \equiv d\cos\theta_k d\phi_k/2\pi$. Since the NDL correction can take place anywhere in the chain of DL emissions, we have two cases to consider: either a soft primary emission at large angles, or any subsidiary soft emission which happens at commensurate angle compared to another soft-collinear emission. If the emission is primary, the ij dipole in Eq. (3.13) corresponds to the initial $q\bar{q}$ (gg) pair and is, therefore, in a back-to-back configuration. In this case, $-2T_i \cdot T_j = 2C_i$ and one can easily show that Eq. (3.13) corresponds exactly to the soft-and-collinear matrix element, Eq. (3.5), and, therefore, no new NDL correction arises. Conversely, if we have the emission of a soft gluon, say k_2 , at an angle commensurate to a previous collinear emission, k_1 , it is well-known that after integrating over the azimuthal angle of the soft gluon, one recovers the property of angular ordering [20, 53], i.e. $\Theta(\theta_2 < \theta_1) = \Theta(\eta_2 > \eta_1)$. This again reproduces the DL result with no NDL correction. Physically, we can view the absence of large-angle contribution at NDL accuracy as a consequence of the fact that the Lund definition of k_t matches the physical relative transverse momentum with respect to the emitting dipole, at least in the soft limit (see also Eq. (3.4)).

In summary, the NDL h_2 function in Eq. (1.1) receives only two non-zero contributions:

$$h_2(\nu) = h_{2,\beta_0}(\nu) + h_{2,\text{hc}}(\nu), \quad (3.14)$$

that are derived in Eqs. (3.19), (3.23), (3.25) and (3.27). The resulting final expression for (3.14) agrees with what was originally obtained in Ref. [24].

While these two contributions could be computed in a similar fashion to Eq. (3.9), we instead propose a new resummation scheme that relies on the above-mentioned observation that for any set of emissions, only one would be associated with the NDL, yielding a contribution of order $\alpha_s L$, with all other emissions being treated in the DL soft-and-collinear approximation. These soft-collinear emissions can then be resummed using explicitly the DL results in Eqs. (3.10) and (3.12).

To illustrate this more concretely, we define $\ell \equiv \ln Q/k_t$, where k_t denotes the scale at which the emission takes place. More concretely, a generic NDL correction can stem either from real emissions or from virtual corrections, and can happen either for an emission from the leading parton (i.e. for an emission in the primary Lund plane) or for an emission off a previous DL emission (at any order in α_s). This leads to a total of four possible contributions that are

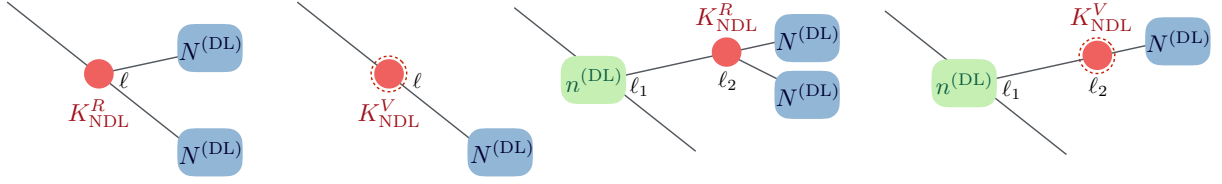


Figure 3: Sketch of the method used to compute NDL corrections from two basic ingredients: a single genuine NDL emission, the (red) solid vertex, and towers of DL emissions, either before (green box, Eq. (3.12)) or after (blue box, Eq. (3.10)) the NDL emission. The four diagrams represent the four options for the NDL vertex: a real emission from the leading parton, a virtual correction from the leading parton, a real emission from any subsidiary DL gluon, or a virtual correction from a subsidiary DL gluon (from left to right).

sketched in Fig. 3. More formally, we can write the NDL correction as

$$\begin{aligned} \delta N_i^{(\text{NDL})} = & \int_0^L d\ell \left\{ K_{\text{NDL}}^R [N_{\text{hard}}^{(\text{DL})}(L; \ell) + N_{\text{soft}}^{(\text{DL})}(L; \ell)] - K_{\text{NDL}}^V N_i^{(\text{DL})}(L; \ell) \right\} \\ & + \int_0^L d\ell_1 n_i^{(\text{DL})}(\ell_1) \int_{\ell_1}^L d\ell_2 \left\{ K_{\text{NDL}}^R [N_{\text{hard}}^{(\text{DL})}(L; \ell_2) + N_{\text{soft}}^{(\text{DL})}(L; \ell_2)] - K_{\text{NDL}}^V N_g^{(\text{DL})}(L; \ell_2) \right\}. \end{aligned} \quad (3.15)$$

This equation requires a few comments. First, we denote by $\delta N_i^{(\text{NDL})} \equiv \sqrt{\alpha_s} h_2^{(i)}$ the NDL corrections to the average Lund plane multiplicity, computed here for a single hemisphere of flavour $i = q, g$. Similarly, $N^{(\text{DL})}(L; \ell)$ denotes the double-logarithmic evolution starting from a parton of transverse momentum scale $e^{-\ell}Q$ down to the cutoff scale $e^{-L}Q$. At this accuracy, $N^{(\text{DL})}(L; \ell) = N^{(\text{DL})}(L - \ell)$. The first line of Eq. (3.15) corresponds to the case where the NDL correction occurs in the primary Lund plane, i.e. is associated with an emission off the leading parton as represented in the leftmost two sketches of Fig. 3. In this case, the NDL factor $\alpha_s L$ arises after integrating over the k_t of the emission (with $\ell = \ln Q/k_t$). Correspondingly, the second line is associated with NDL corrections for an emission off a subsidiary gluon, displayed in the two rightmost sketches of Fig. 3. In this case, we have a tower of DL emissions, yielding a gluon at a relative transverse momentum $k_{t,1}$, with $\ell_1 = \ln(Q/k_{t,1})$. This gluon further splits at a transverse momentum scale $k_{t,2}$, with $\ell_2 = \ln(Q/k_{t,2})$ and the NDL correction, proportional to $\alpha_s L$, stems from the integration over ℓ_2 . Also, we have to take into account that the emission associated with the NDL correction can be either real or virtual. In the former case, both offsprings can further emit DL gluons, hence the two contributions $N_{\text{hard}}^{(\text{DL})}(L; \ell_2)$ (emissions from the $k_{t,1}$ gluon at scales smaller than $k_{t,2}$) and $N_{\text{soft}}^{(\text{DL})}(L; \ell_2)$ (emissions off the $k_{t,2}$ gluon, the soft branch), while for the virtual correction, only one parton can further radiate. This DL radiation follows the same pattern of nested radiation as discussed in Sec. 3.1, except that it covers scales between $k_{t,2}$ and $e^{-L}Q$ as denoted explicitly by the arguments of $N_{\text{hard}}^{(\text{DL})}(L; \ell_2)$ in Eq. (3.15). Finally, the kernels $K_{\text{NDL}}^{R,V}$ denote the genuine NDL corrections, for real and virtual emissions respectively. Since the single-logarithmic contribution has been explicitly written as an integration over ℓ (or ℓ_2), the kernels are proportional to α_s (potentially with extra double-logarithmic factors proportional to $\alpha_s L^2$). The form of Eq. (3.15) also implies that the expressions for the NDL kernels, $K_{\text{NDL}}^{R,V}$, can

be obtained from the study of a single emission (treated at fixed order) and then inserted in Eq. (3.15) to obtain the all-orders result.⁴

In what follows, we use Eq. (3.15) to compute the two contributions appearing in Eq. (3.14) for one hemisphere.

3.2.1 Running coupling effects

We first consider the NDL correction associated to the running of the strong coupling, see Fig. 2a. At 1-loop we have

$$\alpha_s(k_t) = \frac{\alpha_s}{1 - 2\alpha_s\beta_0 \ln \frac{\mu_R}{k_t}} \approx \alpha_s + 2\alpha_s^2\beta_0 \ln \left(\frac{\mu_R}{k_t} \right) + \mathcal{O}(\alpha_s^3), \quad (3.16)$$

where $\alpha_s \equiv \alpha_s(\mu_R)$ with μ_R the renormalisation scale of order Q . Unless explicitly stated otherwise, we set $\mu_R = Q$. Furthermore $\beta_0 = (11C_A - 4n_f T_R)/(12\pi)$ is the 1-loop β function. At NDL accuracy, one of the emissions in the chain will get a correction $2\alpha_s^2\beta_0 \ln(\mu_R/k_t)$, bringing a factor of order $\alpha_s L$ compared to the dominant α_s contribution at DL.

We focus on the contribution from the second line in Eq. (3.15) — the rightmost sketches in Fig. 3 — noting that the contribution from the first line can straightforwardly be deduced by setting ℓ_1 to zero. Consider therefore that an emission with relative transverse momentum $k_{t,2}$ is radiated off a gluon created itself at a scale $k_{t,1}$, as in Fig. 3. This new emission can be emitted over a rapidity range $\ln(k_{t,1}/k_{t,2}) \equiv \ell_2 - \ell_1$ that we can integrate out so as to find

$$K_{\text{NDL},\beta_0} = \frac{2\alpha_s C_A}{\pi} \times (2\alpha_s\beta_0\ell_2) \times (\ell_2 - \ell_1), \quad (3.17)$$

valid for both real emissions and virtual corrections.

Since running coupling corrections do not alter the flavour of the leading parton, the real contribution alongside the hard branch and the virtual correction cancel exactly and we are only left with the real contribution from emissions off the soft branch. Using the fact that $n_i^{(\text{DL})} = n_g^{(\text{DL})} C_i/C_A$, we obtain

$$\delta N_{i,\beta_0}^{(\text{NDL})} = \frac{C_i}{C_A} \int_0^L d\ell_1 \left[\delta(\ell_1) + n_g^{(\text{DL})}(\ell_1) \right] \bar{\alpha} \int_{\ell_1}^L d\ell_2 (2\alpha_s\beta_0\ell_2) (\ell_2 - \ell_1) N_g^{(\text{DL})}(L - \ell_2), \quad (3.18)$$

where the $\delta(\ell_1)$ term in the square bracket accounts for the correction on the primary Lund plane, as given by the first line of Eq. (3.15). Inserting the DL expressions for $N_g^{(\text{DL})}(L - \ell_2)$ and $n_g^{(\text{DL})}(\ell_1)$, Eqs. (3.10) and (3.12), we can perform the integrations and get

$$h_{2,\beta_0}^{(i)} = \frac{C_i}{C_A} \frac{\beta_0}{2} \sqrt{\frac{\pi}{2C_A}} \left[(\nu^2 - 1) \sinh \nu + \nu \cosh \nu \right]. \quad (3.19)$$

⁴We note that there are no Sudakov factors in Eq. (3.15). To understand this, take for example the evolution between ℓ_1 and ℓ_2 in the second line of Eq. (3.15). By construction, all the emissions between these two scales can be taken in the DL approximation. At this accuracy, we have already shown in Sec. 3.1, that the real emissions between ℓ_1 and ℓ_2 exactly cancel the virtual corrections between these two scales and therefore no Sudakov factors appear in the final expression.

3.2.2 Hard-collinear correction

In the hard-collinear regime the emission probability given by Eq. (3.5) has to be amended in order to incorporate the full DGLAP splitting functions, which can be written as:

$$\begin{aligned} P_{g \rightarrow gg}(z) &= 2C_A \left[\frac{1-z}{z} + \frac{z}{2}(1-z) \right], & P_{q \rightarrow qg}(z) &= 2C_F \left(\frac{1-z}{z} + \frac{z}{2} \right), \\ P_{g \rightarrow q\bar{q}}(z) &= n_f T_R [z^2 + (1-z)^2], \end{aligned} \quad (3.20)$$

with n_f the number of flavours and $T_R = 1/2$.⁵ In addition to the DL contribution coming from the soft, $z \ll 1$, limit of the splitting function, i.e. $P_{i \rightarrow ig} \approx 2C_i/z$, this introduces hard-collinear corrections at finite z . For such a hard-collinear emission happening at a rapidity η , one can simply, at NDL accuracy, integrate the non-divergent part of the splitting function over z , yielding the familiar B coefficients [54]:

$$\begin{aligned} B_{gg} &\equiv \int_0^1 dz \left[\frac{1}{2C_A} P_{g \rightarrow gg}(z) - \frac{1}{z} \right] = -\frac{11}{12}, & B_q &\equiv \int_0^1 dz \left[\frac{1}{2C_F} P_{q \rightarrow qg}(z) - \frac{1}{z} \right] = -\frac{3}{4}, \\ B_{gq} &\equiv \int_0^1 dz \frac{1}{2C_A} P_{g \rightarrow q\bar{q}}(z) = \frac{n_f T_R}{3C_A}, \end{aligned} \quad (3.21)$$

and identify the k_t scale of the emission, ℓ , with η_2 , which is equivalent to neglecting any further dependence on the z fraction in subsequent branchings. The NDL kernel associated with hard-collinear branchings, valid for both real and virtual contributions, is therefore

$$K_{\text{NDL,hc}} = \frac{2\alpha_s C_i}{\pi} \times B, \quad (3.22)$$

where C_i and B depend on the flavour channel under consideration.

Below, we consider separately the case of gluon emissions and the case of a flavour-changing $g \rightarrow q\bar{q}$ splitting. We thus split the flavour-diagonal (fd) and flavour-changing (fc) contributions and write

$$h_{2,\text{hc}} = h_{2,\text{hc-fd}} + h_{2,\text{hc-fc}}. \quad (3.23)$$

Flavour-diagonal Real emissions off the hard branch cancel exactly with the virtual corrections, as in the running coupling calculation, leaving only the contributions from DL radiation off the newly emitted parton $k_{t,2}$ in Eq. (3.15). For primary radiation, one gets either a coefficient $B_i = B_q$ or a coefficient $B_i = B_{gg}$ depending on whether the leading jet parton is a quark or a gluon. However, since subsidiary DL emissions are always gluons, their NDL hard-collinear corrections come with a B_{gg} factor. We therefore obtain

$$\delta N_{i,\text{hc-fd}}^{(\text{NDL})} = \frac{C_i}{C_A} \int_0^L d\ell_1 \left[B_i \delta(\ell_1) + B_{gg} n_g^{(\text{DL})}(\ell_1) \right] \bar{\alpha} \int_{\ell_1}^L d\ell_2 N_g^{(\text{DL})}(L - \ell_2), \quad (3.24)$$

where we have used Eq. (3.21) to integrate over the z -coordinate. Performing the remaining integrals yields

$$h_{2,\text{hc-fd}}^{(i)} = \frac{C_i}{C_A} \sqrt{\frac{C_A}{2\pi}} [2B_i \sinh \nu + B_{gg}(\nu \cosh \nu - \sinh \nu)]. \quad (3.25)$$

⁵Note that we have symmetrised $P_{g \rightarrow gg}$ so as to only have a divergence at $z = 0$. This is allowed since both $P_{g \rightarrow gg}$ and the observable definitions are symmetric under the $z \rightarrow 1 - z$ transformation. This is no longer the case for initial-state splittings as we will discuss in Sec. 6.

Flavour-changing The contribution from flavour-changing $g \rightarrow q\bar{q}$ splittings involves two modifications with respect to the flavour-diagonal part. First, primary $g \rightarrow q\bar{q}$ branchings are only possible for gluon jets. Second, while after a real splitting both resulting subjects are quarks, one still has a gluon after a virtual correction. As a consequence, one no longer has an exact cancellation between the real term $N_{\text{hard}}^{(\text{DL})}$ and the virtual correction which involves $N_g^{(\text{DL})}$, meaning that all the contributions have to be kept. Taking these differences into account, one easily arrives at the following expression:

$$\delta N_{i,\text{hc-fc}}^{(\text{NDL})} = \frac{C_i}{C_A} B_{gq} \int_0^L d\ell_1 \left[\delta_{ig} \delta(\ell_1) + n_g^{(\text{DL})}(\ell_1) \right] \bar{\alpha} \int_{\ell_1}^L d\ell_2 \left[2N_q^{(\text{DL})}(L-\ell_2) - N_g^{(\text{DL})}(L-\ell_2) \right], \quad (3.26)$$

where δ_{ig} selects gluon-initiated jets. After integration, we get

$$h_{2,\text{hc-fc}}^{(q)} = \frac{C_F}{C_A} \sqrt{\frac{C_A}{2\pi}} B_{gq} [c_\delta \nu \cosh \nu + (2 - 3c_\delta) \sinh \nu + 2(c_\delta - 1)\nu], \quad (3.27a)$$

$$h_{2,\text{hc-fc}}^{(g)} = \sqrt{\frac{C_A}{2\pi}} B_{gq} [c_\delta \nu \cosh \nu + (2 - c_\delta) \sinh \nu], \quad (3.27b)$$

for quark and gluon-initiated jets respectively. For the sake of conciseness, we have introduced

$$c_\delta \equiv \frac{2C_F - C_A}{C_A}. \quad (3.28)$$

4 Calculation at NNDL accuracy

4.1 Contributions and master formula

We start the NNDL calculation by providing a systematic construction of the physical contributions appearing at NNDL accuracy. Each contribution which is not trivially vanishing will then be discussed in the following subsections. Therefore, here we lay out the main physics arguments, so as to factor them from the more technical calculations in the following sections.

To reach NNDL accuracy, we need to compute the NNDL h_3 function, resumming terms of order $\alpha_s^n L^{2n-2}$, in Eq. (1.1). A term of such form can be obtained by either having (a) a single emission contributing a pure factor α_s with no logarithmic enhancement (together with $n-1$ soft-and-collinear emissions contributing as many factors of $\alpha_s L^2$), or (b) two emissions contributing a factor of order $\alpha_s L$ (together with $n-2$ soft-and-collinear emissions). In what follows, we will consider that the logarithms in this counting are of kinematic origin — i.e. arising from integrations over the phase-space of the emissions — and treat as a third category, (c), the contributions involving the running of the strong coupling. In each category, one should take into account contributions from both real and virtual emissions.

We first discuss the category (a), whose contributions are represented in Fig. 4a-e. Following the discussion at NDL in Sec. 3.2, for a contribution to be of $\mathcal{O}(\alpha_s)$ with no logarithmic enhancements, it should be kinematically confined to a region of $\mathcal{O}(1)$ in the Lund plane. This means either in the vicinity of another emission or in one of the three corners of a (primary or subsidiary) Lund plane: (i) at the top of the plane, (ii) at the collinear end of the $k_{t,\text{cut}}$ bound-

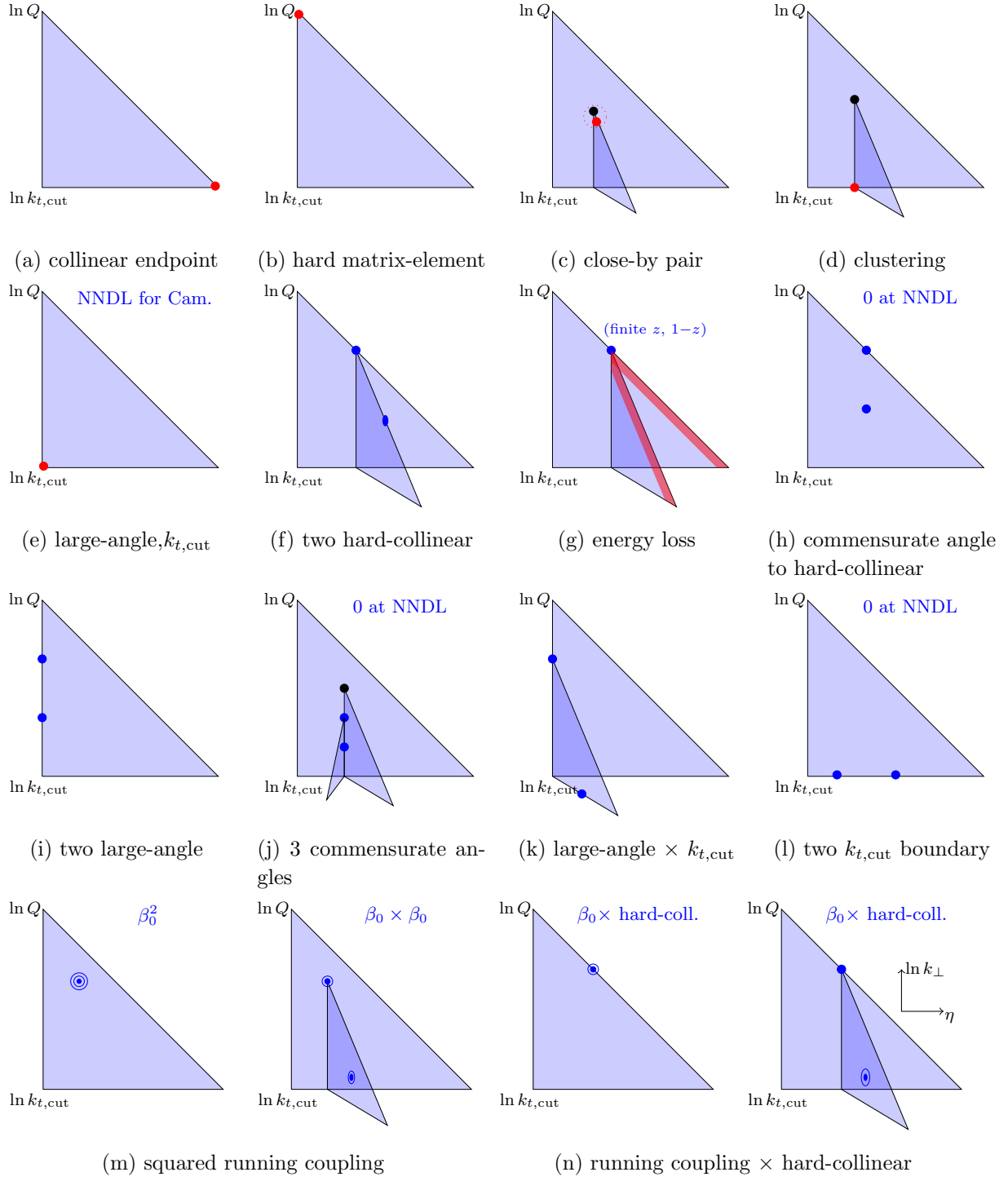


Figure 4: Lund representation of the configurations that contribute to the multiplicity at NNDL. Black dots indicate soft-collinear emissions ($\propto \alpha_s L^2$), blue dots emissions which contribute a factor $\alpha_s L$, and red dots emissions which only contribute a factor α_s with no logarithmic enhancement. Running-coupling corrections ($\propto \alpha_s L$) are represented by open circles.

ary, or (iii) close to the $k_{t,\text{cut}}$ boundary at an angle commensurate to a previous emission.⁶ This directly yields five NNDL-like kinematic configurations compared to what was needed at NDL accuracy. These contributions involve just one emission that is located at:

- The collinear endpoint of the Lund plane (primary or subsidiary), as represented in Fig. 4a. This is related to the exact k_t definition and discussed in Sec. 4.2.1.
- The top of the primary Lund plane, see Fig. 4b. This is associated with fixed-order matrix-element corrections, see Sec. 4.2.2.
- The top of a subsidiary Lund plane or in the vicinity of another emission, i.e. associated with a (close-by) pair of emissions at commensurate k_t and angles. This is shown in Fig. 4c and related to the soft limit of the $1 \rightarrow 3$ splitting function (or to the collinear limit of the double-soft matrix element) as discussed in Sec. 4.2.3 and App. B.
- Close to the $k_{t,\text{cut}}$ boundary at angles commensurate to a previous emission, see Fig. 4d. This is associated with the details of the Cambridge clustering and discussed in Sec. 4.2.4.
- At large angles with $k_t \sim k_{t,\text{cut}}$ in the primary Lund plane, see Fig. 4e. This correction vanishes for the Lund multiplicity but is non-zero for Cambridge, as discussed in Sec. 4.2.5.

We now move on to the kinematic configurations, (b), where two emissions contribute a factor $\alpha_s L$. Following the discussion about NDL multiplicity, for an emission to contribute a factor $\alpha_s L$ it has to be either hard-and-collinear, or at an angle commensurate to a previous emission (including large-angle emissions in the primary Lund plane), or close to the $k_{t,\text{cut}}$ boundary. This results in the following set of configurations, cf. Fig. 4f-1, required at NNDL accuracy:

- Two hard-collinear emissions: this includes of course the contribution where two emissions receive NDL-like corrections from the finite splitting function in the hard-collinear limit, as shown in Fig. 4f and discussed in Sec. 4.3.2. There is however an additional effect to take into account: after a first hard-collinear splitting both daughter partons carry a finite fraction of the energy of the parent parton. This affects the phase-space available for subsequent emissions, shifting the hard-collinear boundary of their Lund planes. This contribution, dubbed *energy loss*, is represented in Fig. 4g, where the (red) bands indicate that after the hard-collinear (blue) emission, this phase-space is no longer accessible. The calculation is presented in Sec. 4.3.1.
- One hard-collinear emission and one commensurate-angle emission. For this, assume we have a set of emissions where one of them, k_1 , is a hard-collinear splitting and one of them, k_2 , occurs at an angle commensurate with that of a previous emission. We need to consider two cases depending on whether the commensurate-angle emission happens at an angle commensurate to the hard-collinear one, i.e. $\theta_1 \approx \theta_2$, or to any other soft-collinear emission, i.e. $\theta_1 \ll \theta_2$ or $\theta_1 \gg \theta_2$. We show in Sec. 4.3.3 that the first case yields no NNDL corrections. For the second case, it is sufficient to realise that emissions well separated

⁶As for our NDL discussion, we include in ‘emissions at commensurate angles’ the case of primary emissions at large angles, technically commensurate with the angle π of the initial $q\bar{q}$ (or $g\bar{g}$) system.

in angle are independent of one another (in particular due to our use of the Cambridge clustering). This would thus result in factorised NDL contributions from k_1 and k_2 . This vanishes as well since commensurate-angle emissions have no NDL corrections (see Sec. 3.2).

- One hard-collinear emission and one emission close to the $k_{t,\text{cut}}$ boundary (not shown in Fig. 4). This vanishes since a hard-collinear emission does not change the k_t of following emissions in the Lund planes of either daughter partons.⁷
- Two emissions at commensurate angles. Here one should distinguish two cases: firstly, the case where the first emission is a primary large-angle emission, Fig. 4i and Sec. 4.3.4; secondly the case of three emissions at commensurate angles (i.e. a first soft-collinear emission followed by two commensurate-angle soft emissions), Fig. 4j, which actually vanishes as explained in Sec. 4.3.5.⁸
- One emission at an angle commensurate to that of a previous emission and one emission close to the $k_{t,\text{cut}}$ boundary. For this to have a non-zero effect, one should be in a configuration where the presence of the commensurate-angle emission leads to a difference between the physical k_\perp of the second emission and its reconstructed Lund k_t , i.e. configurations where Eq. (3.4) has to be revisited. This is only possible when the commensurate-angle emission is a primary emission at large angle, cf. Fig. 4k. In practice, this contribution exactly cancels the one from diagram 4i and we show this explicitly in Sec. 4.3.4.
- Two emissions close to the $k_{t,\text{cut}}$ boundary, Fig. 4l. Due to our choice of using the Cambridge algorithm to define the Lund multiplicity, two emissions close to the $k_{t,\text{cut}}$ boundary and well-separated in angles would never cluster with one another: if they belong to the same Lund plane, the most collinear would cluster with the plane’s leading parton before the larger-angle does, and two collinear emissions in different Lund planes would cluster with the leading parton of their respective plane. This choice of a Cambridge-based multiplicity definition, and the consequence that the contributions from two commensurate- k_t emissions vanish is crucial for the feasibility of the NNDL calculation. For the more standard definition based on the Durham algorithm [24], this diagram would not only be non-zero at NNDL, but it would also depend in an intricate way on the full angular structure of the event, making it extremely difficult to calculate analytically. We elaborate more on this point in App. A.1.

Finally, we discuss the contributions associated with the running of the strong coupling constant. Since the 1-loop running contributes at the NDL accuracy, one would naively expect to have two-loop corrections at NNDL. However, if we write the two-loop running coupling at a scale k_t as

⁷To understand this, consider a hard-and-collinear emission followed by an emission close to the $k_{t,\text{cut}}$ boundary. This soft emission would set the minimum energy in the definition of k_t , Eq. (2.1), regardless of whether the previous emission is hard or not.

⁸This does not cover the case where the two commensurate-angle emissions are emitted off different partons, at widely separated angles (i.e. in independent Lund planes). This contribution however vanishes as the contributions from each commensurate-angle emission would factorise into a product of two commensurate-angle NDL contributions which are themselves zero.

Contribution	h_3	Diagrams	Section	Result
Collinear endpoint	$h_{3,\text{end}}$	4a	4.2.1	(4.8)
Hard matrix-element	$h_{3,\text{hme}}$	4b	4.2.2	(4.18)
Commensurate k_t and angle	$h_{3,\text{pair}}$	4c	4.2.3	(4.29)
Clustering	$h_{3,\text{clust}}$	4d	4.2.4	(4.36)
Large angle and $k_t \sim k_{t,\text{cut}}$	$h_{3,\text{la}\&k_t}$	4e	4.2.5	0 (Lund), (4.39) (Cam)
Energy loss	$h_{3,\text{eloss}}$	4g	4.3.1	(4.44)
(Hard-collinear) ²	h_{3,hc^2}	4f	4.3.2	(4.49)
Hard-coll. \times comm. angles	—	4h	4.3.3	0
First emission at large angles	—	4i, 4k	4.3.4	0
3 commensurate angles	—	4j	4.3.5	0
β_0^2	h_{3,β_0^2}	4m	4.4.1	(4.64)
$\beta_0 \times \text{hard-collinear}$	$h_{3,\beta_0 \times \text{hc}}$	4n	4.4.2	(4.68)
Total	h_3	Fig. 4	4.5	(4.72)-(4.74)

Table 1: Relevant coefficients for the NN DL function h_3 .

a function of $\alpha_s \equiv \alpha_s(Q)$ (taking $\mu_R = Q$ without loss of generality), i.e.

$$\alpha_s(k_t) = \frac{\alpha_s}{1 - 2\alpha_s\beta_0 \ln(Q/k_t)} - \frac{\alpha_s^2\beta_1}{\beta_0} \frac{\ln[1 - 2\alpha_s\beta_0 \ln(Q/k_t)]}{[1 - 2\alpha_s\beta_0 \ln(Q/k_t)]^2}, \quad (4.1)$$

one sees that the two-loop β_1 correction starts as $\beta_1\alpha_s^3 \ln(Q/k_t)$ which, after integration over the phase-space for emissions with $k_t > k_{t,\text{cut}}$, would bring contributions starting at order $\beta_1\alpha_s^3 \ln^3(Q/k_{t,\text{cut}})$, i.e. only arising from N³DL. This means that the running coupling corrections all come from squared NDL corrections and can be split into:

- Terms proportional to $[\alpha_s\beta_0 \ln(Q/k_t)]^2$ where the two β_0 factors can either come from a single emission by expanding the first term of Eq. (4.1) to second order in β_0 , or by having two different emissions, each receiving a β_0 correction. These contributions are depicted in Fig. 4m and computed in Sec. 4.4.1.
- Terms involving one NDL running coupling correction and one NDL hard-collinear correction. In this case, the running-coupling correction can coincide with the hard-collinear emission or can appear for any other soft-collinear emission, Fig. 4n. These are calculated in Sec. 4.4.2.

Putting all the non-vanishing contributions together, we get the following expression for the NN DL function h_3 :

$$h_3 = h_{3,\text{end}} + h_{3,\text{hme}} + h_{3,\text{pair}} + h_{3,\text{clust}} + h_{3,\text{eloss}} + h_{3,\text{hc}^2} + h_{3,\beta_0^2} + h_{3,\beta_0 \times \text{hc}}, \quad (4.2)$$

where all the functions depend only on $\xi = \alpha_s L^2$. For Cambridge multiplicity, we instead find

$$h_3^{(\text{Cam})} = h_3^{(\text{Lund})} + h_{3,\text{la}\&k_t} \quad (4.3)$$

with $h_3^{(\text{Lund})}$ given by Eq. (4.2).

Most of the calculations below are more easily addressed if we consider a single hemisphere, therefore computing the $h_3^{(i)}$ function with $i = q, g$. Although the presence of large-angle contributions, $h_{3,\text{hme}}$ in particular, makes it less obvious that the two hemispheres can be treated independently, one is always entitled to write the NN DL correction to the average Lund multiplicity in $Z \rightarrow q\bar{q}$ and $H \rightarrow gg$ events as $\delta N_Z^{(\text{NNDL})} = \alpha_s h_{3,Z} = 2\alpha_s h_3^{(q)}$ and $\delta N_H^{(\text{NNDL})} = \alpha_s h_{3,H} = 2\alpha_s h_3^{(g)}$.

Table 1 summarises the physical origin of the various NN DL corrections together with the section discussing them and, when non-zero, the equation where to find the final result. Eq. (4.2), together with the individual contributions listed in Table 1 are the main results of this paper. For completeness, the full result for $h_3(\nu)$ is summarised in Sec. 4.5.

4.2 Corrections involving a pure α_s contribution

All the pure α_s contributions involve physical configurations which are new compared to the NDL result. For each of these new kinematic configurations, the α_s -factor arises through a phase-space integration which is only non-exponentially vanishing in a constant region of the Lund plane. This integration typically produces a coefficient $\frac{\alpha_s}{2\pi} D$ with a different constant D for each configuration. This constant can be extracted from a fixed-order calculation before we use it to derive the all-order behaviour by adding an arbitrary number of soft-and-collinear emissions, i.e. following a similar procedure as for the NDL calculation in Sec. 3.2, where the NDL kernel in Eq. (3.15) and in Fig. 3 is now an NN DL kernel.

4.2.1 Hard-collinear endpoint

If we consider a parton of flavour i splitting into two collinear daughter partons of flavours b and c , the contribution of the additional parton to the average multiplicity can be written as

$$\langle N_{i \rightarrow bc}^{(\text{Lund})} \rangle_{\mathcal{O}(\alpha_s)} = \bar{\alpha} \int_0^\infty d\eta \int_0^1 dz \frac{1}{2C_A} P_{i \rightarrow bc}(z) \Theta(\min(z, 1-z)e^{-\eta} > e^{-L}), \quad (4.4)$$

with $P_{i \rightarrow bc}(z)$ the DGLAP splitting kernel (see Sec. 3.2.2) for the flavour channel under consideration. Say we write $P_{i \rightarrow bc}(z) = \frac{2C_i}{z} \delta_{cg} + p_{i \rightarrow bc}^{(\text{finite})}(z)$, separating explicitly the soft-enhanced and finite contributions. For the contribution proportional to $1/z$, an NN DL correction arises from keeping explicitly the $\min(z, 1-z)e^{-\eta}$ in the k_t constraint instead of approximating it by $ze^{-\eta}$ (which would produce the DL result, with no NDL corrections). Similarly, for the finite piece of the splitting function, $p_{i \rightarrow bc}^{(\text{finite})}(z)$, keeping explicitly the $\min(z, 1-z)e^{-\eta}$ in the k_t constraint instead of approximating it by $e^{-\eta}$ (which would produce the hard-collinear NDL contribution) induces an additional NN DL correction. Both contributions, which come from taking into account the exact expression for the reconstructed k_t of the emission, are relevant in the $\mathcal{O}(1)$ phase-space region where z is finite and the reconstructed k_t is close to the cut $k_{t,\text{cut}}$, cf. Fig. 4a.

Considering the two contributions and performing the η integration, one gets an NN DL correction of the form

$$\delta N_{i \rightarrow bc}^{(\text{NNDL})} = \bar{\alpha} \int_{1/2}^1 \frac{dz}{z} \frac{C_i}{C_A} \delta_{cg} \ln\left(\frac{1-z}{z}\right) + \bar{\alpha} \int_0^1 dz \frac{p_{i \rightarrow bc}^{(\text{finite})}(z)}{2C_A} \ln(\min(z, 1-z)) = \frac{\alpha_s}{2\pi} D_{\text{end}}^{i \rightarrow bc}. \quad (4.5)$$

Inserting the explicit expressions from Eq. (3.20) for the splitting kernels, we get

$$D_{\text{end}}^{q \rightarrow qg} = C_F \left(3 + 3 \ln 2 - \frac{\pi^2}{3} \right), \quad (4.6a)$$

$$D_{\text{end}}^{g \rightarrow gg} = C_A \left(\frac{137}{36} + \frac{11}{3} \ln 2 - \frac{\pi^2}{3} \right), \quad (4.6b)$$

$$D_{\text{end}}^{g \rightarrow q\bar{q}} = n_f T_R \left(-\frac{29}{18} - \frac{4}{3} \ln 2 \right). \quad (4.6c)$$

We now proceed with the all-order resummation of the collinear endpoint correction. As discussed in Sec. 4.1, this is achieved by considering a collinear endpoint emission together with a series of DL soft-and-collinear emissions. Since an emission with $k_t \sim k_{t,\text{cut}}$ has no phase-space to further emit a soft-and-collinear gluon — as is evident from Fig. 4a — the collinear endpoint emission should occur as the last step in the series of (nested) DL emissions. We therefore write

$$\alpha_s h_{3,\text{end}}^{(i)} = \frac{\alpha_s}{2\pi} \int_0^L d\ell \left[\delta(\ell) (D_{\text{end}}^{i \rightarrow ig} + \delta_{ig} D_{\text{end}}^{g \rightarrow q\bar{q}}) + \frac{C_i}{C_A} n_g^{(\text{DL})}(\ell) (D_{\text{end}}^{g \rightarrow gg} + D_{\text{end}}^{g \rightarrow q\bar{q}}) \right]. \quad (4.7)$$

The first term in this expression, proportional to $\delta(\ell)$, includes corrections from the leading parton, i.e. from the hard-collinear endpoint of the primary Lund plane. The second term includes the contributions from the hard-collinear endpoints of all the secondary gluon emissions. Performing the integrations explicitly, we find

$$h_{3,\text{end}}^{(q)} = \frac{1}{2\pi} D_{\text{end}}^{q \rightarrow qg} + \frac{1}{2\pi} (D_{\text{end}}^{g \rightarrow gg} + D_{\text{end}}^{g \rightarrow q\bar{q}}) \frac{C_F}{C_A} (\cosh \nu - 1), \quad (4.8a)$$

$$h_{3,\text{end}}^{(g)} = \frac{1}{2\pi} (D_{\text{end}}^{g \rightarrow gg} + D_{\text{end}}^{g \rightarrow q\bar{q}}) \cosh \nu, \quad (4.8b)$$

for quark and gluon jets, respectively.

4.2.2 Hard matrix-element corrections (top of the Lund plane)

We next consider the NNDL contribution, $h_{3,\text{hme}}$, stemming from finite corrections to the Born-level matrix element. As shown in Fig. 4b, this accounts for the $\mathcal{O}(1)$ region at the top of the primary Lund plane where a first primary splitting is both hard and wide-angle.

Let us first consider the calculation at $\mathcal{O}(\alpha_s)$, for which we go back to the full expression for the Lund plane multiplicity, Eq. (3.1). The contribution from the leading parton (the ‘1’ in all three terms) cancels exactly the $\sigma_0 + \sigma_1$, and, for the remaining contribution off the extra emission (the $\Theta(k_t > k_{t,\text{cut}})$ term), σ_1 only contributes at higher orders. As a consequence, Eq. (3.2) is still valid. At order α_s we should therefore consider the exact matrix element for $Z \rightarrow q\bar{q}g$, and for $H \rightarrow ggg$ and $H \rightarrow gq\bar{q}$.

An important technical remark is in order. By definition, the exact matrix element represents the emission probability for an emission anywhere in the Lund plane. Therefore, integrating the matrix element with the $k_{t,\text{cut}}$ condition includes three NNDL corrections: (i) the top of the Lund plane, (ii) the collinear endpoint (see Sec. 4.2.1) and (iii) the large angle, $k_t \sim k_{t,\text{cut}}$ corner. The latter contribution has been shown to vanish in the previous section. To avoid double counting we thus have to subtract the contribution from the collinear endpoint from the full integration.

The exact matrix elements are best written in terms of the energy fractions $x_i = 2E_i/Q$, with $x_1 + x_2 + x_3 = 2$. For a generic decay of a boson X into three particles of momenta k_i , we therefore write the full-event result as

$$\langle N_{X \rightarrow k_1 k_2 k_3}^{(\text{Lund})} \rangle_{\mathcal{O}(\alpha_s)} = \int dx_1 dx_2 dx_3 \frac{|\mathcal{M}^{X \rightarrow k_1 k_2 k_3}|^2}{\sigma_0} \Theta(k_{t,\text{exact}} > k_{t,\text{cut}}) \delta(x_1 + x_2 + x_3 - 2). \quad (4.9)$$

For the different processes we consider, the matrix elements (for the full event, i.e. for both hemispheres) are given by [53, 55]:

$$\frac{|\mathcal{M}^{Z \rightarrow q\bar{q}g}|^2}{\sigma_0} = \frac{\alpha_s C_F}{2\pi} \frac{x_1^2 + x_2^2}{(1-x_1)(1-x_2)}, \quad (4.10)$$

and

$$\frac{|\mathcal{M}^{H \rightarrow ggg}|^2}{\sigma_0} = \frac{\alpha_s C_A}{6\pi} \frac{1 + (1-x_1)^4 + (1-x_2)^4 + (1-x_3)^4}{(1-x_1)(1-x_2)(1-x_3)}, \quad (4.11a)$$

$$\frac{|\mathcal{M}^{H \rightarrow gq\bar{q}}|^2}{\sigma_0} = \frac{\alpha_s n_f T_R}{\pi} \frac{(1-x_2)^2 + (1-x_3)^2}{1-x_1}, \quad (4.11b)$$

where the last line refers to the case of a $H \rightarrow gg$ splitting followed by a $g \rightarrow q\bar{q}$ branching, neglecting the situation where the Higgs boson would directly decay into a $q\bar{q}$ pair. The exact k_t in Eq. (4.9) depends on which pair of particles gets clustered first by the Cambridge algorithm:

$$\begin{aligned} \Theta(k_{t,\text{exact}} > k_{t,\text{cut}}) &= \Theta(\theta_{12} < \theta_{13}, \theta_{23}) \Theta(\min(x_1, x_2) \sin(\theta_{12}) > e^{-L}) \\ &\quad + \Theta(\theta_{13} < \theta_{12}, \theta_{23}) \Theta(\min(x_1, x_3) \sin(\theta_{13}) > e^{-L}) \\ &\quad + \Theta(\theta_{23} < \theta_{12}, \theta_{13}) \Theta(\min(x_2, x_3) \sin(\theta_{23}) > e^{-L}). \end{aligned} \quad (4.12)$$

Explicit integration of (4.9) gives the known DL and NDL contributions, respectively proportional to L^2 and L , negligible terms suppressed by powers of e^{-L} and a constant. This constant is the sum of the collinear endpoints and hard matrix-element NNDL contributions. Subtracting the collinear endpoint computed in Sec. 4.2.1, we find⁹

$$\delta N_{X \rightarrow k_1 k_2 k_3}^{(\text{NNDL})} = \frac{\alpha_s}{\pi} D_{\text{hme}}^{k_1 k_2 k_3} \quad (4.13)$$

with

$$D_{\text{hme}}^{qqg} = C_F \left(\frac{\pi^2}{6} - \frac{7}{4} \right), \quad D_{\text{hme}}^{ggg} = C_A \left(\frac{\pi^2}{6} - \frac{49}{36} \right), \quad D_{\text{hme}}^{gq\bar{q}} = n_f T_R \frac{2}{9}. \quad (4.14)$$

Note that these NNDL hard matrix-element coefficients are independent of the details of the observable. This simply follows from the observation that the hard matrix-element contribution comes from an $\mathcal{O}(1)$ region at the top of the Lund plane while the cut on the observable only affects the soft and/or collinear dynamics. In particular, we have cross-checked Eq. (4.14) using other event shapes like the JADE [56], Durham [27], or Cambridge [30] jet multiplicities.

⁹Note the pre-factor $1/\pi$ instead of $1/(2\pi)$ such that the coefficient D corresponds to the contribution from a single hemisphere, as done for the other NNDL coefficients.

Let us now move to the all-order treatment of the hard matrix-element correction. As we have argued above, the virtual corrections, $|\mathcal{M}_V|^2$, and the NLO correction to the inclusive cross-section, σ_1 , do not contribute at $\mathcal{O}(\alpha_s)$. This holds at all orders, as we prove in what follows. Since we want to compute the correction arising at the top of the Lund plane, it is sufficient to consider explicitly the emission (real or virtual) with the largest k_t . For this emission, the real and virtual contributions can be of two types: (i) associated with an infrared divergence and, (ii) finite hard matrix-element corrections. Up to a sign, the former are the same for the real and virtual terms and, dressed with additional soft-and-collinear emissions, give rise to the DL and NDL multiplicity. The latter are different for real and virtual terms. For simplicity, let us consider a single hemisphere of flavour a . For a given flavour channel, the real contribution is given by $\sigma_0 \frac{\alpha_s}{2\pi} D^{abc}$ with the D^{abc} coefficient computed above. Let us denote the corresponding virtual contribution by $\sigma_0 \frac{\alpha_s}{2\pi} D_V^{abc}$ where the actual value of D_V^{abc} is irrelevant for the following discussion. Given that these contributions arise from an $\mathcal{O}(1)$ region at the top of the primary Lund plane, they should be dressed by additional DL emissions down to the boundary scale $k_{t,\text{cut}}$. We can therefore write

$$N_a^{(\text{NNDL})}(L) = \frac{\sigma_0}{\sigma_0 + \sigma_1} \left\{ N_a^{(\text{NDL})}(L) + \frac{\alpha_s}{2\pi} \sum_{b,c} D^{abc} [N_b^{(\text{DL})}(L) + N_c^{(\text{DL})}(L)] - D_V^{abc} N_a^{(\text{DL})}(L) \right\}, \quad (4.15)$$

where, for real emissions, both products of the splitting are dressed by DL emissions, while virtual corrections only have a single series of DL emissions. Since (again considering a single hemisphere for simplicity)

$$\sigma_1 = \frac{\alpha_s}{2\pi} \sigma_0 \sum_{b,c} D^{abc} - D_V^{abc}, \quad (4.16)$$

Eq. (4.15) can be simplified to

$$N_a^{(\text{NNDL})}(L) = N_a^{(\text{NDL})}(L) + \frac{\alpha_s}{2\pi} \sum_{b,c} D^{abc} [N_b^{(\text{DL})}(L) + N_c^{(\text{DL})}(L) - N_a^{(\text{DL})}(L)], \quad (4.17)$$

where the virtual contribution D_V^{abc} has disappeared as anticipated. Applying this result to the quark and gluon cases, we get

$$h_{3,\text{hme}}^{(q)} = \frac{1}{2\pi} D_{\text{hme}}^{qqg} \cosh \nu, \quad (4.18a)$$

$$h_{3,\text{hme}}^{(g)} = \frac{1}{2\pi} [D_{\text{hme}}^{ggg} \cosh \nu + D_{\text{hme}}^{gq\bar{q}} (c_\delta \cosh \nu + 1 - c_\delta)]. \quad (4.18b)$$

4.2.3 Soft-and-collinear emissions at commensurate angles and k_t

Similarly to the NNDL contribution which appears at the top of the primary Lund plane (Sec. 4.2.2), we must also account for similar corrections on subsidiary planes. Concretely, we must account for contributions where a first soft-and-collinear emission is followed by another at commensurate k_t and angle, as is displayed in Fig. 4c, alongside its virtual corrections.

To help understanding the structure of this correction we first analyse the $\mathcal{O}(\alpha_s^2)$ contribution to the Lund plane multiplicity. We therefore consider the radiation of two partons, soft and collinear compared to the hard leg. It is helpful to decompose the matrix element for emitting

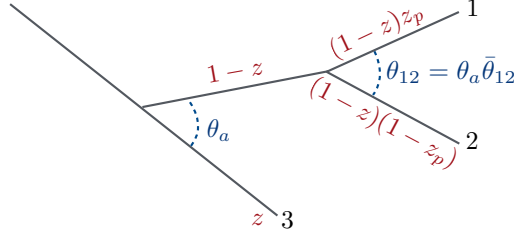


Figure 5: Parametrisation of an $i \rightarrow 123$ splitting. After a first $i \rightarrow 3 + a$ splitting a participates in a further $a \rightarrow 12$ splitting with characteristic angle θ_{12} and energy fraction z_p . The angle θ_a is that between the parent parton a and the final-state parton 3. Note that the soft limit corresponds to $z \rightarrow 1$ while in all previous sections it was parameterised by $z \rightarrow 0$.

two soft particles with momenta k_1 and k_2 into an uncorrelated, factorised, piece and a correlated piece [54], i.e.

$$|\mathcal{M}(k_1, k_2)|^2 = |\mathcal{M}(k_1)|^2 |\mathcal{M}(k_2)|^2 + |\widetilde{\mathcal{M}}(k_1, k_2)|^2. \quad (4.19)$$

The uncorrelated piece does not bring any correction at NNDL since $|\mathcal{M}(k_1)|$ reduces to the soft-and-collinear DL expression in Eq. (3.5) and cancels against the virtual-real contribution. The full NNDL correction is therefore in $|\widetilde{\mathcal{M}}(k_1, k_2)|$. In this case, we can assume that k_1 is emitted first — and is therefore real — and k_2 later (i.e. k_2 is a secondary emission from k_1). Accounting for both cases where k_2 is either real or virtual, the $\mathcal{O}(\alpha_s^2)$ correction to the Lund multiplicity is given by

$$\begin{aligned} \langle N_{\text{corr}}^{(\text{Lund})} \rangle_{\mathcal{O}(\alpha_s^2)} = \frac{1}{\sigma_0} \int [dk_1] \int [dk_2] & |\widetilde{\mathcal{M}}_{RR}(k_1, k_2)|^2 [\Theta(k_{t,1} > k_{t,\text{cut}}) + \Theta(k_{t,2} > k_{t,\text{cut}})] \\ & - |\widetilde{\mathcal{M}}_{RV}(k_1, k_2)|^2 \Theta(k_{t,1} > k_{t,\text{cut}}) \end{aligned} \quad (4.20)$$

where $[dk_i] \equiv d^4k_i \delta(k_i^2)/(2\pi)^3$. Combining the terms involving $\Theta(k_{t,1} > k_{t,\text{cut}})$, we recover a well-known relationship in the literature [57, 58]:

$$\int [dk_2] |\widetilde{\mathcal{M}}_{RR}(k_1, k_2)|^2 - |\widetilde{\mathcal{M}}_{RV}(k_1, k_2)|^2 = |\mathcal{M}(k_1)|^2 \alpha_s \left(-2\beta_0 \ln(k_t/Q) + \frac{K}{2\pi} \right), \quad (4.21)$$

with K the CMW factor [57], or equivalently the 1-loop cusp anomalous dimension, given by

$$K = \left(\frac{67}{18} - \frac{\pi^2}{6} \right) C_A - \frac{10}{9} n_f T_R. \quad (4.22)$$

The $\mathcal{O}(\beta_0)$ term was already accounted for as the running-coupling NDL contribution (Sec. 3.2.1), while the K term presents a new contribution at NNDL accuracy. After integrating over the soft-and-collinear emission k_1 with the phase-space given by Eq. (3.5) we find

$$\delta N_{i,K}^{(\text{NNDL})} = \left(\frac{C_i}{C_A} \frac{\bar{\alpha} L^2}{2} \right) \times \left(\frac{\alpha_s}{2\pi} K \right), \quad (4.23)$$

for a parent parton of flavour i .

We are now left with the computation of the term proportional to $\Theta(k_{t,2} > k_{t,\text{cut}})$ in Eq. (4.20). In practice, $|\widetilde{\mathcal{M}}_{RR}|^2$ can be obtained from the soft limit of the $1 \rightarrow 3$ splitting function, $\hat{P}_{1 \rightarrow 3}$, or, equivalently, from the collinear limit of the double-soft matrix element [59, 60]. In both cases, one should make sure to remove potential uncorrelated contributions.¹⁰ The resulting expressions are explicitly given in Appendix B for all flavour channels. In practice, it is helpful to use the integration variables depicted in Fig. 5, where the splitting is viewed as a first soft emission, at an angle θ_a and with a momentum fraction $1 - z \ll 1$, followed by a second splitting at an angle θ_{12} with momentum fraction z_p . In the limit where $1 - z \ll 1$, one has four flavour channels to consider corresponding to the leading parton, 3, being a quark or a gluon, and to the radiated partons, 1 and 2, being either two gluons or a $q\bar{q}$ pair. In all cases, the remaining part of Eq. (4.20), proportional to $\Theta(k_{t,2} > k_{t,\text{cut}})$, then takes the form

$$\int \frac{dz}{1-z} \frac{d\theta_a^2}{\theta_a^2} \int dz_p \frac{d\bar{\theta}_{12}^2}{\bar{\theta}_{12}^2} \frac{d\phi_{12}}{2\pi} \frac{z_p(1-z_p)(1-z)^2\bar{\theta}_{12}^2}{[1+z_p(1-z_p)\bar{\theta}_{12}^2]^2} \left(\frac{\alpha_s}{2\pi}\right)^2 \hat{P}_{1 \rightarrow 3}^{f_1 f_2 f_3} \Theta(k_{t,21} > k_{t,\text{cut}}). \quad (4.24)$$

for final flavours $f_{1,2,3}$, and with $k_{t,21} = \frac{Q}{2}(1-z)\min(z_p, 1-z_p)\theta_a\bar{\theta}_{12}$ the relative transverse momentum of k_2 with respect to k_1 .¹¹ From this expression, one can extract the pure NNDL contribution from emissions at commensurate angles and k_t by simply subtracting what is obtained in the strongly-angular-ordered limit:

$$\begin{aligned} \delta N_{i,RR}^{(\text{NNDL})} &= \left(\frac{\alpha_s}{2\pi}\right)^2 \int \frac{dz}{1-z} \frac{d\theta_a^2}{\theta_a^2} \int dz_p \frac{d\bar{\theta}_{12}^2}{\bar{\theta}_{12}^2} \frac{d\phi_{12}}{2\pi} \left\{ \frac{z_p(1-z_p)(1-z)^2\bar{\theta}_{12}^2}{[1+z_p(1-z_p)\bar{\theta}_{12}^2]^2} \hat{P}_{1 \rightarrow 3}^{f_1 f_2 f_3} - \mathcal{P} \right\} \Theta(k_{t,21} > k_{t,\text{cut}}), \end{aligned} \quad (4.25)$$

where \mathcal{P} is the appropriate combination of DGLAP splitting function contributing at NDL (see Appendix B for practical details). Note that since we use the exact expression for $k_{t,21}$, the subtraction also gets rid of the contribution computed in Sec. 4.2.1 where k_2 is at the hard-collinear endpoint. Eq. (4.25) follows the expected kinematic behaviour: the integrations over z_p and $\bar{\theta}_{12}$ are only non-zero in an $\mathcal{O}(1)$ region of finite z_p and $\bar{\theta}_{12} \sim 1$ ($\theta_{12} \sim \theta_a$), and the integrations over z and θ_a give a double-logarithmic factor. After integration, we get

$$\delta N_{i,RR}^{(\text{NNDL})} = \left(\frac{C_i}{C_A} \frac{\bar{\alpha} L^2}{2}\right) \times \left(\frac{\alpha_s}{2\pi} D_{\text{pair}}^{123}\right), \quad (4.26)$$

with

$$D_{\text{pair}}^{q\bar{q}} \equiv D_{\text{pair}}^{g \rightarrow q\bar{q}g} = D_{\text{pair}}^{q \rightarrow q\bar{q}'q} = \frac{13}{9} n_f T_R, \quad (4.27a)$$

$$D_{\text{pair}}^{gg} \equiv D_{\text{pair}}^{g \rightarrow ggg} = D_{\text{pair}}^{q \rightarrow gqg} = \left(\frac{\pi^2}{6} - \frac{67}{18}\right) C_A. \quad (4.27b)$$

¹⁰E.g. for $g \rightarrow ggg$ splittings where the triple-collinear splitting function includes an uncorrelated contribution in the C_A^2 colour channel.

¹¹This assumes that the pair (k_1, k_2) of partons clusters first. Strictly speaking, this is only true in the strongly-angular-ordered limit. For commensurate angles, one could have situations where k_1 or k_2 first clusters with the leading parton, in which case $k_{t,21}$ should be replaced by $k_{t,2}$, the relative transverse momentum of k_2 with respect to the leading parton. This difference only matters in the region where $k_{t,2}$ is close to $k_{t,\text{cut}}$ (cf. Fig. 4d). This configuration is kinematically different from the one discussed here and is computed in the next section.

Surprisingly, the contribution coming from $i \rightarrow ggi$ splittings given by Eq. (4.27b) exactly compensates the C_A contribution to the CMW K factor in Eq. (4.23). This means that the correction corresponding to Fig. 4c will only have an $n_f T_R$ colour factor.

To resum these effects to all orders, we follow the usual strategy of considering that the correction can appear at any point in the chain of soft-and-collinear particles. The main subtlety concerns the $i \rightarrow q\bar{q}i$ splitting that, as in previous cases, generates a miscancellation between real and virtual contributions. The resummation formula then reads

$$\alpha_s h_{3,\text{pair}}^{(i)} = \frac{C_i}{C_A} \int_0^L d\ell_1 \left[\delta(\ell_1) + n_g^{(\text{DL})}(\ell_1) \right] \bar{\alpha} \int_{\ell_1}^L d\ell_2 \int_0^{\ell_2 - \ell_1} d\eta_2 \frac{\alpha_s}{2\pi} \quad (4.28)$$

$$\left[\left(D_{\text{pair}}^{gg} + K \right) N_g^{(\text{DL})}(L - \ell_2) + D_{\text{pair}}^{q\bar{q}} \left(2N_q^{(\text{DL})}(L - \ell_2) - N_g^{(\text{DL})}(L - \ell_2) \right) \right].$$

Evaluating the integrals in Eq. (4.28), we get

$$h_{3,\text{pair}}^{(i)} = \frac{C_i}{C_A} \frac{1}{2\pi} \left[(1 - c_\delta) D_{\text{pair}}^{q\bar{q}} (\cosh \nu - 1) + \left(K + D_{\text{pair}}^{gg} + c_\delta D_{\text{pair}}^{q\bar{q}} \right) \frac{\nu}{2} \sinh \nu \right]. \quad (4.29)$$

with c_δ given by Eq. (3.28).

4.2.4 Clustering corrections

We now discuss the kinematic configuration where we have two emissions (in any Lund plane) at commensurate angles, Fig. 4d. More specifically, say we have a ‘parent parton’, k_0 (either the leading parton or any emission spawning its own Lund plane) in colour representation C_i , accompanied by two extra gluon emissions: a first, k_1 , soft-and-collinear in the bulk of the Lund plane, and a second one, k_2 , much softer and with a transverse momentum of order $k_{t,\text{cut}}$.

In the angular-ordered limit we have two well-separated contributions: (i) ‘primary’ radiation, where k_2 is radiated off k_0 . This comes with a C_i^2 colour factor, and the transverse momentum of k_2 is measured with respect to k_0 , i.e. $k_{t,2} \equiv k_{t,20}$; (ii) ‘secondary radiation’, where k_2 is radiated off k_1 . This comes with a $C_i C_A$ colour factor, and the transverse momentum of k_2 is measured with respect to k_1 , i.e. $k_{t,2} \equiv k_{t,21}$. When the emissions have commensurate angles, i.e. when $\theta_{01} \sim \theta_{02} \sim \theta_{12}$, one must take exactly into account the Cambridge clustering used to build the Lund multiplicity. One can therefore be in a situation where a primary emission k_2 is first clustered with k_1 , meaning that its relative k_t would actually be $k_{t,21}$ instead of $k_{t,20}$, or in a situation where a secondary emission k_2 is first clustered with k_0 , meaning that its relative k_t would be $k_{t,20}$ instead of $k_{t,21}$. When $k_{t,2}$ is close to $k_{t,\text{cut}}$, finite differences between $k_{t,20}$ and $k_{t,21}$ can put the emission below or above the cut, introducing an NNDL correction compared to what strict angular ordering would give. We call this a *clustering* correction since it is associated with details of the Cambridge clustering.

As usual, we first compute the NNDL correction at fixed order, here $\mathcal{O}(\alpha_s^2)$. The emission of k_1 off k_0 , at any angle, can be described using the soft-collinear matrix element in Eq. (3.5). Since the second emission is soft and at angles commensurate with θ_{01} , we instead describe it using the eikonal factor given by Eq. (3.13). We further assume that all three angles θ_{01} , θ_{02} and θ_{12} are small and strongly separated from all the other angles in the event. In this case, k_2 can

be emitted from any of the three dipoles formed by k_0 , k_1 and the recoiling system, k_r ,¹² and the sum over dipoles

$$C_A(k_2|k_0k_1) + C_A(k_2|k_1k_r) + (2C_i - C_A)(k_2|k_0k_r), \quad (4.30)$$

simplifies considerably. One gets to the following expression for the NNDL clustering correction:

$$\begin{aligned} \delta N_{i,\text{clust},\mathcal{O}(\alpha_s^2)}^{(\text{NNDL})} = & \left(\frac{2\alpha_s}{\pi} \right)^2 C_i \int \frac{dk_{t,1}}{k_{t,1}} d\eta_1 \int \frac{dE_2}{E_2} \frac{d^2\theta_2}{2\pi} \left\{ \left[\frac{C_A}{2} \frac{1}{\theta_{12}^2} + \frac{C_A}{2} \frac{\theta_{01}^2}{\theta_{02}^2 \theta_{12}^2} + \left(C_i - \frac{C_A}{2} \right) \frac{1}{\theta_{02}^2} \right] \right. \\ & \times [\Theta_{\text{clust},0} \Theta(k_{t,20} > k_{t,\text{cut}}) + \Theta_{\text{clust},1} \Theta(k_{t,21} > k_{t,\text{cut}})] \\ & \left. - \frac{C_i}{\theta_{02}^2} \Theta(k_{t,20} > k_{t,\text{cut}}) - \frac{C_A}{\theta_{12}^2} \Theta(\theta_{21} < \theta_{01}) \Theta(k_{t,21} > k_{t,\text{cut}}) \right\}, \quad (4.31) \end{aligned}$$

where $\Theta_{\text{clust},i}$ encodes the condition for k_2 to be reconstructed as an emission from k_i :

$$\Theta_{\text{clust},1} \equiv \Theta(\theta_{12} < \theta_{01}, \theta_{02}) \quad \text{and} \quad \Theta_{\text{clust},0} = 1 - \Theta_{\text{clust},1}. \quad (4.32)$$

When writing Eq. (4.31), the NNDL clustering correction is explicitly written as the difference between the full result including the exact clustering (the first two lines) and the already-computed NDL expression with angular ordering (the last line).

Treating separately the C_i^2 and $C_i C_A$ contributions one sees that the integration over k_2 in Eq. (4.31) is finite. The constraints on $k_{t,20}$ or $k_{t,21}$ can be used to perform the integration over E_2 and are non-zero only in a region where $\theta_{02} \sim \theta_{12} \sim \theta_{01}$. We can then do the θ_2 integration, yielding

$$\delta N_{i,\text{clust},\mathcal{O}(\alpha_s^2)}^{(\text{NNDL})} = \left(\frac{2\alpha_s C_i L^2}{\pi} \right) \times \left[\frac{\alpha_s}{2\pi} \left(C_i D_{\text{clust}}^{(\text{prim})} + C_A D_{\text{clust}}^{(\text{sec})} \right) \right], \quad (4.33)$$

with

$$D_{\text{clust}}^{(\text{prim})} = -\frac{5\pi^2}{54}, \quad \text{and} \quad D_{\text{clust}}^{(\text{sec})} = \frac{\pi^2}{27}. \quad (4.34)$$

The generalisation to all orders is relatively straightforward: for each DL gluon emission k_2 , emitted from a parent k_1 , one should include an NNDL correction of the form of Eq. (4.33). One should just properly separate the case where k_2 is a primary emission, i.e. k_1 is the leading parton, for which C_i is given by the flavour of the leading parton, from all subsidiary emissions where $C_i = C_A$. We therefore write

$$\alpha_s h_{3,\text{clust}}^{(i)} = \frac{\alpha_s C_i}{2\pi} \left[\frac{\bar{\alpha} L^2}{2} \left(\frac{C_i}{C_A} D_{\text{clust}}^{(\text{prim})} + D_{\text{clust}}^{(\text{sec})} \right) + \int_0^L d\ell \left(n_g^{(\text{DL})}(\ell) - \bar{\alpha} \ell \right) \left(D_{\text{clust}}^{(\text{prim})} + D_{\text{clust}}^{(\text{sec})} \right) \right], \quad (4.35)$$

where the first (second) term corresponds to primary (subsidiary) emissions. In particular, one recognises $\int d\ell (\bar{\alpha} \ell) = \bar{\alpha} L^2/2$ as the multiplicity of primary emissions. Eq. (4.35) evaluates to:

$$h_{3,\text{clust}}^{(i)} = \frac{C_i}{2\pi} \left\{ \left[\cosh \nu - 1 - \left(1 - \frac{C_i}{C_A} \right) \frac{\nu^2}{2} \right] D_{\text{clust}}^{(\text{prim})} + (\cosh \nu - 1) D_{\text{clust}}^{(\text{sec})} \right\}. \quad (4.36)$$

¹²At our accuracy, the recoiling system can be viewed as a unique object as long as it is at much larger angles.

4.2.5 A primary large-angle emission with $k_t \sim k_{t,\text{cut}}$: the Cambridge multiplicity

The last pure α_s contribution that we consider is that of a first, primary, emission at large angles and with transverse momentum of order $k_{t,\text{cut}}$. The precise definition of k_t plays a central role in this correction and, therefore, differences between the Lund (2.1) and Cambridge (2.2) k_t definitions are expected.

As already discussed in our NDL calculation, the definition of the Lund-plane transverse momentum k_t , Eq. (2.1), coincides exactly with the relative transverse momentum of the emission with respect to the initial $q\bar{q}$ (or gg) dipole, i.e. the relation in Eq. (3.5) is also valid for soft emissions at large angles. Hence, this contribution vanishes for the Lund multiplicity. However, this is not the case for the Cambridge definition of k_t , which is related to the Lund one by

$$k_t^{(\text{Cam})} = k_t^{(\text{Lund})} \sqrt{1 + e^{-2\eta}}. \quad (4.37)$$

The last factor in Eq. (4.37) results in an NNDL correction. At $\mathcal{O}(\alpha_s)$, the contribution of this large-angle, $k_t \sim k_{t,\text{cut}}$ primary emission is, after subtracting the DL contribution:

$$\langle N_{i,\text{la}\&k_t}^{(\text{Cam})} \rangle_{\mathcal{O}(\alpha_s)} = \bar{\alpha} \frac{C_i}{C_A} \int_0^Q \frac{dk_\perp}{k_\perp} \int_0^\infty d\eta \Theta(k_\perp \sqrt{1 + e^{-2\eta}} > Qe^{-L} > k_\perp) = \frac{\alpha_s}{2\pi} C_i \frac{\pi^2}{12}. \quad (4.38)$$

Noting that, first, a large-angle emission has to be the last clustering in the Cambridge sequence and, second, an emission with $k_t \sim k_{t,\text{cut}}$ leaves no DL phase-space for subsequent emission, this result is valid to all orders. We therefore find that the difference between the Cambridge and Lund multiplicities is (see Appendix A.3 for further details)

$$h_3^{(i,\text{Cam})} - h_3^{(i,\text{Lund})} = h_{3,\text{la}\&k_t}^{(i,\text{Cam})} = \frac{C_i}{2\pi} \frac{\pi^2}{12}. \quad (4.39)$$

4.3 Corrections involving two $\alpha_s L$ factors

4.3.1 Energy loss

In Sec. 3.2.2 we accounted for the NDL correction corresponding to a single hard-and-collinear splitting. In the NDL case, once a hard-collinear splitting has happened, further emissions from both branches can be treated as if the branch was carrying the same energy as the parent parton. In other words, if $z \sim \mathcal{O}(1)$ is the momentum fraction of the hard-collinear splitting, the factors z and $1 - z$ in the daughter branches can be neglected and set to 1. These factors, which we discuss in this section, can however not be neglected at NNDL accuracy. Conceptually, finite z and $1 - z$ effects limit the available phase-space for further emissions, as indicated by the red region in Fig. 4g. Consequently we name this correction *energy loss*.

The energy loss NNDL contribution can be computed following our generic approach of describing NNDL contributions as subleading corrections dressed by an arbitrary number of double-logarithmic, nested, soft-and-collinear emissions. One therefore starts either with the leading parton or with any (DL) gluon emitted from it via nested soft-collinear radiation at a transverse momentum scale ℓ_1 . This parton then undergoes a (real or virtual) hard-collinear splitting at a transverse scale ℓ_2 , with a momentum fraction z . For a real splitting, the resulting “hard” and “soft” branches will then radiate DL soft-collinear emissions from (relative) transverse momentum $k_{t,\text{hard}} = (1 - z)e^{-\ell_2}$ and $k_{t,\text{soft}} = ze^{-\ell_2}$, respectively, taking into account the exact

energy sharing in the hard-collinear branching. One therefore writes, summing over all possible flavour configurations,

$$\langle N_{i,\text{e-loss}}^{(\text{Lund})} \rangle = \sum_{abc} \int_0^L d\ell_1 \left[\delta_{ai} \delta(\ell_1) + \delta_{ag} n_i^{(\text{DL})}(\ell_1) \right] \int_{\ell_1}^L d\ell_2 \int dz \frac{\alpha_s}{\pi} P_{a \rightarrow bc}(z) \quad (4.40)$$

$$\left[N_b^{(\text{DL})}(L - \ell_2 + \ln(1 - z)) + N_c^{(\text{DL})}(L - \ell_2 + \ln(z)) - N_a^{(\text{DL})}(L - \ell_2) \right].$$

Again, it is convenient to separate the splitting function into a soft-divergent component (for gluon emissions) and a finite piece, i.e. $P_{a \rightarrow bc}(z) = \frac{2C_a}{z} \delta_{cg} + p_{a \rightarrow bc}^{(\text{finite})}(z)$. In the small- z limit, only the singular part contributes. Combined with the $N_c^{(\text{DL})}(L - \ell_2 + \ln(z))$ term in the second line, it gives rise to the DL behaviour. For the remaining terms, the z integral has no logarithmic enhancements. Next, one recognises the NDL contribution coming from the finite part of the splitting function, neglecting the $\ln(1 - z)$ and $\ln(z)$ offsets in $N_b^{(\text{DL})}$ and $N_c^{(\text{DL})}$. These offsets however start contributing at NNDL accuracy, either from the soft part of the splitting function together with $N_b^{(\text{DL})}(L - \ell_2 + \ln(1 - z))$, or from the finite part of the splitting function with both N_b and N_c in the second line. Up to subleading corrections, we can use the expansion:

$$N_b^{(\text{DL})}(L - \ell_2 + \ln(1 - z)) \simeq N_b^{(\text{DL})}(L - \ell_2) + n_b^{(\text{DL})}(L - \ell_2) \ln(1 - z), \quad (4.41a)$$

$$N_c^{(\text{DL})}(L - \ell_2 + \ln(z)) \simeq N_c^{(\text{DL})}(L - \ell_2) + n_c^{(\text{DL})}(L - \ell_2) \ln(z), \quad (4.41b)$$

with NNDL corrections associated with the right-most terms. The z integration can then be carried out for each flavours yielding ($n_q^{(\text{DL})} = C_F/C_A n_g^{(\text{DL})}$)

$$\langle N_{i,\text{e-loss}}^{(\text{Lund})} \rangle = \frac{C_i}{C_A} \frac{\alpha_s}{2\pi} \int_0^L d\ell_1 \left[D_{\text{e-loss}}^i \delta(\ell_1) + D_{\text{e-loss}}^g n_g^{(\text{DL})}(\ell_1) \right] \int_{\ell_1}^L d\ell_2 n_g^{(\text{DL})}(L - \ell_2). \quad (4.42)$$

with, the following NNDL coefficients

$$D_{\text{e-loss}}^q = 2 \int dz \left[P_{q \rightarrow qg}(z) \ln(1 - z) + \frac{C_A}{C_F} p_{q \rightarrow qg}^{(\text{finite})}(z) \ln(z) \right] = \frac{7}{2} C_A + \left(\frac{5}{2} - \frac{2\pi^2}{3} \right) C_F, \quad (4.43a)$$

$$D_{\text{e-loss}}^g = 2 \int dz \left\{ P_{g \rightarrow gg}(z) \ln(1 - z) + p_{g \rightarrow gg}^{(\text{finite})}(z) \ln(z) + \frac{C_F}{C_A} P_{g \rightarrow q\bar{q}}(z) [\ln(1 - z) + \ln(z)] \right\}$$

$$= \left(\frac{67}{9} - \frac{2\pi^2}{3} \right) C_A - \frac{26}{9} \frac{C_F}{C_A} n_f T_R. \quad (4.43b)$$

The remaining integrations are easily performed using the DL results to give

$$h_{3,\text{e-loss}}^{(q)} = \frac{C_F}{C_A} \frac{1}{2\pi} \left[D_{\text{e-loss}}^g \frac{1}{2} \nu \sinh \nu + (D_{\text{e-loss}}^q - D_{\text{e-loss}}^g) (\cosh \nu - 1) \right], \quad (4.44a)$$

$$h_{3,\text{e-loss}}^{(g)} = \frac{1}{2\pi} D_{\text{e-loss}}^g \frac{1}{2} \nu \sinh \nu. \quad (4.44b)$$

4.3.2 Squared hard-collinear correction

We continue by considering the NNDL correction when two emissions in the nested chain receive a contribution from the finite part of the splitting function in the hard-collinear limit. In this case we directly perform the resummation. Since the two NDL corrections are strongly-ordered in

angle (and hence in k_t as they happen at the hard-collinear edge of the Lund plane), we can even simplify Eq. (3.9) a bit further by inserting explicitly only the NDL correction associated with the larger angle (larger k_t) emission and rely on the (resummed) NDL expressions, Eqs. (3.25) and (3.27) to handle the second NDL correction.

We split the calculation in three parts, according to whether (i) the two NDL emissions are both flavour-diagonal, (ii) one is flavour-diagonal and the other flavour-changing, or (iii) both emissions are flavour-changing:

$$h_{3,\text{hc}^2} = h_{3,\text{fd}^2} + h_{3,\text{fd+fc}} + h_{3,\text{fc}^2}. \quad (4.45)$$

For the sake of brevity we give the integral form of each contribution below and write the full, integrated, result for the sum at the end of the section.

Two flavour diagonal. Here, one has a first hard-collinear splitting occurring either on the primary branch or on a subsidiary one. The next NDL correction has to happen in the secondary (gluon) branch of the first splitting for which we can recycle the NDL multiplicity results from Sec. 3.2.¹³ We thus write

$$\alpha_s h_{3,\text{fd}^2}^{(i)} = \frac{C_i}{C_A} \int_0^L d\ell_1 \left[\delta(\ell_1) B_i + n_g^{(\text{DL})}(\ell_1) B_{gg} \right] \bar{\alpha} \int_{\ell_1}^L d\ell_2 N_{g,\text{hc-fd}}^{(\text{NDL})}(L; \ell_2), \quad (4.46)$$

with $B_i = B_q$ (B_{gg}) for a quark (gluon) given by Eq.(3.21), and $N_{g,\text{hc-fd}}^{(\text{NDL})}(L; \ell_2) = N_{g,\text{hc-fd}}^{(\text{NDL})}(L - \ell_2)$ obtained from Eq. (3.25).

One flavour changing, one flavour diagonal. We move on to the case when one of the two hard-collinear emissions is a gluon splitting to a $q\bar{q}$ pair. This proceeds as for the flavour-diagonal case except for two modifications: (i) the first hard-collinear splitting can either be the hard gluon emission or the $g \rightarrow q\bar{q}$ splitting, and, (ii) after a $g \rightarrow q\bar{q}$ splitting a miscancellation between real and virtual splittings occur as we have discussed in several previous cases (cf. Sec. 4.2.3). This yields

$$\begin{aligned} \alpha_s h_{3,\text{fd-fc}}^{(i)} = & \frac{C_i}{C_A} \left\{ \int_0^L d\ell_1 \left[\delta(\ell_1) B_i + n_g^{(\text{DL})}(\ell_1) B_{gg} \right] \bar{\alpha} \int_{\ell_1}^L d\ell_2 N_{g,\text{hc-fc}}^{(\text{NDL})}(L; \ell_2) \right. \\ & \left. + \int_0^L d\ell_1 \left[\delta(\ell_1) \delta_{ig} + n_g^{(\text{DL})}(\ell_1) \right] B_{gq} \bar{\alpha} \int_{\ell_1}^L d\ell_2 \left[2N_{q,\text{hc-fd}}^{(\text{NDL})}(L; \ell_2) - N_{g,\text{hc-fd}}^{(\text{NDL})}(L; \ell_2) \right] \right\}. \end{aligned} \quad (4.47)$$

The first (resp. second) line corresponds to the flavour-diagonal (resp. flavour-changing) splitting happening first. The two terms in the square brackets under the ℓ_1 integration describe, as above, emissions from the primary branch or from any subsidiary one. Finally, the δ_{ig} factor on the last line ensures that $g \rightarrow q\bar{q}$ splitting on the primary branch are only included for gluon jets.

Two flavour changing. Finally we consider the case of two flavour-changing $g \rightarrow q\bar{q}$ splittings. Following the same logic and accounting again for the first splitting being either on the primary

¹³As in the NDL case, the primary branch has no corrections as the real and virtual contributions from the first hard-collinear splitting cancel.

branch or on any subsidiary one, we get

$$\alpha_s h_{3,\text{fc}^2}^{(i)} = \frac{C_i}{C_A} \int_0^L d\ell_1 \left[\delta(\ell_1) \delta_{ig} + n_g^{(\text{DL})}(\ell_1) \right] \bar{\alpha} \int_{\ell_1}^L d\ell_2 B_{gq} \left[2N_{q,\text{hc-fc}}^{(\text{NDL})}(L; \ell_2) - N_{g,\text{hc-fc}}^{(\text{NDL})}(L; \ell_2) \right]. \quad (4.48)$$

where $N_{g,\text{hc-fc}}^{(\text{NDL})}(L; \ell_2) = N_{g,\text{hc-fc}}^{(\text{NDL})}(L - \ell_2)$, obtained from Eq. (3.27).

Final result for $h_{3,\text{hc}^2}^{(i)}$. The overall contribution to h_3 from two hard-collinear branchings is the sum of the above three terms, Eqs. (4.46)-(4.48). Using the explicit NDL results, the integrations are relatively straightforward and give

$$\begin{aligned} h_{3,\text{hc}^2}^{(q)} = \frac{C_F}{4\pi} \{ & (B_{gg} + c_\delta B_{gq})^2 \nu^2 \cosh \nu + 8 [2c_\delta B_{gg} - 2c_\delta B_q - (1 - 3c_\delta^2) B_{gq}] B_{gq} \cosh \nu \\ & + [4B_q(B_{gg} + (2c_\delta + 1)B_{gq}) - (B_{gg} + c_\delta B_{gq})(B_{gg} + 9c_\delta B_{gq})] \nu \sinh \nu \\ & + 4(1 - c_\delta^2) B_{gq}^2 \nu^2 + 8 [2c_\delta B_q - 2c_\delta B_{gg} + (1 - 3c_\delta^2) B_{gq}] B_{gq} \} \end{aligned} \quad (4.49a)$$

$$\begin{aligned} h_{3,\text{hc}^2}^{(g)} = \frac{C_A}{4\pi} \{ & (B_{gg} + c_\delta B_{gq})^2 \nu^2 \cosh \nu - 8(1 - c_\delta^2) B_{gq}^2 (\cosh \nu - 1) \\ & + [(B_{gg} + c_\delta B_{gq})(3B_{gg} - 5c_\delta B_{gq}) + 4(1 + c_\delta) B_{gq} B_q] \nu \sinh \nu \}. \end{aligned} \quad (4.49b)$$

4.3.3 A hard-collinear emission with a soft emission at commensurate angle

We investigate the case of a first hard-and-collinear emission which is followed by a soft-and-commensurate-angle emission, as depicted in Fig. 4h. To see that this contribution does not contribute at the NNDL accuracy, it is sufficient to show it at $\mathcal{O}(\alpha_s^2)$. We therefore consider a parton k_0 with colour factor C_i which radiates a hard-and-collinear gluon k_1 followed by a subsequent emission of a soft gluon k_2 at a commensurate angle. The arguments below can also be carried on with an initial flavour-changing splitting. The contribution of this system to the Lund multiplicity at $\mathcal{O}(\alpha_s^2)$ is¹⁴

$$\begin{aligned} \langle N_{i,\text{hc} \times \text{comm}}^{(\text{Lund})} \rangle_{\mathcal{O}(\alpha_s^2)} = & \left(\frac{\alpha_s}{\pi} \right)^2 \int_0^\infty d\eta_1 \int_0^1 dz_1 P_{i \rightarrow ig}(z_1) \int \frac{dE_2}{E_2} \frac{d^2\theta_2}{2\pi} \\ & \times \left[\frac{C_A}{2} (k_2 | k_1 k_0) + \frac{C_A}{2} (k_2 | k_1 k_r) - \frac{C_A}{2} (k_2 | k_0 k_r) \right] \Theta(k_{t,21} > k_{t,\text{cut}}), \end{aligned} \quad (4.50)$$

where $P_{i \rightarrow ig}(z)$ is the appropriate DGLAP splitting function, defined in Eq. (3.20), k_r is the recoiling system (at angles much larger than the ones between k_0 , k_1 and k_2) and the eikonal functions $(k|i j)$ were defined in Eq. (3.13). Integrating over the azimuthal angle of k_2 one easily recovers, in the limit $\theta_{10}, \theta_{20}, \theta_{21} \ll 1$, the standard angular-ordered result, namely,

$$\langle N_{i,\text{hc} \times \text{comm}}^{(\text{Lund})} \rangle_{\mathcal{O}(\alpha_s^2)} = \bar{\alpha} \frac{\alpha_s}{\pi} \int_0^\infty d\eta_1 \int_0^1 dz_1 P_{i \rightarrow ig}(z_1) \int_0^{z_1} \frac{dx_2}{x_2} \int_0^{\eta_1} d\eta_{21} \Theta(x_2 e^{-\eta_{21}} > e^{-L}), \quad (4.51)$$

where $\eta_{21} = -\ln(\theta_{21}/2)$, and $x_2 = 2E_2/Q$. Due to exact angular ordering being recovered, Eq. (4.51) represents precisely the NDL accurate contribution to the multiplicity described in Sec. 3.2.2, with no NNDL correction.

¹⁴This expression already accounts for the cancellation of the term proportional to $C_i(k_2 | k_0 k_r)$ in the square bracket including both real and virtual contributions for the k_1 gluon.

A key point in the above argument is that the θ_{21} angle in Eq. (4.51) is bounded by the physical angle θ_{10} , i.e. the angle between the daughter partons after the $k_0 k_1$ branching. Technically, working in the collinear limit, one could choose to impose angular-ordering with a different definition of the angle (e.g. the angle of the emission with respect to the parent parton). In this case, the contribution discussed in this section would no longer vanish. However, such a change would also affect the definition of η in the hard-collinear endpoint, Eq. (4.4), reshuffling a contribution between the hard-collinear and hard-matrix-element coefficients. We have checked explicitly that this does not change the final resummed result.

4.3.4 A primary large-angle emission

In Sec. 3.2 we showed that a first soft-and-large-angle primary emission does not yield a NDL correction. We now study the effect of such a soft-and-large-angle emission on subsequent ones. Concretely, following the discussion in Sec. 4.1 we investigate two possible kinematic configurations for the second emission: (i) soft and at commensurate angles to the first, Fig. 4i, and (ii) soft and collinear with $k_t \sim k_{t,\text{cut}}$, Fig. 4k. We therefore write

$$D_{\text{la}} = D_{\text{la}^2} + D_{\text{la} \times k_t}. \quad (4.52)$$

We show below that the contributions cancel each other exactly.

We start with the configuration in Fig. 4i, where an initial system $(k_0 k_r)$ emits a soft-and-large-angle parton, k_1 , which then radiates a soft emission k_2 at a commensurate angle. The contribution to the Lund multiplicity is (after cancelling the real and virtual contributions for the first emission)

$$\begin{aligned} \langle N_{i,\text{la}^2}^{(\text{Lund})} \rangle_{\mathcal{O}(\alpha_s^2)} &= \left(\frac{\alpha_s}{\pi} \right)^2 \int \frac{dE_1}{E_1} \frac{d^2\theta_1}{2\pi} \int \frac{dE_2}{E_2} \frac{d^2\theta_2}{2\pi} \\ &\times C_i(k_1|k_0 k_r) \left[\frac{C_A}{2}(k_2|k_1 k_0) + \frac{C_A}{2}(k_2|k_1 k_r) - \frac{C_A}{2}(k_2|k_0 k_r) \right] \Theta(k_{t,21} > k_{t,\text{cut}}). \end{aligned} \quad (4.53)$$

After integrating over the solid angle of the second emission and subtracting the DL term in which the two emissions are angular-ordered, we obtain the following NNDL correction

$$\delta N_{i,\text{la}^2}^{(\text{NNDL})} = \frac{C_i}{C_A} \frac{\bar{\alpha} L^2}{2} \frac{\alpha_s}{2\pi} D_{\text{la}^2} \quad \text{with} \quad D_{\text{la}^2} = -\frac{\pi^2}{6} C_A. \quad (4.54)$$

Let us now move to the case where the first soft-and-large-angle emission is followed by a soft-and-collinear emission with $k_t \sim k_{t,\text{cut}}$, as in Fig. 4k. The Lund multiplicity at $\mathcal{O}(\alpha_s^2)$ is given by

$$\langle N_{i,\text{la} \times k_t}^{(\text{Lund})} \rangle_{\mathcal{O}(\alpha_s^2)} = \frac{4\alpha_s^2 C_i C_A}{\pi^2} \int d\eta_1 \int \frac{dk_{t,1}}{k_{t,1}} \int_{\eta_1}^{\infty} d\eta_2 \int \frac{dz_2}{z_2} \Theta(k_{t,21} > k_{t,\text{cut}}), \quad (4.55)$$

where we have replaced the eikonal factor for the second emission by its soft-and-collinear limit. The NNDL correction stems from taking into account the exact expression for $k_{t,21}$, namely

$$k_{t,21} = E_2 \sin(\theta_{21}) \approx E_2 \theta_{21} \approx z_2 E_1 \theta_{21} \approx z_2 k_{t,1} 2 \cosh \eta_1 e^{-\eta_{21}}, \quad (4.56)$$

where, for the last equality, we have used the generalisation of Eq. (3.4) beyond the collinear limit, $E_1 = k_{t,1} \cosh \eta_1$, and $\theta_{21} \approx 2e^{-\eta_{21}}$. This expression differs from the soft-collinear limit by a factor $2e^{-\eta_1} \cosh \eta_1 = 1 + e^{-2\eta_1}$, so that, after subtracting the DL contribution from Eq. (4.55), one is left with the NNDL correction (with $\ell_1 = \ln(Q/k_{t,1})$)

$$\begin{aligned} \langle N_{i,\text{la} \times k_t}^{(\text{Lund})} \rangle_{\mathcal{O}(\alpha_s^2)} &= \frac{4\alpha_s^2 C_i C_A}{\pi^2} \int_0^L d\ell_1 \int_0^{L-\ell_1} d\eta_{21} \int_0^\infty d\eta_1 \ln(1 + e^{-2\eta_1}) \\ &= \frac{C_i}{C_A} \frac{\bar{\alpha} L^2}{2} \frac{\alpha_s}{2\pi} D_{\text{la} \times k_t} \quad \text{with} \quad D_{\text{la} \times k_t} = \frac{\pi^2}{6} C_A = -D_{\text{la}^2}. \end{aligned} \quad (4.57)$$

The sum of (4.54) and (4.57) therefore vanishes and it is relatively straightforward to see that this relation holds to all orders.¹⁵

4.3.5 Three emissions at commensurate angles

We consider the case where a first soft-and-collinear emission k_1 is followed by two subsequent emissions, k_2 and k_3 , strongly ordered in energy, $E_1 \gg E_2 \gg E_3$, and at commensurate angles, $\theta_1 \sim \theta_2 \sim \theta_3$, as depicted in Fig. 4j. In the NDL limit, once both real and virtual emissions are taken into account, the only left-over contribution comes from the angular-ordered DL result, $\theta_{23} < \theta_{12} < \theta_1$, proportional to $C_i C_A^2$. We show here that this is still the case at NNDL accuracy, i.e. that the contribution of Fig. 4j vanishes.

It is sufficient to consider this configuration at $\mathcal{O}(\alpha_s^3)$. The first gluon, k_1 , is emitted off a (k_0, k_r) dipole according to the eikonal factor $(k_1|k_0, k_r)$ in Eq. (3.13), where for a collinear k_1 emission the specific choice of the large-angle recoiling momentum k_r is irrelevant. The second gluon k_2 can then be emitted from any of the three dipoles (k_0, k_r) , (k_0, k_1) or (k_1, k_r) resulting in the combination in Eq. (4.30). Finally, the third emission k_3 can be emitted from any dipole in the (k_0, k_1, k_2, k_r) system. The full matrix element for all three emissions can be deduced from the expression in Refs. [60, 61], valid for $E_3 \sim E_2$, which, after taking the limit $E_3 \ll E_2$ can be cast into the following form:

$$\begin{aligned} &C_i \frac{C_A^2}{4} (1|0r) \left\{ (2|10) [(3|20) + (3|21) + (3|1r) - (3|0r)] + (2|1r) [(3|2r) + (3|21) + (3|10) - (3|0r)] \right. \\ &\quad \left. - (2|0r) [(3|20) + (3|2r) + (3|10) + (3|1r)] \right\} \\ &+ C_i^2 \frac{C_A}{2} (1|0r) \left\{ (3|0r) [(2|10) + (2|1r)] + (2|0r) [(3|20) + (3|2r) + (3|10) + (3|1r) - 2(3|0r)] \right\} \\ &+ C_i^3 (1|0r) (2|0r) (3|0r), \end{aligned} \quad (4.58)$$

where for the sake of readability we used the shorthand notation $(c|ab)$ to denote the factor $(k_c|k_a k_b)$.

Besides the matrix element proportional to Eq. (4.58) we need to account for the fact that each of the three emissions can be either real or virtual. Summing over all possible emission

¹⁵One can for example realise that both contributions shift the boundary of the secondary Lund plane spawned by the first soft-large-angle emission by an equal amount proportional to $\int_0^\infty d\eta \ln(1 + e^{-2\eta})$. The “la²” shifts the large-angle boundary of the secondary plane, reducing the phase-space, while the “la \times k_t” contributions shifts the lower edge, enhancing the phase-space by the same amount. This results in an overall shift which has no net effect on the NNDL multiplicity.

configurations we find that the Lund multiplicity at $\mathcal{O}(\alpha_s^3)$ is¹⁶

$$\begin{aligned} \langle N_{i,3\text{comm}}^{(\text{Lund})} \rangle_{\mathcal{O}(\alpha_s^3)} &= \left(\frac{\alpha_s C_A}{2\pi} \right)^3 \frac{2C_i}{C_A} \int \frac{dE_1}{E_1} \frac{d^2\theta_1}{2\pi} \int \frac{dE_2}{E_2} \frac{d^2\theta_2}{2\pi} \int \frac{dE_3}{E_3} \frac{d^2\theta_3}{2\pi} (k_1|k_0k_r) \\ &\quad \times \left\{ (k_2|k_1k_0) [(k_3|k_2k_0) + (k_3|k_2k_1) - (k_3|k_1k_0)] \right. \\ &\quad + (k_2|k_1k_r) [(k_3|k_2k_r) + (k_3|k_2k_1) - (k_3|k_1k_r)] \\ &\quad \left. - (k_2|k_0k_r) [(k_3|k_2k_0) + (k_3|k_2k_r) - (k_3|k_0k_r)] \right\} \times \Theta(k_{t,3} > k_{t,\text{cut}}). \end{aligned} \quad (4.59)$$

A few comments about Eq. (4.59) are in order. Since all emissions are above the $k_{t,\text{cut}}$, we can ignore differences in the $k_{t,3}$ definition, i.e. we can treat $k_{t,30}, k_{t,31}, k_{t,32}$ indistinctly. More interestingly, only the term proportional to $C_i C_A^2$ survives, as was already the case at DL accuracy.

At small angles, all the eikonal factors can be simplified according to $(c|ab) \approx 2\theta_{ab}^2/(\theta_{ac}^2\theta_{bc}^2)$ for $b, c \neq r$ and $(c|ar) \approx 2/\theta_{ac}^2$. After performing the (2-dimensional) integrations over θ_2 and θ_3 , one finds that Eq. (4.59) reproduces angular-ordered result with no NNDL correction. Thus, the contribution corresponding to Fig. 4j vanishes to all orders. Although the appearance of angular ordering seems to appear somewhat fortuitously, one wonders if it extends beyond three commensurate-angle emissions.

4.4 Corrections involving the running of the strong coupling

The last family of NNDL corrections we have to compute is the one involving the running of the QCD coupling. Since one-loop running is sufficient, we can follow a similar strategy as for two hard-collinear emissions (Sec. 4.3.2) and insert an extra subleading correction in the NDL calculation.

Naturally, such a calculation would make use of the NDL multiplicity $N_{i,\text{rc}}^{(\text{NDL})}(L; \ell)$ of a parton of flavour i initially created at a transverse momentum scale $e^{-\ell}Q$ down to a transverse momentum cut $e^{-L}Q$. However, since the QCD running coupling is not scale invariant, $N_{i,\text{rc}}^{(\text{NDL})}(L; \ell) \neq N_{i,\text{rc}}^{(\text{NDL})}(L - \ell)$ one cannot simply reuse Eq. (3.19) as we did for the hard-collinear NDL corrections. Instead, $N_{i,\text{rc}}^{(\text{NDL})}(L; \ell)$ has to be explicitly computed. Following the same strategy as in Sec. 3.2.1, we get

$$\begin{aligned} N_{i,\text{rc}}^{(\text{NDL})}(L; \ell) &= \frac{C_i}{C_A} \int_{\ell}^L d\ell_1 \left[\delta(\ell_1) + n_g^{(\text{DL})}(\ell_1; \ell) \right] \bar{\alpha} \int_{\ell_1}^L d\ell_2 (2\alpha_s \beta_0 \ell_2) (\ell_2 - \ell_1) N_g^{(\text{DL})}(L; \ell_2), \\ &= \frac{C_i}{C_A} \frac{\beta_0}{2} \sqrt{\frac{\alpha_s \pi}{2C_A}} \left[(\nu^2 - \nu_0^2 - 1) \sinh(\nu - \nu_0) + (\nu - \nu_0) \cosh(\nu - \nu_0) \right], \end{aligned} \quad (4.60)$$

with $\nu_0 = \sqrt{\bar{\alpha}}\ell$.

4.4.1 Squared running-coupling correction

We first consider the case of NNDL corrections proportional to β_0^2 . If we expand the running coupling according to

$$\alpha_s(k_t) = \frac{\alpha_s}{1 - 2\alpha_s \beta_0 \ln \frac{Q}{k_t}} \approx \alpha_s + 2\alpha_s^2 \beta_0 \ln(Q/k_t) + 4\beta_0^2 \alpha_s^3 \ln(Q/k_t)^2 + \mathcal{O}(\alpha_s^4), \quad (4.61)$$

¹⁶The contributions proportional to $\Theta(k_{t,2} > k_{t,\text{cut}})$ and $\Theta(k_{t,1} > k_{t,\text{cut}})$ vanish when summing the cases where the third soft emission is either real or virtual.

we see that we can get NNDL corrections either by having a single $\mathcal{O}([\alpha_s \beta_0 \ln(Q/k_t)]^2)$ correction to one of the DL emissions, $h_{3,\mathcal{O}(\beta_0^2)}$, or by having $\mathcal{O}(\alpha_s \beta_0 \ln(Q/k_t))$ corrections to two emissions along the chain of nested emissions, $h_{3,\beta_0 \times \beta_0}$, Fig. 4m. The two cases can be written as

$$\alpha_s h_{3,\mathcal{O}(\beta_0^2)}^{(i)} = \frac{C_i}{C_A} \int_0^L d\ell_1 \left[\delta(\ell_1) + n_g^{(\text{DL})}(\ell_1) \right] \bar{\alpha} \int_{\ell_1}^L d\ell_2 (2\alpha_s \beta_0 \ell_2)^2 (\ell_2 - \ell_1) N_g^{(\text{DL})}(L; \ell_2), \quad (4.62)$$

$$\alpha_s h_{3,\beta_0 \times \beta_0}^{(i)} = \frac{C_i}{C_A} \int_0^L d\ell_1 \left[\delta(\ell_1) + n_g^{(\text{DL})}(\ell_1) \right] \bar{\alpha} \int_{\ell_1}^L d\ell_2 (2\alpha_s \beta_0 \ell_2) (\ell_2 - \ell_1) N_{g,\text{rc}}^{(\text{NDL})}(L; \ell_2). \quad (4.63)$$

For the first of the two contributions, a DL emission, which was created at scale $k_{t,1} = Qe^{-\ell_1}$, dresses a gluon with a β_0^2 correction down to the scale $k_{t,2} = Qe^{-\ell_2}$. For the second contribution, the β_0 correction occurs at the scale ℓ_2 and a second NDL correction happens at a lower k_t scale as encoded by $N_{g,\text{rc}}^{(\text{NDL})}(L; \ell_2)$, given by Eq. (3.18). Evaluating the integrals using the known DL and NDL multiplicities, we get

$$h_{3,\beta_0^2}^{(i)}(\nu) = \frac{C_i}{C_A} \frac{\pi \beta_0^2}{16 C_A} [3\nu(2\nu^2 - 1) \sinh \nu + (\nu^4 + 3\nu^2) \cosh \nu]. \quad (4.64)$$

4.4.2 Running-coupling and hard-collinear correction

We now consider the case where one emission in the chain of nested emissions correctly receives running coupling correction $\mathcal{O}(\beta_0)$, while also allowing one hard-and-collinear splitting. As in Sec. 3.2.2, we split the discussion in terms of whether the hard-collinear splitting is flavour-conserving or flavour-changing. Accordingly, we write the NNDL correction as

$$h_{3,\beta_0 \times \text{hc}} = h_{3,\beta_0 \times \text{hc,fd}} + h_{3,\beta_0 \times \text{hc,fc}}. \quad (4.65)$$

Flavour-diagonal. In the case of a flavour-diagonal hard-collinear splitting, we can write

$$\begin{aligned} \alpha_s h_{3,\beta_0 \times \text{hc,fd}}^{(i)} = & \frac{C_i}{C_A} \left[\int_0^L d\ell_1 \left[\delta(\ell_1) B_i + n_g^{(\text{DL})}(\ell_1) B_{gg} \right] \bar{\alpha} \int_{\ell_1}^L d\ell_2 (2\alpha_s \beta_0 \ell_2) N_g^{(\text{DL})}(L; \ell_2) \right. \\ & + \int_0^L d\ell_1 \left[\delta(\ell_1) B_i + n_g^{(\text{DL})}(\ell_1) B_{gg} \right] \bar{\alpha} \int_{\ell_1}^L d\ell_2 N_{g,\text{rc}}^{(\text{NDL})}(L; \ell_2) \\ & \left. + \int_0^L d\ell_1 n_{\text{RC}}^{(\text{NDL})}(\ell_1) \bar{\alpha} \int_{\ell_1}^L d\ell_2 B_{gg} N_g^{(\text{DL})}(L; \ell_2) \right]. \end{aligned} \quad (4.66)$$

where $n_{\text{RC}}^{(\text{NDL})}(\ell_1)$ is defined as the derivative of Eq. (3.18) for gluons with respect to L . This expression covers the three physical cases: if the hard-collinear splitting occurs at a scale ℓ_2 , the running-coupling correction can happen either for the same emission (the first line), or for a later emission (the second line), or for an earlier emission (the last line). For the first two lines, the hard-collinear emission can either be from the primary branch, proportional to $\delta(\ell_1)$ with $B_i = B_q$ for a quark and $B_i = B_{gg}$ for a gluon, or from a subsequent gluon emission.

Flavour-changing. The case where the hard-collinear splitting is a $g \rightarrow q\bar{q}$ branching is computed the same way with the usual care that after a real $g \rightarrow q\bar{q}$ branching both branches behave like quarks while the virtual corrections involve gluon-initiated emissions. Modulo this detail,

we still have to include three contributions for the running-coupling NDL correction happening earlier, at the same emission, or later than the $g \rightarrow q\bar{q}$ branching:

$$\begin{aligned} \alpha_s h_{3,\beta_0 \times \text{hc,fc}}^{(i)} = & \frac{C_i}{C_A} B_{gq} \left\{ \int_0^L d\ell_1 n_{\text{rc}}^{(\text{NDL})}(\ell_1) \bar{\alpha} \int_{\ell_1}^L d\ell_2 \left[2N_q^{(\text{DL})}(L; \ell_2) - N_g^{(\text{DL})}(L; \ell_2) \right] \right. \\ & + \int_0^L d\ell_1 \left[\delta_{ig} \delta(\ell_1) + n_g^{(\text{DL})}(\ell_1) \right] \bar{\alpha} \int_{\ell_1}^L d\ell_2 (2\alpha_s \beta_0 \ell_2) \left[2N_q^{(\text{DL})}(L; \ell_2) - N_g^{(\text{DL})}(L; \ell_2) \right] \\ & \left. + \int_0^L d\ell_1 \left[\delta_{ig} \delta(\ell_1) + n_g^{(\text{DL})}(\ell_1) \right] \bar{\alpha} \int_{\ell_1}^L d\ell_2 \frac{2C_F - C_A}{C_A} N_{g,\text{rc}}^{(\text{NDL})}(L; \ell_2) \right\}, \end{aligned} \quad (4.67)$$

where we have used that $N_{q,\text{rc}}^{(\text{NDL})} = C_F N_{g,\text{rc}}^{(\text{NDL})} / C_A$ in the last line.

Integrated contribution. Evaluating the integrals in the flavour-diagonal and flavour-changing contributions, we get

$$\begin{aligned} h_{3,\beta_0 \times \text{hc}}^{(q)} = & \frac{C_F \beta_0}{C_A} \frac{1}{4} \{ (B_{gg} + c_\delta B_{gq}) \nu^3 \sinh \nu + [2B_q - 2B_{gg} + (6 - 8c_\delta) B_{gq}] \nu \sinh \nu \\ & + 2(B_q + B_{gg} + B_{gq}) \nu^2 \cosh \nu - 4(1 - c_\delta) B_{gq} (2 \cosh \nu - 2 + \nu^2) \}, \end{aligned} \quad (4.68a)$$

$$\begin{aligned} h_{3,\beta_0 \times \text{hc}}^{(g)} = & \frac{\beta_0}{4} \{ (B_{gg} + c_\delta B_{gq}) \nu^3 \sinh \nu + 6(1 - c_\delta) B_{gq} \nu \sinh \nu \\ & + 2[2B_{gg} + (1 + c_\delta) B_{gq}] \nu^2 \cosh \nu - 8B_{gq} (1 - c_\delta) (\cosh \nu - 1) \}. \end{aligned} \quad (4.68b)$$

4.5 Final result

For completeness, we gather here the full expression for the NNDL multiplicity, as obtained from Eq. (4.2) with the individual contributions computed in the previous subsections (see also Table 1). We give results for both $\langle N_Z^{(\text{Lund})} \rangle$ and $\langle N_H^{(\text{Lund})} \rangle$ corresponding respectively to rest-frame $e^+e^- \rightarrow Z \rightarrow q\bar{q}$ and $e^+e^- \rightarrow H \rightarrow gg$ collisions with centre-of-mass energy Q . We define $\alpha_s = \alpha_s(Q)$, $L = \ln(Q/k_{t,\text{cut}})$, $\xi = \alpha_s L^2$, $\nu = \sqrt{2C_A \alpha_s L^2 / \pi}$ and $c_\delta = (2C_F - C_A)/C_A$. The equations are written in terms of coefficients summarised in Table 2.

The generic all-order structure of the Lund multiplicity is

$$\langle N_{Z,H}^{(\text{Lund})}(L; \alpha_s) \rangle = 2[h_1^{(q,g)}(\xi) + \sqrt{\alpha_s} h_2^{(q,g)}(\xi) + \alpha_s h_3^{(q,g)}(\xi)]. \quad (4.69)$$

Using $\nu = \sqrt{2C_A \xi / \pi}$, the DL contribution is

$$h_1^{(q)} = 1 + \frac{C_F}{C_A} (\cosh \nu - 1) \quad (4.70a)$$

$$h_1^{(g)} = \cosh \nu, \quad (4.70b)$$

the NDL function h_2 is given by

$$h_2^{(q)} = \frac{C_F}{\sqrt{2\pi C_A}} \left\{ \frac{\pi\beta_0}{2C_A} [(\nu^2 - 1) \sinh \nu + \nu \cosh \nu] + (B_{gg} + c_\delta B_{gq}) \nu \cosh \nu \right. \\ \left. + [2B_q - B_{gg} + (2 - 3c_\delta) B_{gq}] \sinh \nu + 2(c_\delta - 1) B_{gq} \nu \right\}, \quad (4.71a)$$

$$h_2^{(g)} = \sqrt{\frac{C_A}{2\pi}} \left\{ \frac{\pi\beta_0}{2C_A} [(\nu^2 - 1) \sinh \nu + \nu \cosh \nu] \right. \\ \left. + (B_{gg} + c_\delta B_{gq}) \nu \cosh \nu + [B_{gg} + (2 - c_\delta) B_{gq}] \sinh \nu \right\}. \quad (4.71b)$$

The DL (4.70) and NDL (4.71) accurate expressions also apply to any k_t -based jet multiplicity, for example Durham multiplicity [24]. The main new result of this paper is the NNDL function h_3 which is found to be

$$2\pi h_3^{(q)} = D_{\text{end}}^{q \rightarrow qq} + (D_{\text{end}}^{g \rightarrow gg} + D_{\text{end}}^{g \rightarrow q\bar{q}}) \frac{C_F}{C_A} (\cosh \nu - 1) + D_{\text{hme}}^{qqg} \cosh \nu \quad (4.72) \\ + \frac{C_F}{C_A} \left[(1 - c_\delta) D_{\text{pair}}^{q\bar{q}} (\cosh \nu - 1) + \left(K + D_{\text{pair}}^{gg} + c_\delta D_{\text{pair}}^{q\bar{q}} \right) \frac{\nu}{2} \sinh \nu \right] \\ + C_F \left[\left(\cosh \nu - 1 - \frac{1 - c_\delta}{4} \nu^2 \right) D_{\text{clust}}^{(\text{prim})} + (\cosh \nu - 1) D_{\text{clust}}^{(\text{sec})} \right] \\ + \frac{C_F}{C_A} \left[D_{\text{e-loss}}^g \frac{\nu}{2} \sinh \nu + (D_{\text{e-loss}}^q - D_{\text{e-loss}}^g) (\cosh \nu - 1) \right] \\ + \frac{C_F}{2} \left\{ (B_{gg} + c_\delta B_{gq})^2 \nu^2 \cosh \nu + 8 [2c_\delta B_{gg} - 2c_\delta B_q - (1 - 3c_\delta^2) B_{gq}] B_{gq} \cosh \nu \right. \\ \left. + [4B_q (B_{gg} + (2c_\delta + 1) B_{gq}) - (B_{gg} + c_\delta B_{gq}) (B_{gg} + 9c_\delta B_{gq})] \nu \sinh \nu \right. \\ \left. + 4(1 - c_\delta^2) B_{gq}^2 \nu^2 + 8 [2c_\delta B_q - 2c_\delta B_{gg} + (1 - 3c_\delta^2) B_{gq}] B_{gq} \right\} \\ + \frac{C_F}{C_A} \frac{\pi\beta_0}{2} \left\{ (B_{gg} + c_\delta B_{gq}) \nu^3 \sinh \nu + [2B_q - 2B_{gg} + (6 - 8c_\delta) B_{gq}] \nu \sinh \nu \right. \\ \left. + 2(B_q + B_{gg} + B_{gq}) \nu^2 \cosh \nu - 4(1 - c_\delta) B_{gq} (2 \cosh \nu - 2 + \nu^2) \right\} \\ + \frac{C_F}{C_A} \frac{\pi^2 \beta_0^2}{8C_A} [3\nu(2\nu^2 - 1) \sinh \nu + (\nu^4 + 3\nu^2) \cosh \nu]$$

for quarks, and

$$2\pi h_3^{(g)} = (D_{\text{end}}^{g \rightarrow gg} + D_{\text{end}}^{g \rightarrow q\bar{q}}) \cosh \nu + [D_{\text{hme}}^{ggg} \cosh \nu + D_{\text{hme}}^{gq\bar{q}} (c_\delta \cosh \nu + 1 - c_\delta)] \quad (4.73) \\ + \left[(1 - c_\delta) D_{\text{pair}}^{q\bar{q}} (\cosh \nu - 1) + \left(K + D_{\text{pair}}^{gg} + c_\delta D_{\text{pair}}^{q\bar{q}} \right) \frac{\nu}{2} \sinh \nu \right] \\ + C_A \left(D_{\text{clust}}^{(\text{prim})} + D_{\text{clust}}^{(\text{sec})} \right) (\cosh \nu - 1) + D_{\text{e-loss}}^g \frac{\nu}{2} \sinh \nu \\ + \frac{C_A}{2} \left\{ (B_{gg} + c_\delta B_{gq})^2 \nu^2 \cosh \nu - 8(1 - c_\delta^2) B_{gq}^2 (\cosh \nu - 1) \right. \\ \left. + [(B_{gg} + c_\delta B_{gq}) (3B_{gg} - 5c_\delta B_{gq}) + 4(1 + c_\delta) B_{gq} B_q] \nu \sinh \nu \right\} \\ + \frac{\pi\beta_0}{2} \left\{ (B_{gg} + c_\delta B_{gq}) \nu^3 \sinh \nu + 6(1 - c_\delta) B_{gq} \nu \sinh \nu + 2 [2B_{gg} + (1 + c_\delta) B_{gq}] \nu^2 \cosh \nu \right. \\ \left. - 8B_{gq} (1 - c_\delta) (\cosh \nu - 1) \right\} + \frac{\pi^2 \beta_0^2}{8C_A} [3\nu(2\nu^2 - 1) \sinh \nu + (\nu^4 + 3\nu^2) \cosh \nu]$$

Contribution	Coefficient
Running coupling	$\beta_0 = \frac{11C_A - 4n_f T_R}{12\pi}$
Hard-collinear correction	$B_q = -\frac{3}{4}, B_{gg} = -\frac{11}{12}, B_{gq} = \frac{n_f T_R}{3C_A}$
Collinear endpoint	$D_{\text{end}}^{q \rightarrow qq} = C_F(3 + 3 \ln 2 - \frac{\pi^2}{3})$ $D_{\text{end}}^{g \rightarrow gg} = C_A(\frac{137}{36} + \frac{11}{3} \ln 2 - \frac{\pi^2}{3})$ $D_{\text{end}}^{g \rightarrow q\bar{q}} = n_f T_R(-\frac{29}{18} - \frac{4}{3} \ln 2)$
Hard matrix-element	$D_{\text{hme}}^{qqg} = C_F(\frac{\pi^2}{6} - \frac{7}{4}), D_{\text{hme}}^{ggg} = C_A(\frac{\pi^2}{6} - \frac{49}{36}), D_{\text{hme}}^{gq\bar{q}} = n_f T_R \frac{2}{9}$
Commensurate k_t and angle	$D_{\text{pair}}^{q\bar{q}} = \frac{13}{9} n_f T_R, D_{\text{pair}}^{gg} = (\frac{\pi^2}{6} - \frac{67}{18}) C_A$ $K = \left(\frac{67}{18} - \frac{\pi^2}{6}\right) C_A - \frac{10}{9} n_f T_R$
Clustering	$D_{\text{clust}}^{(\text{prim})} = -\frac{5\pi^2}{54}, D_{\text{clust}}^{(\text{sec})} = \frac{\pi^2}{27}$
Energy loss	$D_{\text{e-loss}}^q = \frac{7}{2} C_A + (\frac{5}{2} - \frac{2\pi^2}{3}) C_F$ $D_{\text{e-loss}}^g = (\frac{67}{9} - \frac{2\pi^2}{3}) C_A - \frac{26}{9} \frac{C_F}{C_A} n_f T_R$

Table 2: Coefficients entering the NNDL h_3 function.

for gluons, with different contributions separated in different colours, except for those involving ingredients already present at NDL accuracy which have been gathered (in orange).

At NNDL accuracy, the Cambridge multiplicity is simply obtained from Eq. (4.69):

$$\langle N^{(\text{Cam})}(\alpha_s, L) \rangle = \langle N^{(\text{Lund})}(\alpha_s, L) \rangle + \frac{\alpha_s C_i}{2\pi} \frac{\pi^2}{6}. \quad (4.74)$$

To gain insight into the relative sizes of the NNDL contributions, the top panels of Fig. 6 show the ratios $h_{2,3}/h_1$ as a function of $\xi = \alpha_s L^2$ for quark (left) and gluon (right) hemispheres. We note that the NDL corrections are negative at low values of ξ , driven by hard-collinear corrections, while the NNDL result remains positive for all ξ . Unless we go to large values of ξ , the NNDL function h_3 is roughly of the same magnitude as the NDL function h_2 . That said, for physical values of $\alpha_s \sim 0.1$, the size of the NNDL corrections, $\alpha_s h_3(\xi)$, would be commensurate to the NDL contribution $\sqrt{\alpha_s} h_2(\xi)$, motivating the study of their phenomenological impact, which we carry out in Sec. 5.2.

In the bottom row of Fig. 6, we investigate the relative sizes of the NNDL contributions to the total $h_3(\xi)$ for quarks (left) and gluons (right), with line colours matching those in Eqs. (4.72) and (4.73). For conciseness, we have grouped the corrections stemming only from NDL hard-collinear or running coupling corrections into a unique (NDL)² contribution, i.e. $h_{3,\text{NDL}^2} \equiv h_{3,\text{hc}^2} + h_{3,\beta_0 \times \text{hc}} + h_{3,\beta_0^2}$ (Sects. 4.3.2 and 4.4). We note that there are particularly large cancellations between the $h_{3,\beta_0 \times \text{hc}}$ and h_{3,β_0^2} functions, further motivating their grouping.

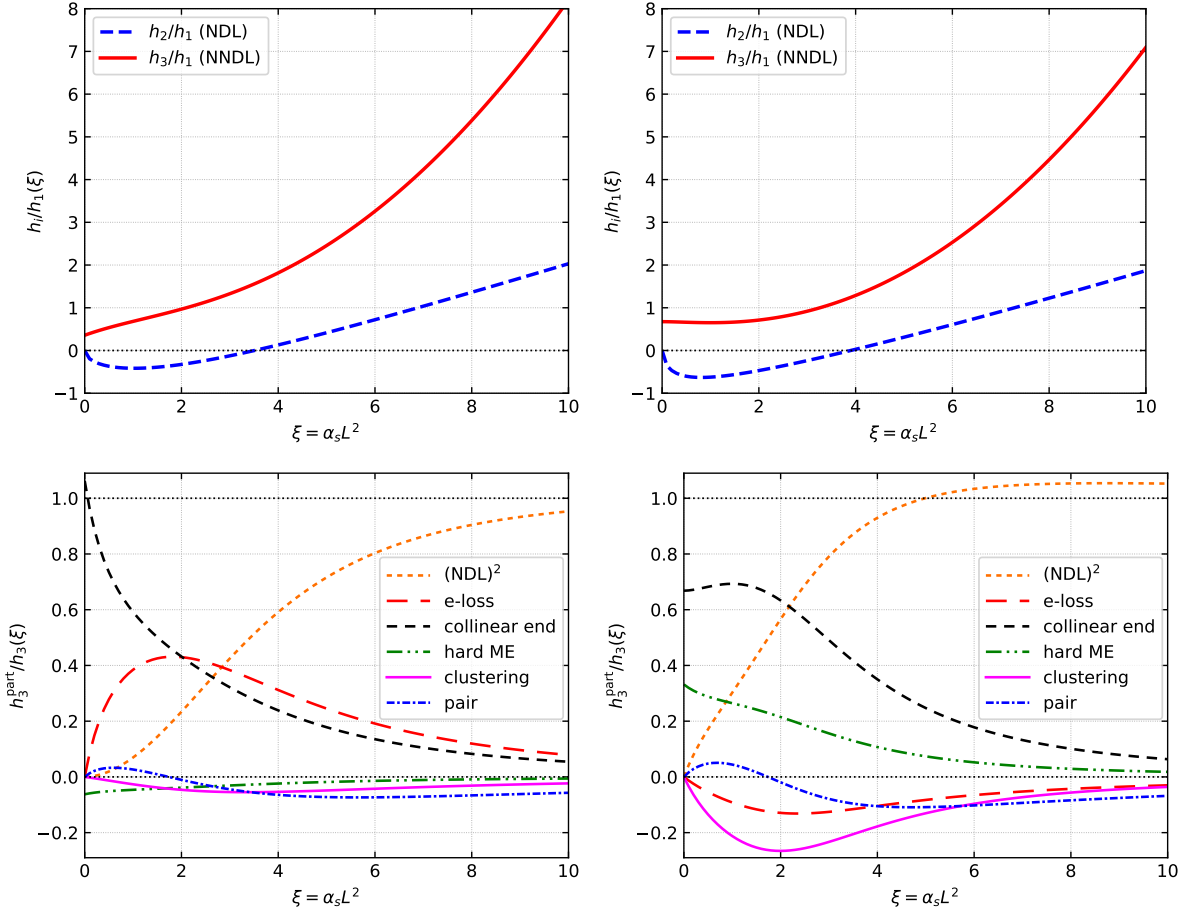


Figure 6: Top: Ratio of NDL (blue) and NN DL (red) resummation functions to the DL result as a function of $\alpha_s L^2$ for quark (left) and gluon hemispheres (right). Bottom: Relative weight of the NN DL contributions to h_3 for quark (left) and gluon hemispheres (right).

We observe that these $(\text{NDL})^2$ corrections become dominant when $\xi \gtrsim 3$ for both the quark and gluon cases. This can be traced to the running-coupling corrections which, relative to h_1 , scale like ξ^2 (ξ for the NDL contribution). More generally, one should expect that pure running-coupling corrections would bring contributions of order ξ^{k-1} to h_k/h_1 , so that for $\sqrt{\xi}(\alpha_s L) = \sqrt{\alpha_s} \xi \sim 1$, the N^kDL approach of expanding in series of $\sqrt{\alpha_s}$ at fixed $\xi = \alpha_s L^2$, Eq. (1.1), should be revisited so as to resum an arbitrary number of running-coupling corrections.¹⁷ This is actually reminiscent of the LL, NLL, NNLL, ... logarithmic counting where running-coupling corrections are included already in the LL Sudakov factor [54]. It is also interesting to recall that, while the original result from Ref. [24] is strictly speaking NDL, the use of a generating functional potentially includes an arbitrary number of running-coupling corrections, partly resumming them in the above sense to all orders. In this context we have checked explicitly that parts of the h_{3,NDL^2} function are already included in the expansion of the result from [24] to NN DL order, in

¹⁷In this case, mixed running-coupling and hard-collinear corrections are expected to be numerically significant.

particular terms which dominate at large values of ξ (i.e. the terms proportional to ξ^2 , $\xi^{3/2}$ and ξ , multiplied by $\cosh \nu$ or $\sinh \nu$). Further investigation on how to include this in a perturbatively controlled way in our formalism is left for future work.

For phenomenologically-accessible values of ξ , $\xi \lesssim 5$, we observe in Fig. 6 that the contributions from the collinear endpoint and energy loss are in the 20-40% range¹⁸ for the quark case. For gluons we observe a larger sensitivity, $\sim 10\%$, to other contributions, like hard matrix-element, clustering and soft pairs.

The relative weight of each contribution to the NNDL multiplicity is an important piece of information to gauge the constraining power of Lund multiplicity on parton shower validation, as it probes the full multiple branching structure of QCD. This was explicitly demonstrated in Ref. [44] (and Ref. [26] at full colour) where the NLL PanScales family of showers were shown to successfully reproduce the NDL jet multiplicity analytic resummation [24], among other observables. Thus, the NNDL analytic result presented in this paper would be a key element towards testing a future generation of NNLL showers. Since, as discussed above, some of the physical contributions to h_3 can be relatively small, an excellent control of the numerical precision in the shower would be required.

5 Validation and phenomenology

In this section we first cross-check the fixed-order expansion of our resummed result against the **Event2** generator [46, 47]. We then discuss the phenomenological impact of the NNDL resummation at LEP energies, including matching our resummed result to exact NLO from **Event2**. We finish this section with a brief comparison to existing OPAL data, taking into account non-perturbative corrections obtained by means of Monte Carlo simulations.

5.1 Fixed-order validation

The **Event2** generator provides exact results for the multiplicity in $e^+e^- \rightarrow Z \rightarrow q\bar{q}$ Born-level events up to $\mathcal{O}(\alpha_s^2)$:

$$\langle N^{(\text{Lund})}(\alpha_s, L) \rangle = 2 + \frac{\alpha_s}{2\pi} \langle N_1^{(\text{Lund})}(L) \rangle + \left(\frac{\alpha_s}{2\pi} \right)^2 \langle N_2^{(\text{Lund})}(L) \rangle + \mathcal{O}(\alpha_s^3). \quad (5.1)$$

The fixed-order coefficients have the following dependence on L :

$$\frac{1}{2\pi} \langle N_1^{(\text{Lund})}(L) \rangle = h_{11}L^2 + h_{21}L + h_{31} + \mathcal{O}(e^{-L}), \quad (5.2a)$$

$$\frac{1}{(2\pi)^2} \langle N_2^{(\text{Lund})}(L) \rangle = h_{12}L^4 + h_{22}L^3 + h_{32}L^2 + h_{42}L + h_{52} + \mathcal{O}(e^{-L}), \quad (5.2b)$$

where the h_{ij} coefficients correspond to the j -th order α_s expansion of the h_i resummed expressions, e.g. h_{11} is the first-order expansion of the DL h_1 function, h_{32} is the second-order expansion of the NNDL h_3 function and so on. The extraction of the α_s and $\alpha_s^2 L^2$ contributions from **Event2** therefore provides a validation of our NNDL resummed calculation. More

¹⁸Or even more at small ξ , although this region would in practice be affected by fixed-order corrections.

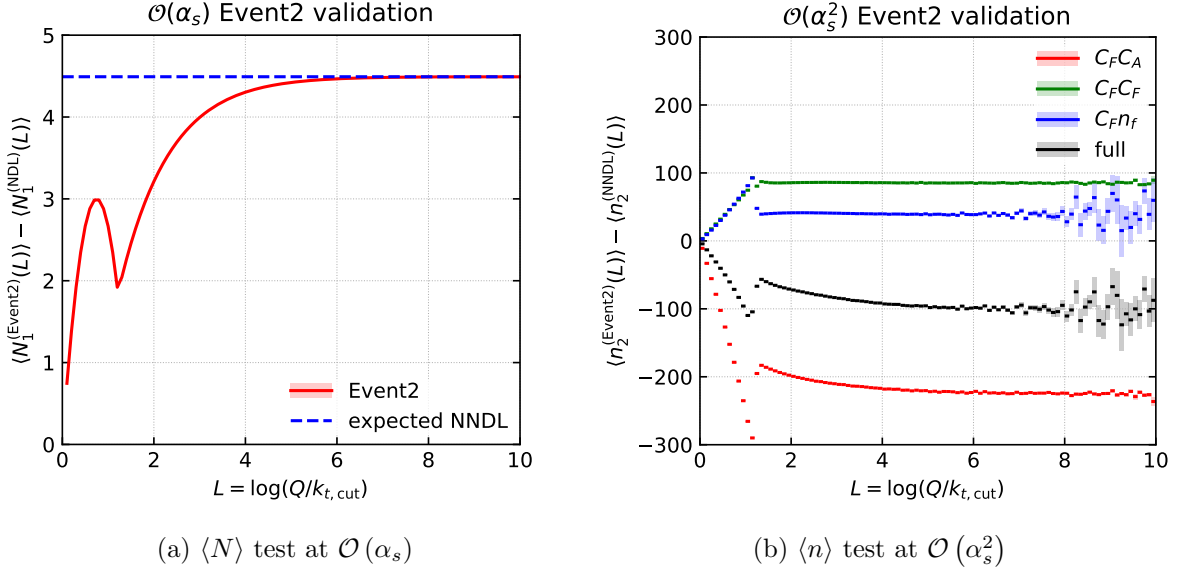


Figure 7: Comparison between our NNDL calculation expanded in series of α_s and exact fixed-order results obtained numerically with **Event2**: (a) the multiplicity difference $\langle N_1^{\text{Event2}} \rangle - \langle N_1^{\text{NNDL}} \rangle$ at order α_s , expected to tend to the NNDL constant represented by the dashed (blue) line, cf. Eq. (5.2a); (b) the differential multiplicity difference $\langle n_2^{\text{Event2}} \rangle - \langle n_2^{\text{NNDL}} \rangle$ at order α_s^2 which is expected to go to a (N³DL) constant if the results agree at NNDL, cf. Eq. (5.2b).

specifically, from the results in Sec. 4, we find

$$h_{31} = \frac{1}{\pi} (D_{\text{hme}}^{qqg} + D_{\text{end}}^{q \rightarrow qq}), \quad (5.3a)$$

$$h_{32} = \frac{C_A}{\pi^2} D_{\text{hme}}^{qqg} + \frac{C_F}{\pi^2} \left(D_{\text{end}}^{g \rightarrow gg} + D_{\text{end}}^{g \rightarrow q\bar{q}} + K + D_{\text{pair}}^{gg} + D_{\text{pair}}^{q\bar{q}} + D_{\text{e-loss}}^q + C_F D_{\text{clust}}^{(\text{prim})} + C_A D_{\text{clust}}^{(\text{sec})} \right) + \frac{4C_F C_A}{\pi^2} B_q (B_{gg} + B_{gq}) + \frac{4C_F}{\pi} B_q \beta_0. \quad (5.3b)$$

In order to check that these coefficients are indeed correct, we have performed two tests, shown in Fig. 7. First, focusing on the first order in α_s , we subtract from the **Event2** multiplicity $\langle N_1^{\text{Event2}} \rangle$ the NDL expectation, $\langle N_1^{\text{NNDL}} \rangle$. This is plotted as the solid (red) line in Fig. 7a. Our NNDL expectation is that it should tend asymptotically to $2\pi h_{31}$, plotted as the dashed (blue) line in Fig. 7a. The solid curve indeed matches the dashed one at large L as expected.

Next, focusing on the second order, $\mathcal{O}(\alpha_s^2)$, we subtract from the *differential Event2* multiplicity distribution, $\langle n_2^{\text{Event2}} \rangle$, the NNDL expectation, $\langle n_2^{\text{NNDL}} \rangle$, obtained through a simple derivative of our NNDL result. This is plotted in Fig. 7b for both the full multiplicity and for the contributions of each colour channel. The expectation is that the NNDL-subtracted result tends to a constant (associated with h_{42} in Eq. (5.2b)) at large L , which it does. Similar tests, reported in Appendix A.3, have been performed for the Cambridge multiplicity.

These two tests show that our NNDL calculation is correct, at least up to order α_s^2 for $e^+e^- \rightarrow Z \rightarrow q\bar{q}$ events. If the tools become available, it would be interesting to extend these tests to $e^+e^- \rightarrow H \rightarrow gg$ events, as well as one order higher in α_s . This would for example allow

us to probe the NNDL contributions starting at $\mathcal{O}(\alpha_s^2)$ beyond their first non-trivial contribution, as well as probing the NNDL coefficients which start only at $\mathcal{O}(\alpha_s^3)$, such as the β_0^2 correction or the vanishing of the contribution from three emissions at commensurate angles.

Note that we have performed additional checks beyond the comparison with **Event2**. The fixed-order expansion up to $\mathcal{O}(\alpha_s^2)$ of $h_{3,\text{end}}$ (Sec. 4.2.1), $h_{3,\text{e-loss}}$ (Sec. 4.3.1) and h_{3,hc^2} (Sec. 4.3.2) has been checked against the **MicroJet** results [62]. Finally, the large-angle components of the calculation, see Secs. 4.3.4 and 4.2.4, have been cross-checked against the $\mathcal{O}(\alpha_s^2)$ expansion of a toy dipole shower described in Ref. [39].

5.2 Matching with fixed-order

In order to produce reliable phenomenological predictions of the Lund multiplicity in $e^+e^- \rightarrow Z$ events for all values of $L = \ln(Q/k_{t,\text{cut}})$, the resummed distribution obtained in Sec. 4, relevant at large L , needs to be matched with a fixed-order calculation, relevant at small L . For this observable, we use an additive matching scheme:

$$\langle N^{(\text{Lund})} \rangle_{\text{match}} = \langle N^{(\text{Lund})} \rangle_{\text{fo}} + \langle N^{(\text{Lund})} \rangle_{\text{resum}} - \langle N^{(\text{Lund})} \rangle_{\text{resum,fo}}, \quad (5.4)$$

where $\langle N^{(\text{Lund})} \rangle_{\text{fo}}$ is the exact fixed-order result obtained with **Event2** as described in Sec. 5.1, taken here at NLO i.e. at order α_s^2 , $\langle N^{(\text{Lund})} \rangle_{\text{resum}}$ is the NNDL-accurate resummed result, Eq. (4.69), and $\langle N^{(\text{Lund})} \rangle_{\text{resum,fo}}$ avoids double counting by subtracting the $\mathcal{O}(\alpha_s^2)$ expansion of the resummed result $\langle N^{(\text{Lund})} \rangle_{\text{resum}}$. At our accuracy, the fixed-order distribution can be normalised to the NLO inclusive cross-section, $\sigma_0 + \sigma_1 = \sigma_0(1 + \alpha_s/\pi)$. The scale uncertainty is probed by varying the renormalisation scale and the resummation scale. For this, we introduce two dimensionless parameters, x_R and x_L . The renormalisation scale is taken as $\mu_R = x_R Q$, both in the resummation and in the fixed-order results, and the resummation scale is varied by redefining L as $\ln(x_L Q/k_t)$. When varying x_R and x_L , one must introduce counter-terms to preserve the perturbative accuracy, both at fixed order and for the resummed result. For the resummed result, we get

$$\begin{aligned} \langle N^{(\text{Lund})} \rangle_{\text{resum}} &= h_1(\xi) + \sqrt{\alpha_s} [h_2(\xi) - 2 \ln x_L \sqrt{\xi} h'_1(\xi)] \\ &+ \alpha_s [h_3(\xi) + (2\beta_0 \ln x_R \xi + \ln^2 x_L) h'_1(\xi) + 2 \ln^2 x_L \xi h''_1(\xi) - 2 \ln x_L \sqrt{\xi} h'_2(\xi)], \end{aligned} \quad (5.5)$$

with h_i defined in Sec. 4.5, $\alpha_s \equiv \alpha_s(\mu_R = x_R Q)$, $\xi = \alpha_s L^2 = \alpha_s \ln^2(x_L Q/k_t)$, and h'_i, h''_i the first and second derivatives of h_i with respect to ξ . In practice, we estimate the scale uncertainty by separately varying either x_L or x_R between 1/2 and 2, taking the envelopes of the variations, and summing in quadrature the renormalisation and resummation uncertainties.

Finally, to account for the fact that the endpoints of the resummed and fixed-order distributions do not coincide, we redefine the L in the argument of $\langle N^{(\text{Lund})} \rangle_{\text{resum}}$ according to [63]

$$L = \ln \frac{Q}{k_{t,\text{cut}}} \rightarrow L = \ln \left(\frac{x_L Q}{k_{t,\text{cut}}} - \frac{x_L Q}{k_{t,\text{max}}} + 1 \right), \quad (5.6)$$

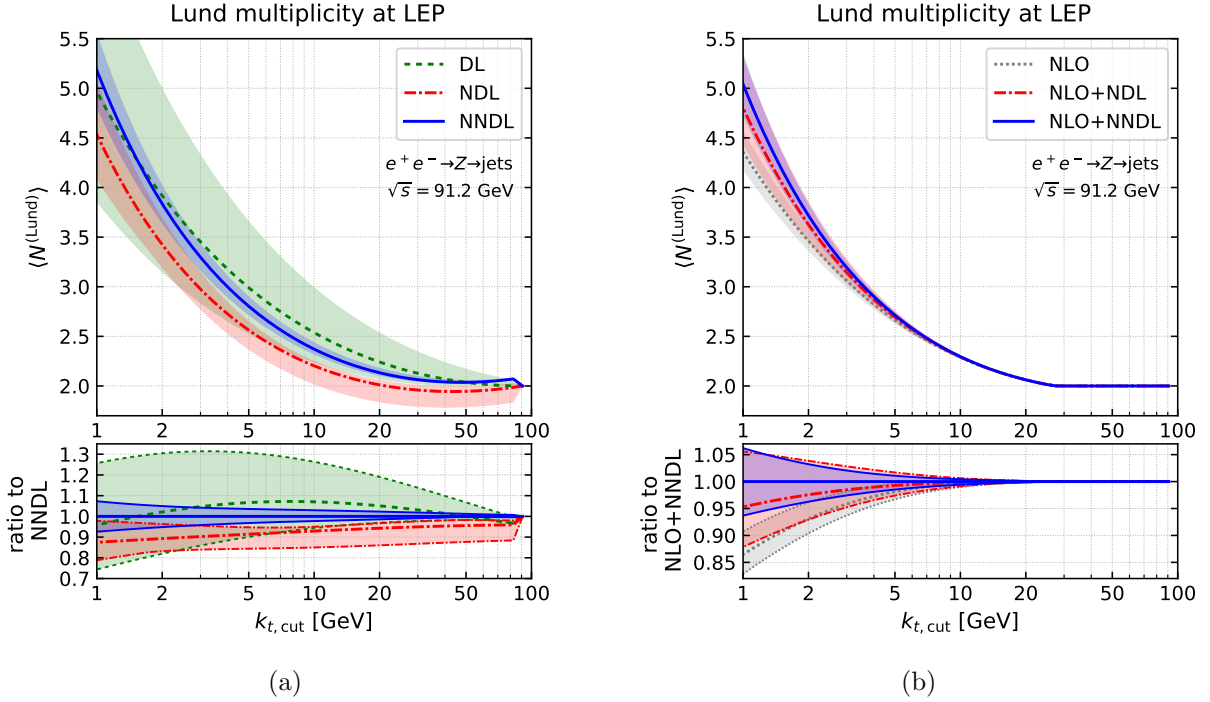


Figure 8: Left: Resummed Lund multiplicity at DL (dashed, green), NDL (dash-dotted, red) and NNDL (solid, blue) as a function of $k_{t,\text{cut}}$ for LEP kinematics. Right: Lund multiplicity after matching with NLO. The pure NLO result is shown in dotted (grey) for reference, together with matched NLO+NDL (dash-dotted, red) and NLO+NNDL (solid, blue). The bottom panels display the ratio to the most accurate result (NNDL on the left and NLO+NNDL on the right).

with $k_{t,\text{max}}$ the smallest k_t value at which the fixed-order distribution is equal to its Born-level value, i.e. 2.¹⁹ At large L , this replacement only generates power corrections in $k_{t,\text{cut}}$ and so does not spoil the logarithmic accuracy.

Fig. 8 shows the Lund multiplicity, together with its uncertainty, as a function of $k_{t,\text{cut}}$ for LEP $e^+e^- \rightarrow Z$ events at $\sqrt{s} = 91.2$ GeV. A common feature to all curves is that the Lund multiplicity increases significantly when $k_{t,\text{cut}}$ decreases. In Fig. 8a, we focus on the resummed results at different degrees of logarithmic accuracy. We find that while NDL corrections reduce the multiplicity, NNDL corrections cause a non-negligible increase, as one would expect from Fig. 6. Furthermore, increasing the logarithmic accuracy significantly reduces the perturbative uncertainty. Working for example at $k_{t,\text{cut}} = 5$ GeV, The DL uncertainty of $\sim 20\%$ is reduced to 5.6% at NDL and to $\sim 3.4\%$ at NNDL. For $k_{t,\text{cut}} = 1$ GeV, these numbers are around 27%, 11% and 7%, showing a similar reduction from NDL (the current state-of-the-art) to NNDL. The NNDL uncertainty band is also more symmetric than the NDL one. It is also interesting to notice that the NDL and NNDL uncertainty bands only barely overlap.

Fig. 8b shows the effect of matching with NLO ($\mathcal{O}(\alpha_s^2)$) fixed-order results. We first see

¹⁹At $\mathcal{O}(\alpha_s)$, we find $k_{t,\text{max}}^2 = \frac{5\sqrt{5}-11}{2}Q^2 \approx 0.0902Q^2$ ($\ln Q/k_{t,\text{max}} \approx 1.203$). At $\mathcal{O}(\alpha_s^2)$ we determine $k_{t,\text{max}}$ numerically from the `Event2` distribution, finding $k_{t,\text{max}}^2 \approx 0.1062Q^2$, i.e. $\ln Q/k_{t,\text{max}} \approx 1.121$.

that the effect of the resummation is to increase the average Lund multiplicity, even further so with NNDL matching than with NDL matching, showing the necessity for the resummation at small $k_{t,\text{cut}}$. Besides the sheer increase in multiplicity, NLO+NNDL matched results also bring a significant reduction in scale uncertainty compared to what is observed at NLO+NDL. This reduction is of about 50% at almost all $k_{t,\text{cut}}$ values, e.g. going from $\sim 9\%$ (2%) to $\sim 6\%$ (1.3%) at $k_{t,\text{cut}} = 5$ GeV (1 GeV).

5.3 Comparison to LEP data

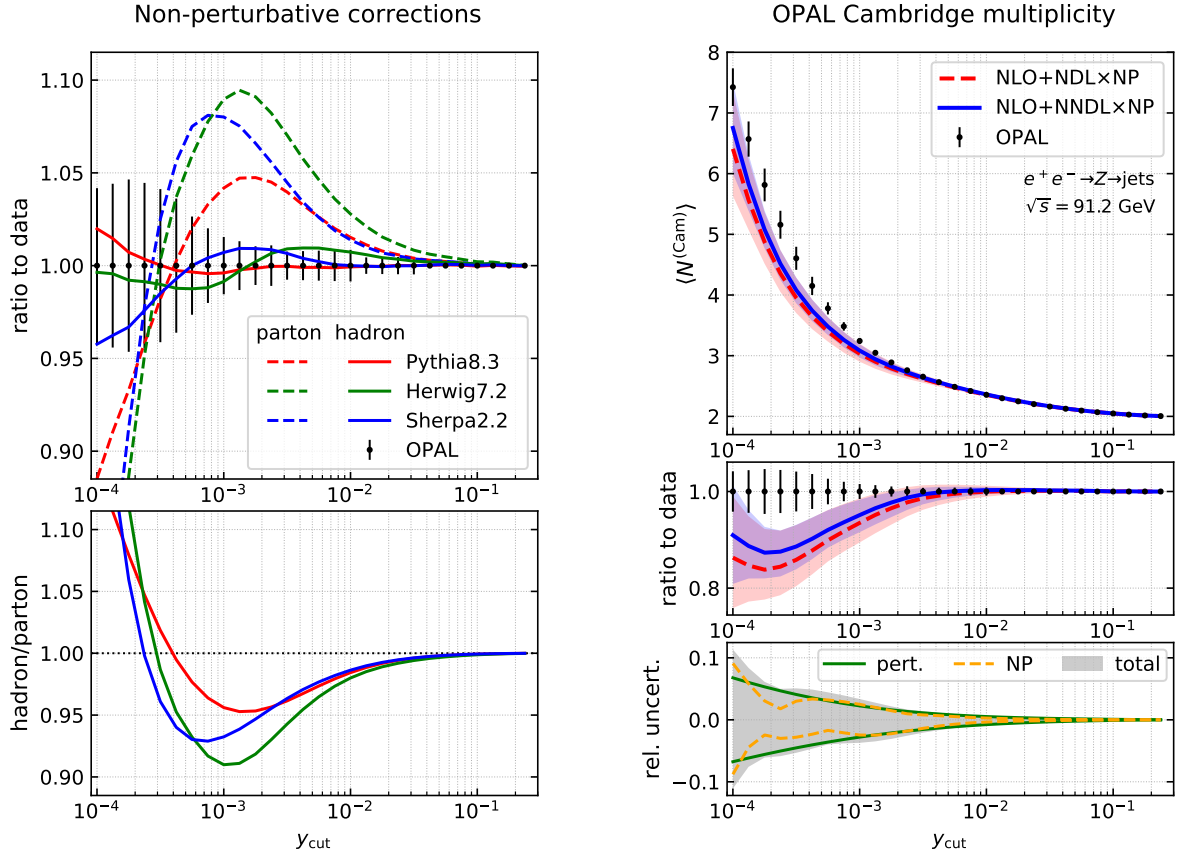
We conclude this section with a short comparison between our analytic results and the existing measurement [45] done by the OPAL collaboration at LEP. Here, we focus solely on the results for $\sqrt{s} = 91.2$ GeV.

From the viewpoint of perturbative QCD, the same approach we just discussed for the Lund multiplicity can be applied to the Cambridge multiplicity: our NNDL resummed result, Eq. (4.74), can be matched to `Event2` exact NLO multiplicities using additive matching, Eq. (5.4). For a phenomenological comparison to the LEP data, we need to supplement our perturbative result by non-perturbative corrections. In this brief study, we have extracted these from standard general-purpose Monte Carlo generators. Namely, we have run `Pythia`(v8.306) [64], `Herwig`(v7.2.0) [65, 66], and `Sherpa`(v2.2.11) [7, 67] each at parton level and hadron level separately. This is plotted on the top panel of Fig. 9a showing that hadron-level predictions for the three generators do reproduce the data, although their respective parton-level distributions are quite different. Hadronisation corrections (and uncertainties) are then taken as the average (and envelope) of the three ratios of hadron- to parton-level distributions, cf. the lower panel of Fig. 9a.

The non-perturbative corrections are applied as a multiplicative factor to the matched perturbative results. The uncertainty is obtained by adding the perturbative and non-perturbative uncertainties in quadrature. The resulting distributions are shown in Fig. 9b for the NDL and NNDL resummations. Globally speaking, we see a decent degree of agreement with the OPAL data, although the predictions are systematically below the data for $y_{\text{cut}} \lesssim 10^{-3}$, i.e. for $k_{t,\text{cut}} \lesssim 3$ GeV. Including the NNDL corrections shows both an increase in multiplicity, bringing the predictions closer to the data, and a reduction in uncertainty. This agrees with the observations made in the previous subsection. We note as well that for the matched NNDL results, the perturbative and non-perturbative uncertainties are of the same order for $y_{\text{cut}} \lesssim 0.002$ with the perturbative uncertainties marginally dominating at larger values.

As a side comment, we observe that non-perturbative corrections become larger than 10% for $y_{\text{cut}} \lesssim 10^{-4}$, corresponding to $k_{t,\text{cut}} \lesssim 1.5$ GeV, in quantitative agreement with Fig. 15 of the original Cambridge paper [30]. We also note that the uncertainty on the non-perturbative corrections also grows significantly below $k_{t,\text{cut}} \sim 1.5$ GeV.

From a phenomenological viewpoint, the significant reduction of the perturbative uncertainties at NNDL compared to NDL, seen both in this section and in the previous one, is the most important phenomenological result of this paper. It suggests that it would be interesting to perform a more extensive comparison to the OPAL data. Such a study could include matching to exact NNLO results, as well as an improved resummation of the running-coupling corrections (see the discussion at the end of Sec. 4.5). These would hopefully further reduce the perturbative



(a) Comparison of the data to standard Monte Carlo generators at parton (dashed) and hadron (solid) levels.

(b) Comparison of the data to NDL (red) and NNDL (blue) resummed results matched to NLO and corrected for non-perturbative effects.

Figure 9: Comparison of Monte Carlo (left) and analytic (right) results to the existing average Cambridge jet multiplicity measurement [45] from the OPAL collaboration at LEP.

uncertainty and produce a better agreement with the data at low values of $k_{t,\text{cut}}$. This could then potentially serve as a way to make an additional extraction of the strong coupling constant α_s . It would also be of interest to measure the average Lund plane multiplicity as a function of $k_{t,\text{cut}}$ — or the difference between the Lund and Cambridge multiplicities —, especially in the context of the renewed interest in the community for the analysis of archived ALEPH data to study new observables (see e.g. [68]) or phenomena (see e.g. [69]). From a theoretical viewpoint, one could expect that higher-order running-coupling corrections would also increase the multiplicity at small y_{cut} , reemphasising the interest already stated in Sec. 4.5.

6 A byproduct: multiplicity in hadron collisions at NDL accuracy

In order to demonstrate the flexibility of the resummation strategy that we introduced in Sec. 3.2, we proceed to extend the Lund multiplicity calculation to hadronic collisions or, equivalently,

including initial-state radiation, up to NDL accuracy (see Sec. 2 for how the definition of the multiplicity is adapted to hadronic collisions).

We consider colour singlet production, i.e. Drell-Yan ($pp \rightarrow q\bar{q} \rightarrow Z$) and Higgs production via gluon fusion ($pp \rightarrow gg \rightarrow H$). The colourless boson $X = Z, H$ is produced at a virtuality $Q^2 = M_X^2$ and rapidity $y_X = \frac{1}{2} \ln \frac{x_1}{x_2}$ from a pair of incoming partons a, b with fixed flavour and fixed longitudinal momentum fractions x_1, x_2 . Since we are interested in the event-averaged Lund multiplicity, for fixed Q^2 and y_X , we normalise the Lund multiplicity to the differential cross section for colour singlet production which schematically reads

$$\frac{d^2\sigma_{pp \rightarrow X}}{dQ^2 dy_X} = \frac{d^2\hat{\sigma}_{ab \rightarrow X}}{dQ^2 dy_X} \times f_a(x_1, Q^2) f_b(x_2, Q^2), \quad (6.1)$$

where the differential cross section in Eq. (6.1) is written in terms of a hard partonic cross section $d^2\hat{\sigma}_{ab \rightarrow X}$ and the parton distribution functions (PDFs) $f(x_i, Q^2)$.

We note that as long as $\alpha_s(Q) \ln^2(1 - x_i) \ll 1$, ensuring that we are sufficiently far from the quasi-elastic regime [31], both partons may be viewed, up to NDL accuracy, as evolving independently from one another. We therefore analyse the multiplicity contribution of only one of the legs, akin to the procedure of Sec. 3. We also note that the leading-order value of the multiplicity is zero in this process, i.e. we do not count the colour singlet.

Differences with final-state multiplicity. In a colour singlet process we have to consider (primary) initial-state radiation from the incoming leg and their subsequent final-state evolution. A first natural question is whether the jet radius, introduced in a somewhat arbitrary way in the reconstruction of the Lund multiplicity in the pp case, affects the multiplicity calculation, preventing us from recycling the e^+e^- calculation. In principle, radiation from the incoming parton with $\theta \sim R$ could be mistagged due to clustering as (secondary) final-state radiation and vice-versa, similarly to the clustering correction in Sec. 4.2.4. For these emissions close to the jet boundary, the k_t with respect to the beam and the k_t with respect to the jet axis differ by a factor of $\mathcal{O}(R)$, so that for a finite jet radius, the difference between the two is NNDL [39, 70]. Therefore, up to NDL accuracy we can neglect the effect of the jet radius.

A direct consequence of the above discussion is that the only differences between the Lund multiplicity measured in pp and that measured in e^+e^- collisions come from radiation off the leading partons, which, instead of evolving through final-state radiation like in e^+e^- collisions, now evolves through initial-state radiation. For concreteness, let us therefore write the Lund multiplicity for one incoming leg of a pp collision as a difference with respect to the e^+e^- case:

$$N_{i,\text{IS}}(x, L) = N_{i,\text{FS}}(L) - 1 + \delta N_{i,\text{IS}}(x, L), \quad (6.2)$$

where the ‘ -1 ’ subtracts the incoming parton/beam — which is counted as part of the final state in $N_{i,\text{FS}}$ but should not be counted in the initial-state case — and we ought to compute $\delta N_{i,\text{IS}}$ up to NDL accuracy, including potential differences already at DL accuracy. Let us therefore proceed as in Sec. 3.2 and list all the possible contributions to $\delta N_{i,\text{IS}}$ up to NDL accuracy. Two obvious candidates are the NDL corrections already present in the final-state case, namely one-loop running coupling corrections and hard-collinear branchings. Since the running of the coupling does not affect the kinematics of the incoming parton, and, in particular, does not affect

the longitudinal momentum entering the PDFs, its NDL correction is the same in the initial- and final-state cases and its contribution to $\delta N_{i,\text{IS}}$ is zero. Conversely, hard-collinear initial-state branchings differ from their final-state equivalent in two ways: first, they lead to an increase of the x -fraction of the incoming parton leading to a non-trivial dependence on the PDF factor; second, the (flavour) structure of the branching differs from that in the final state in a similar way that initial-state backwards evolution in a parton shower differs from forwards final-state evolution.

Besides these corrections, one should also account for the fact that computing the multiplicity at a hadron collider involves a PDF factor. When measuring the multiplicity of Lund declusterings with a relative transverse momentum above $k_{t,\text{cut}}$, this PDF factor has to be evaluated at the scale $k_{t,\text{cut}}$ which differs from the scale Q^2 used in Eq. (6.1) for normalisation of the Lund multiplicity.²⁰ Including both the primary hard-collinear splittings and the PDF scale contributions, we can therefore write

$$N_{i,\text{IS}}^{(\text{NDL})}(x, L) = N_{i,\text{FS}}^{(\text{NDL})}(L) - 1 + \delta N_{i,\text{IS}}^{\text{prim}}(x, L) + \delta N_{i,\text{IS}}^{\mu_F}(x, L). \quad (6.4)$$

Factorisation scale contribution. Evaluating the PDF at the scale $k_{t,\text{cut}}$ and taking into account the normalisation in Eq. (6.1), we can write

$$\delta N_{i,\text{IS}}^{\mu_F}(x, L) \simeq \left[\frac{f_i(x, k_{t,\text{cut}}^2)}{f_i(x, Q^2)} - 1 \right] [N_{i,\text{FS}}^{(\text{DL})}(L) - 1] \simeq -2L \frac{\partial \ln f_i(x, Q^2)}{\partial \ln Q^2} [N_{i,\text{FS}}^{(\text{DL})}(L) - 1]. \quad (6.5)$$

When writing this equation we have made a few approximations valid at NDL accuracy. For the second equality, we have used the DGLAP evolution equation. Since $\partial \ln f_i(x, Q^2)/\partial \ln Q^2$ is of order α_s with no logarithmic enhancement, it is sufficient to expand this DGLAP evolution to first order at NDL accuracy. For the first equality, we have changed the scale of the PDFs, but kept both the flavour and the longitudinal fraction x constant. For the first equality, since the change of PDF scale from Q to $k_{t,\text{cut}}$ already induces an NDL correction, we are allowed to keep the flavour and x fraction of the incoming parton unchanged, and to evaluate the multiplicity in the second square bracket at DL accuracy. Note that a direct consequence of Eq. (6.5) is that, at DL accuracy we simply have

$$N_{i,\text{IS}}^{(\text{DL})}(x, L) = N_{i,\text{FS}}^{(\text{DL})}(L) - 1. \quad (6.6)$$

Hard-collinear initial-state branching. Let us now evaluate $\delta N_{i,\text{IS}}^{\text{prim}}(x, L)$. This takes into account differences between hard-collinear branchings in the initial-state and in the final state. In

²⁰In practice, the average multiplicity can be written as the following cross-section-weighted average:

$$\langle N_i(x, L) \rangle = \left[f_i(x, Q^2) \frac{d\hat{\sigma}_i}{dQ^2} \right]^{-1} \left[\sum_j \int dx' f_j(x', k_{t,\text{cut}}^2) \frac{d\hat{\sigma}_i}{dQ^2} \langle N_{i|j}(x|x', L) \rangle \right], \quad (6.3)$$

where $\frac{d\hat{\sigma}_i}{dQ^2}$ is the Born-level hard partonic cross-section and we have normalised by the total cross-section at a fixed x (i.e. the equivalent of Eq. (6.1) for a single hemisphere or, equivalently, for DIS). In this expression, one integrates over all possible incoming partons of flavour j and momentum fraction x' and $\langle N_{i|j}(x|x', L) \rangle$ denotes the average Lund multiplicity with a given $k_{t,\text{cut}} = Qe^{-L}$ for fixed x' and j . In this case, the PDFs in the numerator have to be evaluated at the final scale $k_{t,\text{cut}}^2$.

particular, we should consider that such an initial-state splitting affects the longitudinal momentum fraction entering the PDFs, taking it from its initial value x_{old} to a new value $x_{\text{new}} = x_{\text{old}}/\zeta$, where ζ is the transmitted collinear momentum fraction of the splitting. Note that we now define the soft limit as corresponding to $\zeta \rightarrow 1$ and that the transmitted ζ and emitted z momentum fractions are related by $\zeta = 1 - z$. Furthermore when hard-collinear branchings also change the flavour of the incoming parton, the PDFs also have to be evaluated with the new flavour. As in the final-state case, hard-collinear branchings affect quarks (i.e. Drell-Yan or Deep Inelastic Scattering (DIS)) and gluons (i.e. $gg \rightarrow H$) differently, so we discuss the two cases separately.

Quark-initiated. The contribution to the Lund multiplicity of a primary, hard-collinear splitting from an initial-state quark-leg at a scale ℓ is given by

$$\begin{aligned} \delta N_{q,\text{IS}}^{\text{prim}}(x, L) = & \frac{\alpha_s}{\pi} \int_0^L d\ell \int_x^1 \frac{d\zeta}{\zeta} P_{qq}^{\text{IS}}(\zeta) \frac{f_q(x/\zeta, Q^2)}{f_q(x, Q^2)} \left[N_{q,\text{IS}}^{(\text{DL})}(L) + N_g^{(\text{DL})}(L - \ell) \right] \\ & - \frac{\alpha_s}{\pi} \int_0^L d\ell \int_0^1 d\zeta P_{qq}^{\text{IS}}(\zeta) N_{q,\text{IS}}^{(\text{DL})}(L) \\ & - \frac{\alpha_s}{\pi} \int_0^L d\ell \int_0^1 d\zeta P_{q \rightarrow qg}(1 - \zeta) N_g^{(\text{DL})}(L - \ell) \\ & + \frac{\alpha_s}{\pi} \int_0^L d\ell \int_x^1 \frac{d\zeta}{\zeta} P_{qg}^{\text{IS}}(\zeta) \frac{f_g(x/\zeta, Q^2)}{f_q(x, Q^2)} \left[N_{q,\text{IS}}^{(\text{DL})}(L) + N_g^{(\text{DL})}(L - \ell) \right], \end{aligned} \quad (6.7)$$

where the standard, initial-state, DGLAP splitting functions read

$$P_{qq}^{\text{IS}}(z) = C_F \left(\frac{1+z^2}{1-z} \right), \quad P_{qg}^{\text{IS}}(z) = T_R [z^2 + (1-z)^2], \quad (6.8)$$

In Eq. (6.7) the first line represents the real emission of a gluon from a quark while backwards evolving into a quark. All legs involved in the splitting are dressed by a chain of soft-and-collinear emissions $N_i^{(\text{DL})}$, Eq. (3.10) or Eq. (6.6), evaluated at $L - \ell$ for the final state gluon and at L for the initial-state quark. In the second line, we consider the virtual correction for which only the incoming quark leg is dressed with $N_{q,\text{IS}}^{(\text{DL})}(L)$. The third line subtracts the hard-collinear splitting contribution in the final-state case (after the real-virtual cancellation of the radiation off the quark), remembering that we are computing the difference between initial- and final-state multiplicities, Eq. (6.4). There is no PDF ratio in this term. Furthermore, $P_{q \rightarrow qg}(z) = P_{qq}^{\text{IS}}(1 - z)$ and we have used $z = 1 - \zeta$. Finally, the fourth term in Eq. (6.7) accounts for the backwards evolution of a quark into a gluon by emitting a quark. Since this splitting does not exist in the final-state case we do not have to consider any subtraction term.

Grouping terms proportional to N_q and N_g and performing the ℓ integrations we obtain

$$\begin{aligned} \delta N_{q,\text{IS}}^{\text{prim}}(x, L) = & \frac{\alpha_s}{\pi} \int_x^1 \frac{d\zeta}{\zeta} \left[P_{qq,+}^{\text{IS}}(\zeta) \frac{f_q(x/\zeta, Q^2)}{f_q(x, Q^2)} + P_{qg}^{\text{IS}}(\zeta) \frac{f_g(x/\zeta, Q^2)}{f_q(x, Q^2)} \right] N_{q,\text{IS}}^{(\text{DL})} L \\ & + \frac{\alpha_s}{\pi} \int_x^1 \frac{d\zeta}{\zeta} \left[P_{qq,+}^{\text{IS}}(\zeta) \frac{f_q(x/\zeta, Q^2)}{f_q(x, Q^2)} + P_{qg}^{\text{IS}}(\zeta) \frac{f_g(x/\zeta, Q^2)}{f_q(x, Q^2)} \right] \frac{\sinh \nu}{\sqrt{\alpha}} \end{aligned} \quad (6.9)$$

Where $P_{qq,+}^{\text{IS}}$ includes the ‘plus’ prescription in the P_{qq}^{IS} splitting function of Eq. (6.8). Using the DGLAP evolution equation

$$\frac{\partial \ln f_q(x, Q^2)}{\partial \ln Q^2} = \frac{\alpha_s}{2\pi} \int_x^1 \frac{d\zeta}{\zeta} \left[P_{qq}^{\text{IS},+}(\zeta) \frac{f_q(x/\zeta, Q^2)}{f_q(x, Q^2)} + P_{qg}^{\text{IS}}(\zeta) \frac{f_g(x/\zeta, Q^2)}{f_q(x, Q^2)} \right], \quad (6.10)$$

we realise that the first line of Eq. (6.9) is identical, but with opposite sign, to the $\delta N_{q,\text{IS}}^{\mu_F}(x, L)$ contribution given by Eq. (6.5), cancelling the $N_{q,\text{IS}}$ term in the first line of (6.9). The final result for the quark-initiated Lund multiplicity in hadronic collisions is then given by

$$N_{q,\text{IS}}^{(\text{NDL})}(x, L) = N_{q,\text{FS}}^{(\text{NDL})}(L) - 1 + \frac{2 \sinh \nu}{\sqrt{\alpha}} \frac{\partial \ln f_q(x, Q^2)}{\partial \ln Q^2}. \quad (6.11)$$

This result agrees with the one obtained in Ref. [32] using the initial-state generating functional formalism in the context of DIS. In fact, since the choice of clustering algorithm does not impact the resummation at NDL accuracy, the Lund multiplicity in deep-inelastic scattering is identical to that of Ref. [32] which was instead defined using a k_t -like algorithm.

Finally, we proceed to extend the calculation to Drell-Yan where the incoming parton entering into the hard process does not have a fixed flavour. In this case, the normalisation is given by

$$\frac{d^2 \sigma_{pp \rightarrow X}}{dQ^2 dy_X} = \frac{d^2 \hat{\sigma}_{q\bar{q} \rightarrow X}}{dQ^2 dy_X} \times \sum_q Q_q^2 [f_q(x_1, Q^2) f_{\bar{q}}(x_2, Q^2) + (q \leftrightarrow \bar{q})], \quad (6.12)$$

where an additional sum over all possible quark flavours weighted by their electric charge is included with respect to Eq. (6.1). This translates into our final formula for the NDL accurate Drell-Yan multiplicity

$$\begin{aligned} \langle N^{(\text{Lund})}(x_1, x_2, L) \rangle_{\text{DY,NDL}} &= \langle N^{(\text{Lund})}(L) \rangle_{e^+e^-, \text{NDL}} - 2 \\ &+ \frac{2 \sinh \nu}{\sqrt{\alpha}} \frac{\partial}{\partial \ln Q^2} \ln \sum_q Q_q^2 [f_q(x_1, Q^2) f_{\bar{q}}(x_2, Q^2) + (q \leftrightarrow \bar{q})]. \end{aligned} \quad (6.13)$$

Gluon-initiated The contribution to the Lund multiplicity of a primary, hard-collinear splitting from an initial-state gluon-leg at a scale ℓ is given by

$$\begin{aligned} \delta N_{g,\text{IS}}^{\text{prim}}(x, L) &= \frac{\alpha_s}{\pi} \int_0^L d\ell \int_x^1 \frac{d\zeta}{\zeta} P_{gg}^{\text{IS}}(\zeta) \frac{f_g(x/\zeta, Q^2)}{f_g(x, Q^2)} [N_{g,\text{IS}}^{(\text{DL})}(L) + N_g^{(\text{DL})}(L - \ell)] \\ &- \frac{\alpha_s}{\pi} \int_0^L d\ell \int_0^1 d\zeta [P_{gg}^{\text{IS}}(\zeta) + P_{qg}^{\text{IS}}(\zeta)] N_{g,\text{IS}}^{(\text{DL})}(L) \\ &- \frac{\alpha_s}{\pi} \int_0^L d\ell \int_0^1 d\zeta P_{g \rightarrow gg}(1 - \zeta) N_g^{(\text{DL})}(L - \ell) \\ &+ \frac{\alpha_s}{\pi} \int_0^L d\ell \int_x^1 \frac{d\zeta}{\zeta} P_{gq}^{\text{IS}}(\zeta) \frac{f_\Sigma(x/\zeta, Q^2)}{f_g(x, Q^2)} [N_{g,\text{IS}}^{(\text{DL})}(L) - N_g^{(\text{DL})}(L - \ell) + 2N_q^{(\text{DL})}(L - \ell)] \\ &- \frac{\alpha_s}{\pi} \int_0^L d\ell \int_0^1 d\zeta P_{g \rightarrow q\bar{q}}(1 - \zeta) [2N_q^{(\text{DL})}(L - \ell) - N_g^{(\text{DL})}(L - \ell)], \end{aligned} \quad (6.14)$$

where the initial-state, DGLAP splitting functions read

$$P_{gg}^{\text{IS}}(z) = 2C_A \left[\frac{z}{1-z} + \frac{1-z}{z} + z(1-z) \right], \quad P_{gq}^{\text{IS}}(z) = C_F \left[\frac{1 + (1-z)^2}{z} \right], \quad (6.15)$$

and we have defined the singlet distribution $f_\Sigma(x, \mu_F^2) \equiv \sum_i^{n_f} [f_{q_i}(x, \mu_F^2) + f_{\bar{q}_i}(x, \mu_F^2)]$. The ordering of the terms in Eq. (6.14) follows the same logic as of the quark-initiated case. The first three lines of Eq. (6.14) are related to the backwards evolution of a gluon into a gluon by emitting another gluon: the first line describes real emissions, the second line subtracts virtual corrections and the third one subtracts the final-state contribution. The last two lines describe the backwards evolution of a gluon into a quark/anti-quark pair of any flavour. Note that the final-state subtraction in this case has the usual mismatch between real and virtual emissions, see e.g. Eq. (3.26), that leads to the $[2N_q^{(\text{DL})}(L - \ell) - N_g^{(\text{DL})}(L - \ell)]$ term.

Recalling that DGLAP evolution for a gluon reads (using the ‘plus’ prescription for P_{gg})

$$\frac{\partial \ln f_g(x, Q^2)}{\partial \ln Q^2} = \frac{\alpha_s}{2\pi} \int_x^1 \frac{d\zeta}{\zeta} \left[P_{gg}^{\text{IS},+} \frac{f_g(x/\zeta, Q^2)}{f_g(x, Q^2)} + P_{gq}^{\text{IS}}(\zeta) \frac{f_\Sigma(x/\zeta, Q^2)}{f_g(x, Q^2)} \right], \quad (6.16)$$

we can re-write Eq. (6.14) as

$$\begin{aligned} \delta N_{g,\text{IS}}^{\text{prim}}(x, L) &= \frac{\partial \ln f_g(x, Q^2)}{\partial \ln Q^2} \left[2L + \frac{2 \sinh \nu}{\sqrt{\bar{\alpha}}} \right] \\ &+ \frac{2\alpha_s}{\pi} \int_0^L d\ell \int \frac{d\zeta}{\zeta} P_{gq}^{\text{IS}}(\zeta) \frac{f_\Sigma(x/\zeta, Q^2)}{f_g(x, Q^2)} [N_q^{\text{DL}}(L) - N_g^{(\text{DL})}(L - \ell)] \\ &- \frac{2\alpha_s}{\pi} \int_0^L d\ell \int d\zeta P_{g \rightarrow q\bar{q}}(1 - \zeta) [N_q^{\text{DL}}(L) - N_g^{(\text{DL})}(L - \ell)]. \end{aligned} \quad (6.17)$$

As in the Drell-Yan case, the first term of Eq. (6.17) exactly cancels $\delta N_{g,\text{IS}}^{\mu_F}(x, L)$. After integrating over ℓ we obtain the NDL gluon-initiated Lund multiplicity in hadronic collisions

$$N_{g,\text{IS}}^{(\text{NDL})}(x, L) = N_{g,\text{FS}}^{(\text{NDL})}(L) - 1 + \frac{2 \sinh \nu}{\sqrt{\bar{\alpha}}} \frac{\partial \ln f_g(x, Q^2)}{\partial \ln Q^2} + \frac{4\alpha_s}{\pi} (C_F - C_A) \left(\frac{\sinh \nu}{\sqrt{\bar{\alpha}}} - L \right) (B_\Sigma - B_{gq}), \quad (6.18)$$

with

$$B_\Sigma = \frac{1}{2C_A} \int_x^1 \frac{d\zeta}{\zeta} P_{gq}^{\text{IS}}(\zeta) \frac{f_\Sigma(x/\zeta, Q^2)}{f_g(x, Q^2)}, \quad (6.19)$$

and B_{gq} defined as in Eq. (3.21). A clear difference exists between Eq. (6.18) and the quark-initiated case, Eq. (6.11): besides the DGLAP evolution of the initiator’s PDF, the gluon-initiated case contains an additional term proportional to f_Σ . This second term can be traced back to the hard-collinear contribution where a gluon backwards-evolve into a $q\bar{q}$ pair, creating a mismatch between the N_q and N_g contributions. As with Eq. (6.11), Eq. (6.18) has been cross-checked against the result from Ref. [32] obtained with a generating-functional approach.

Finally, the Lund multiplicity in Higgs production via gluon-gluon fusion can be constructed from Eq. (6.18) by simply summing the contributions over both initial-state partons. We get

$$\begin{aligned} \langle N^{(\text{Lund})}(x_1, x_2, L) \rangle_{gg \rightarrow H} &= \langle N^{(\text{Lund})}(L) \rangle_{e^+e^-} - 2 + \frac{2 \sinh \nu}{\sqrt{\bar{\alpha}}} \frac{\partial}{\partial \ln Q^2} \ln [f_g(x_1, Q^2) f_g(x_2, Q^2)] \\ &+ \frac{4\alpha_s}{\pi} (C_F - C_A) \left(\frac{\sinh \nu}{\sqrt{\bar{\alpha}}} - L \right) (B_{\Sigma,1} + B_{\Sigma,2} - 2B_{gq}), \end{aligned} \quad (6.20)$$

with $B_{\Sigma,i}$ given by Eq. (6.19) evaluated at x_i for each beam.

7 Conclusions and outlook

This paper has presented the first theoretical determination of subjet multiplicity for angular-ordered based clustering algorithms at NNDL accuracy in e^+e^- collisions. In particular, we have explored two definitions of subjet multiplicity: (i) a novel procedure based on Lund declustering as explained in Sec. 2 and (ii) the more standard average jet multiplicity obtained when running the Cambridge algorithm [30] with $y_{\text{cut}} = k_{t,\text{cut}}^2/Q^2$. We have found that these two definitions are identical at NNDL up to a term related to the precise definition of k_t for large-angle emissions (see Eqs. (4.72), (4.73) and (4.74)). Our calculation thus achieves an order higher in logarithmic accuracy than the current state-of-the-art [24].

A key aspect allowing for this improvement is the use of an angular-ordered clustering sequence instead of the typical Durham clustering algorithm. The latter receives additional contributions where one has a pair of emissions with $k_t \simeq k_{t,\text{cut}}$ and widely separated in angle (Fig. 4l). At all orders, when adding an arbitrary number of soft-and-collinear emissions, this would yield complex situations depending on fine details of the clustering history (see App. A.1). This configuration is absent when defining the multiplicity based on the Cambridge clustering algorithm. This is similar to the original argument motivating the Cambridge algorithm [30].

Another cornerstone of our work is the use of a novel resummation approach which does not rely on generating functionals. Instead, it is based on the observation that subleading contributions can be obtained from configuration where the subleading part is associated with only a handful of emissions — a single one giving a contribution proportional to $\alpha_s L$ at NDL, one or two giving a contribution proportional either to α_s or to $(\alpha_s L^2)$ at NNDL— dressed with an arbitrary number of soft-and-collinear emissions. Once these subleading contributions have been systematically enumerated and computed (at fixed order), their all-order treatment largely recycles results from lower orders and is therefore straightforward (see e.g. Fig. 3). This approach can be extended, at least in principle, to higher resummation orders.

The final NNDL formulæ for quark ($e^+e^- \rightarrow Z \rightarrow q\bar{q}$) and gluon ($e^+e^- \rightarrow H \rightarrow gg$) hemispheres, the main results of this paper, can be found in Sec. 4.5. Besides its purely theoretical interest, this compact formulæ could be useful to test the logarithmic accuracy of the next-generation of NNLL parton showers. As a proof of concept, in addition to the e^+e^- result, we have presented the extension of our formalism to initial-state radiation in Sec. 6 and computed the Lund multiplicity at NDL accuracy for deep-inelastic scattering and colour singlet production in hadronic collisions, i.e. Drell-Yan and Higgs production via gluon fusion.

We have performed an exploratory study of the Lund multiplicity at LEP energies. To that end, the resummed predictions were additively matched to the NLO result obtained via **Event2**. We have shown that the inclusion of NNDL corrections leads to a strong reduction of the theoretical uncertainty of about 50% for almost all $k_{t,\text{cut}}$ values. Our work thus provides a precise pQCD benchmark for eventual theory-to-data comparisons. We have also shown that, after a simple inclusion of non-perturbative corrections, we obtained a decent description of the measurements of the average Cambridge multiplicity from the OPAL collaboration [45, 71]. In the future, the short analysis presented in this paper could be extended into a deeper phenomenological study. In this context, one could combine our increased perturbative accuracy with recent efforts to reach NNLO fixed-order accuracy [72–75] and study if it could lead to a new determination of

the strong coupling constant. Furthermore, it would be interesting to see if the Lund multiplicity (or the difference between the Lund and Cambridge multiplicities which may have a simple perturbative structure) could also be measured from LEP data, following e.g. the recent interest for reanalyses of the archived ALEPH data [68].

Besides these direct phenomenological application at LEP, there are multiple possible extensions of this work. On the e^+e^- side, one first task would be to understand the all-orders resummation of an arbitrary number of hard-collinear and running-coupling corrections in a perturbatively-controlled manner, since these two contributions are expected to dominate at large $\alpha_s L^2$. In this case, we expect that the expansion in Eq. (1.1) should be revisited. Another option would be to generalise the proposed resummation scheme so as to calculate higher-order moments of the Lund multiplicity distribution. This would amount to accounting for correlations between different splittings, an effect which may break the simplifications arising from angular-ordering. From a phenomenological viewpoint, a dedicated study of hadronisation corrections is required for practical applications to precision physics. In this context, it would be interesting to see if recent approaches either on the analytic front [76], using Monte Carlo techniques [77], or even methods based on Deep-Learning [78], could be helpful.

It would also be interesting to extend the calculation to other processes like $e^+e^- \rightarrow W^+W^-$, relevant for FCC-ee studies, but also to deep-inelastic scattering at the forthcoming Electron-Ion Collider (EIC). Finally, a natural continuation of this work would be to compute the Lund multiplicity at NNDL for high-energy jets produced at hadron colliders, in processes such as dijet or $Z + \text{jet}$ events at the LHC (or for the average associated jet rate introduced in Ref. [79]). This calculation would be relevant for at least two reasons. On the one hand, one could probe multiplicity distributions over an energy range much larger than that is available at LEP. This might ultimately provide a new handle on the measurement of the strong coupling constant at the LHC. In this context, one could fit the multiplicity together with (an)other Lund-plane observable(s) (e.g. the primary Lund plane density computed at NLL in [39]) so as to simultaneously constrain the strong coupling constant and the quark-gluon fraction. On the other hand, the measurement of a quantity such as the multiplicity, which is sensitive to the dynamics of the jet across all scales from its transverse momentum down to a $k_{t,\text{cut}}$ as low as a few GeV, could help constraining Monte Carlo generators. This could for example improve the determination of crucial quantities such as the Jet Energy Scale for quark- and gluon-initiated jets which is currently affected by large Monte Carlo uncertainties, in particular from parton showers [80, 81].

Acknowledgements

We wish to thank Keith Hamilton and Gavin Salam for collaboration in the early stages of this work. We are grateful to our PanScales collaborators (Melissa van Beekveld, Mrinal Dasgupta, Frédéric Dreyer, Basem El-Menoufi, Silvia Ferrario Ravasio, Keith Hamilton, Alexander Karlberg, Pier Monni, Gavin Salam, Ludovic Scyboz and Rob Verheyen), as well as to Bryan Webber for discussions and comments on this manuscript. RM is grateful for the hospitality of Université Paris-Saclay, and ASO and GS are grateful for the hospitality of the University of Oxford where part of this research was conducted. This work has been supported by the European Research

Council (ERC) under the European Union’s Horizon 2020 research and innovation programme (grant agreement No. 788223, PanScales).

A Subject multiplicity definition and logarithmic accuracy

Here, we discuss why an angular-ordered clustering sequence is essential for the viability of NNDL resummation of the average multiplicity (App. A.1). We then show that the choice of recombination scheme in the initial clustering does not affect the NNDL accuracy of the resummed average multiplicity (App. A.2). Finally, we relate Lund and Cambridge multiplicity (App. A.3).

A.1 Angular ordered vs k_t -based clustering algorithms

As pointed out in Sec. 4.1, the main difference at NNDL between k_t -based [27] and angular-ordered [30] clustering algorithms comes from configurations with multiple emissions with $k_t \sim k_{t,\text{cut}}$, Fig. 41. We briefly discuss here how the presence of such a contribution drastically complicates the calculation for k_t -based algorithms.

To illustrate this, consider the case of three primary emissions off a leading quark, all with identical azimuthal angle relative to it. Take their angles such that $\theta_{3q} \gg \theta_{1q} \gg \theta_{2q}$ and assume that $k_{t,1q} \gg k_{t,\text{cut}}$ is in the double-logarithmic region, while emissions 2 and 3 are just below $k_{t,\text{cut}}$ such that $k_{t,\text{cut}}/2 < k_{t,2q} < k_{t,3q} < k_{t,\text{cut}}$. If we compute the multiplicity using a k_t -based algorithm, e.g. the Durham algorithm [27], emission 3 is first clustered with 1 and does not contribute to the multiplicity as $k_{t,3q} < k_{t,\text{cut}}$; emission 2 is then clustered with the leading parton and thus does not contribute to the multiplicity either. If we instead consider the same situation in which emission 1 is absent (e.g. virtual), emissions 2 and 3 would be clustered together resulting in a k_t of the pair above the $k_{t,\text{cut}}$. This mismatch creates a logarithmic contribution of order $(\alpha_s L^2)_1 (\alpha_s L)_2 (\alpha_s L)_3 = \alpha_s^3 L^4$, i.e. NNDL. Conversely, with Cambridge clustering, emissions 2 and 3 would be clustered with the leading parton in both cases, leaving only an effect beyond NNDL accuracy when the emissions further satisfy $\theta_{23} \sim \theta_{2q}$. More generally, computing the average multiplicity for k_t -based algorithms would require knowledge of the full fragmentation process for a pair of emissions with $k_t \sim k_{t,\text{cut}}$ accompanied by an arbitrary number of soft-collinear emissions. This is a very complex task which depends in a non-trivial way on the geometry of all the emissions and could most likely only be achieved (semi-)numerically.

A.2 Recombination scheme independence

We comment on why the choice of recombination scheme for the initial Cambridge (e^+e^-) or C/A (pp) clustering affects the average Lund multiplicity beyond NNDL.

As a case study, we contrast the usual E -scheme, where one simply adds the 4-momenta of the two pseudo-jets, to the winner-takes-all (WTA) recombination scheme [51, 82], where the transverse momenta p_t of the two pseudo-jets are added linearly, but the direction of the recombined jet is determined by the direction of the higher p_t pseudo-jet. As a case study, let us consider the case of two emissions. When one emission is much softer than the other, their possible recombination would yield the same result with E -scheme and WTA recombination, up to power corrections in their relative energy fractions. This would only generate effects beyond our accuracy, including, for example, for the clustering correction of Sec. 4.2.4. When the emissions

are strongly ordered in angles, the difference between the recombination schemes would then be power-suppressed by the ratio of the angles. This only leaves a potential effect when the two emissions have both commensurate angles and energies, i.e. the “pair” contribution from Sec. 4.2.3. In this case, the relative difference between the two recombination schemes would be of order 1. This would only be relevant for $k_t \sim k_{t,\text{cut}}$ which would therefore contribute only at the N³DL. To sum up, the E -scheme and WTA Lund multiplicities are the same at NN DL accuracy. The above argument would hold for any infrared-and-collinear-safe recombination scheme which would reproduce the E -scheme up to power corrections in either the soft or collinear limit.

A.3 Lund and Cambridge multiplicities

In this Appendix, we discuss a specific aspect which allows us to relate the Lund and Cambridge multiplicities. Specifically, we argue that if we take the full clustering tree obtained by running the Cambridge algorithm with $y_{\text{cut}} = 1$, the total number of clusterings for which k_t , defined in the Lund sense, Eq. (2.1), is above $k_{t,\text{cut}}$ is equal to the Lund multiplicity.

The only possible situation which could result in these two multiplicities to differ is one where the Lund declustering procedure hits a declustering $i \rightarrow j+k$ ($E_j > E_k$) with $k_t < k_{t,\text{cut}}$ such that one of the clusterings that led to the softer branch, k , had a relative k_t above $k_{t,\text{cut}}$. Indeed, in such a situation, this last clustering would be counted as part of the Cambridge multiplicity, but missed in the Lund declustering procedure as the latter would not recurse into subjet k . Since the energy can only grow throughout clustering, this situation can only happen if the clustering angles are reduced. We argue below that, even if the angles can decrease, it never creates a situation where the Lund multiplicity would miss a Cambridge clustering above $k_{t,\text{cut}}$.

We start by considering a simple situation with 3 particles, p_1, p_2, p_3 , at small angles (with a fourth one recoiling against this system for energy-momentum conservation). For definiteness, let us assume that p_1 and p_2 cluster first, followed by p_3 clustering with the $p_1 + p_2$ combination. We are interested in a configuration when $k_{t,12} > k_{t,\text{cut}}$, but $k_{t3,1+2} < k_{t,\text{cut}}$. Still without loss of generality, we can parameterise the energies as $E_1 = (1-z)z_p E$, $E_2 = (1-z)(1-z_p)E$, $E_3 = zE$ with $E = Q/2$, and assume that the angle between particles 1 and 2 is $\theta_{12} = \Delta$. The Lund procedure would first obtain the $k_{t3,1+2}$ associated with the last clustering. Next, if $z \leq 1/2$, $k_{t,12}$ would be reconstructed by following the hard branch. However, since $k_{t3,1+2} < k_{t,\text{cut}}$, if $z > 1/2$, the $p_1 + p_2$ clustering would be ignored. Hence, we want to show that we can never have $k_{t,12} > k_{t3,1+2}$ if $z > 1/2$, i.e. if the $p_1 + p_2$ system is on the soft branch of the final clustering.

Geometrically, the smallest possible $k_{t3,1+2}$ requires the smallest possible angular distance $\Delta_{3,1+2}$, which is achieved when p_3 is at a distance $\Delta + \varepsilon$ (with $\varepsilon \ll \Delta$) from both p_1 and p_2 , as depicted in Fig. 10. It is easy to show that, in such a configuration,

$$\frac{k_{t,21}}{k_{t3,1+2}} = \frac{z_p}{\sqrt{\frac{3}{4} + \left(\frac{1}{2} - z_p\right)^2}} \leq \frac{1}{\sqrt{3}}, \quad (\text{A.1})$$

where the maximum value is reached for $z_p = 1/2$. Since this maximal value is below 1, we never face a situation where a soft branch can hide a clustering with a k_t larger than the parent one. With a bit of an effort, the above argument can be shown to hold beyond the small-angle limit, with the small-angle case still giving the extremal value.

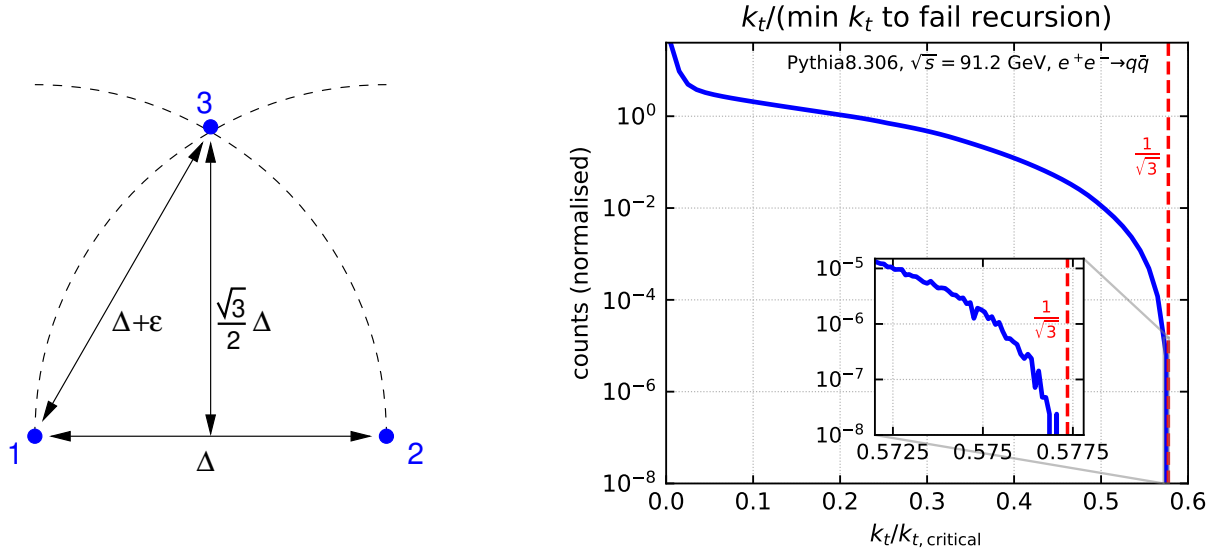


Figure 10: Left: Sketch of a 3 particle system where angles between particles become smaller after clustering. Right: Number of events as a function of the ratio between the k_t of each declustering and the critical k_t as defined in the text. Since the number of events drops at $k_t/k_{t,\text{critical}} = 1/\sqrt{3} < 1$, this plot illustrates that the Lund multiplicity is equivalent to counting the Cambridge clusterings with a k_t above a given $k_{t,\text{cut}}$.

We have not been able to prove that the upper bound derived in Eq. (A.1) was still valid for an arbitrary number of particles. Instead, we approach the problem numerically. We run a Pythia [83] simulation of $e^+e^- \rightarrow Z \rightarrow q\bar{q}$ events at $\sqrt{s} = 91.2$ GeV and for each event reconstruct the Cambridge clustering tree. For each branching, \mathcal{B} , associated with a relative transverse momentum k_t , we look at all the earlier Lund declusterings for which reaching \mathcal{B} would, at some point, require following a soft branch. Of these declusterings, we define $k_{t,\text{critical}}$ as the one with the smallest k_t . Seeing a value of $k_t/k_{t,\text{critical}}$ above 1 would mean that for a value of $k_{t,\text{cut}}$ between k_t and $k_{t,\text{critical}}$, the branching \mathcal{B} would be counted as part of the Cambridge multiplicity but not as part of the Lund multiplicity. The distribution of $k_t/k_{t,\text{critical}}$ is plotted in Fig. 10 and clearly shows that the upper bound in Eq. (A.1), derived for 3 particles, is still valid in general and that, in particular, the ratio never exceeds 1.

The above discussion shows that, if an event is clustered with the Cambridge algorithm with $y_{\text{cut}} = 1$, counting Lund declusterings with a k_t (defined as in Eq. (2.1)) above $k_{t,\text{cut}}$, i.e. following the algorithm defined in Sec. 2, is equivalent to counting declusterings satisfying the same condition in the full clustering tree. In practice, one could instead consider the Cambridge jet multiplicity, obtained by running the Cambridge algorithm with $y_{\text{cut}} = k_{t,\text{cut}}^2/Q^2$ and counting the number of resulting jets. Procedurally this is very similar to the Lund multiplicity, however it differs from it in two ways, which we can account for within the Lund multiplicity algorithm. First, we modify the definition of the relative transverse momentum to use $k_t^{(\text{Cam})}$, Eq. (2.2),

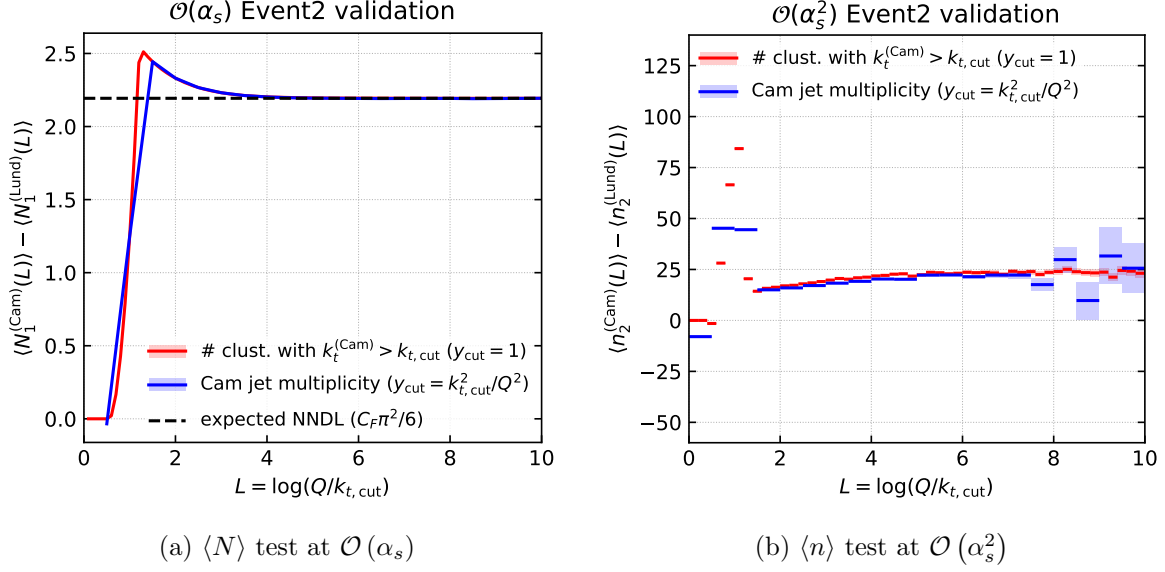


Figure 11: Comparison between the Lund and Cambridge multiplicities at fixed-order with the `Event2` program: (a) the (cumulative) multiplicity difference $\langle N_1^{(\text{Cam})} \rangle - \langle N_1^{(\text{Lund})} \rangle$ at order α_s , compared to the NNDL analytic expectation (b) the differential multiplicity difference $\langle n_2^{(\text{Cam})} \rangle - \langle n_2^{(\text{Lund})} \rangle$ at order α_s^2 , which is expected to go to a (N³DL) constant if the results agree at NNDL.

and, second, we run the initial Cambridge clustering sequence with the recombination scheme

$$\text{recombine}(p_i, p_j) = \begin{cases} p_i + p_j, & \text{if } k_t < k_{t,\text{cut}} \\ \max(p_i, p_j), & \text{if } k_t > k_{t,\text{cut}} \end{cases}, \quad (\text{A.2})$$

where $\max(p_i, p_j)$ is the most energetic of p_i and p_j . This describes the feature of the Cambridge algorithm that each newly resolved jet is removed from the list of particles [30]. We have already discussed in the main text that trading the Lund definition of k_t for $k_t^{(\text{Cam})}$ does impact the average multiplicity starting from NNDL accuracy, with the result in Eq. (4.39). Furthermore, the effect of the recombination scheme in Eq. (A.2) is beyond our targeted NNDL accuracy.²¹ To see this, we need to consider a situation where the second line of Eq. (A.2) is used and see its impact on subsequent clusterings. For this to impact the counting (compared to an E -scheme approach), one should be in a situation where p_i and p_j have commensurate energies, i.e. in the case of a hard-collinear branching (with $k_t \geq k_{t,\text{cut}}$). For the difference between p_i (assuming $E_i > E_j$) and $p_i + p_j$ to have an impact on the $k_{t,\text{cut}}$ condition for a subsequent clustering, this new clustering must have a k_t commensurate to $k_{t,\text{cut}}$ with p_i on its soft branch. This kinematic configuration is clearly beyond NNDL accuracy.

To further check the relation between the Lund and Cambridge multiplicities, we run some fixed-order tests with the `Event2` program, similarly to what was done in Sec. 5.1. We study the difference between the Lund multiplicity and one of the following two Cambridge-based definitions: (i) running the Cambridge algorithm with $y_{\text{cut}} = 1$ and counting the clusterings with $k_t^{(\text{Cam})} > k_{t,\text{cut}}$, i.e. using the Cambridge definition of k_t instead of the Lund definition, and (ii)

²¹Note that the recombination scheme in Eq. (A.2) does not satisfy the criteria discussed at the end of App. A.2.

using the Cambridge jet multiplicity with $y_{\text{cut}} = k_{t,\text{cut}}^2/Q^2$. Our results are shown in Fig. 11. In Fig. 11a, we plot differences between the multiplicities at order α_s . We see that the Lund and Cambridge multiplicities indeed differ by a constant which corresponds to the NNDL expectation of $C_F\pi^2/6$ for the full event, cf. Sec. 4.2.5, Eq. (4.39). At $\mathcal{O}(\alpha_s^2)$, Fig. 11b, we instead consider the difference in the differential multiplicity (as done in Fig. 7b, Sec. 5.1). The fact that the differences tend to a constant at large L indicates that the two distributions agree at NNDL accuracy, as expected from our analytic calculations.

B $1 \rightarrow 3$ splitting functions in the soft limit

We provide explicit expressions for the key two ingredients in Eq. (4.25): the (soft limit of the) $1 \rightarrow 3$ splitting function $\hat{P}_{1 \rightarrow 3}$ describing the emission of two collinear particles at commensurate energies and angles from an initial hard parton, and the corresponding NDL subtraction term, \mathcal{P} . The $1 \rightarrow 3$ splitting function were computed in Ref. [60], where we can set $\varepsilon = 0$ and take the soft limit, $z_3 \rightarrow 1$. In this limit, the energy fractions and invariant masses entering the splitting functions are related to the variables introduced in Fig. 5 through²²

$$z_1 = (1 - z)z_p, \quad z_2 = (1 - z)(1 - z_p), \quad (\text{B.1a})$$

$$s_{12} = (1 - z)^2 z_p (1 - z_p) \theta_a^2 \bar{\theta}_{12}^2, \quad (\text{B.1b})$$

$$s_{13} = (1 - z) \theta_a^2 z_p [1 + 2(1 - z_p) \cos \phi_{12} \bar{\theta}_{12} + (1 - z_p)^2 \bar{\theta}_{12}^2], \quad (\text{B.1c})$$

$$s_{23} = (1 - z) \theta_a^2 (1 - z_p) [1 - 2z_p \cos \phi_{12} \bar{\theta}_{12} + z_p^2 \bar{\theta}_{12}^2], \quad (\text{B.1d})$$

$$s_{123} = s_{12} + s_{13} + s_{23} \stackrel{z_3 \rightarrow 1}{\approx} s_{13} + s_{23} = (1 - z) \theta_a^2 [1 + z_p(1 - z_p) \bar{\theta}_{12}^2], \quad (\text{B.1e})$$

$$t_{12,3} = 2 \frac{z_1 s_{23} - z_2 s_{13}}{z_1 + z_2} + \frac{z_1 - z_2}{z_1 + z_2} s_{12} \stackrel{z_3 \rightarrow 1}{\approx} 2[z_p s_{23} - (1 - z_p) s_{13}]. \quad (\text{B.1f})$$

Note that s_{12} is proportional to $(1 - z)^2$ while all other invariants scale as $1 - z$. Also, only s_{13} and s_{23} (and, hence $t_{12,3}$) carry a dependence on the azimuthal angle ϕ .

The various $1 \rightarrow 3$ splitting functions given below are taken with the same normalisation as in the original reference [60]. When using them in practice in Eq. (4.25), we need to insert the appropriate symmetry factors.

Quark-initiated The splitting of a quark can lead to two different configurations: (i) a quark and two gluons, $\hat{P}_{g_1 g_2 q_3}$ with an Abelian contribution proportional to C_F^2 and a non-Abelian contribution proportional to $C_F C_A$, or (ii) a quark plus a $q\bar{q}$ pair, $\hat{P}_{\bar{q}_1 q_2 q_3} \propto C_F n_f T_R$.²³ We begin by considering case (i). It is straightforward to see that in the limit $z \rightarrow 1$ the C_F^2 contribution factorises in a product of independent soft-collinear emissions $(2C_F)^2/(z_1 z_2)$ and therefore does not bring any NNDL contribution. For the non-Abelian contribution, the matrix

²²In principle, the invariant masses are proportional to the square of the energy of the initial parton. Since we are always working with ratios of s_{ij} , these factors cancel and have been omitted for simplicity.

²³The case in which all quarks have identical flavours includes a term proportional to $C_F(C_F - C_A/2)$. Since this term is finite in the $z \rightarrow 1$ limit (see e.g. [58]) it is beyond our NNDL accuracy.

element is given by Eq. (62) in Ref. [60] and its soft limit reads:

$$z_p(1-z_p)(1-z)^2\hat{P}_{g_1g_2q_3} = C_F C_A \left\{ 2 \frac{[z_p s_{23} - (1-z_p)s_{13}]^2}{s_{12}\theta_a^2\bar{\theta}_{12}^2} + \frac{s_{123}}{s_{13}}(z_p r - 1)(2-z_p) \right. \\ \left. + \frac{s_{123}}{s_{23}}[(1-z_p)r - 1](1+z_p) + r[1 - 8z_p(1-z_p)] \right\} \quad (\text{B.2})$$

with $r \equiv (1-z)s_{123}/s_{12} = [1+z_p(1-z_p)\bar{\theta}_{12}^2]/[z_p(1-z_p)\bar{\theta}_{12}^2]$. The NDL contribution corresponds to the $P_{g \rightarrow gg}$ splitting function that, with our choice of variables, reads

$$\int \frac{d\phi_{12}}{2\pi} \mathcal{P}_{g_1g_2q_3} = 4C_F C_A \frac{[1-z_p(1-z_p)]^2}{z_p(1-z_p)} \Theta(\bar{\theta}_{12} < 1). \quad (\text{B.3})$$

where the factor 4 appears due to the phase-space definition in Eq. (4.25). We have explicitly performed the ϕ -integration to highlight that at NDL the two emissions are angular ordered and as encompassed by the $\Theta(\bar{\theta}_{12} < 1)$ constraint.

We now treat the case in which a quark emits a soft gluon that subsequently decays into a quark/anti-quark pair with commensurate energies and angle. After taking the soft limit of the triple collinear splitting function given in this case by Eq. (57) in Ref. [60], we obtain

$$z_p(1-z_p)(1-z)^2\hat{P}_{\bar{q}_1q_2q_3} = 2C_F n_f T_R \left[-\frac{[z_p s_{23} - (1-z_p)s_{13}]^2}{s_{12}\theta_a^2\bar{\theta}_{12}^2} + z_p(1-z_p)r \right]. \quad (\text{B.4})$$

In this case, the NDL subtraction term is given by

$$\int \frac{d\phi_{12}}{2\pi} \mathcal{P}_{\bar{q}_1q_2q_3} = 4C_F n_f T_R [z_p^2 + (1-z_p)^2] \Theta(\bar{\theta}_{12} < 1). \quad (\text{B.5})$$

Gluon-initiated We have again two cases to consider for a gluon splitting since it can generate: (i) two more gluons, $\hat{P}_{g_1g_2g_3} \propto C_A^2$, or (ii) a $q\bar{q}$ pair, $\hat{P}_{q_1\bar{q}_2g_3}$, with a contribution proportional to $C_A n_f T_R$ which survives in the soft limit $z_3 \rightarrow 1$ and a contribution proportional to $C_F C_A$ which does not. The $q\bar{q}$ channel is then given by the soft limit of Eq. (69) in Ref. [60],²⁴ i.e.

$$z_p(1-z_p)(1-z)^2\hat{P}_{q_1\bar{q}_2g_3} = 2C_A n_f T_R \left[-\frac{[z_p s_{23} - (1-z_p)s_{13}]^2}{s_{12}\theta_a^2\bar{\theta}_{12}^2} + z_p(1-z_p)r \right] \quad (\text{B.6})$$

and the subtraction term is given by Eq. (B.5) with the overall factor C_F replaced by C_A . Note that this result is equivalent to the production of a $q\bar{q}$ pair from an initial hard quark, up to the overall colour factor (C_A or C_F). This explains why the $D_{\text{pair}}^{g \rightarrow q\bar{q}g}$ and $D_{\text{pair}}^{q \rightarrow q\bar{q}'q}$ coefficients in Eq. (4.27a) are equal.

Finally, we tackle the case of a $g \rightarrow ggg$ splitting. Two complications arise with respect to the previous cases due to the indistinguishability of the gluons: (i) all six permutations of the gluon momenta have to be taken into account in the splitting function and (ii) the full $g \rightarrow g_1g_2g_3$ splitting function also includes logarithmically-enhanced contributions where either g_1 or g_2 is collinear to g_3 . The corresponding NDL contributions should also be subtracted in order to

²⁴Compared to [60], we have reordered the indices so that the gluon is the third parton and the soft limit still corresponds to $z_3 \rightarrow 1$.

obtain the NN DL correction. The triple collinear splitting function is provided in Eq. (70) of Ref. [60]. After taking the $z_3 \rightarrow 1$ limit in all 6 permutations it reduces to

$$z_p(1-z_p)(1-z)^2 \hat{P}_{g_1 g_2 g_3} = C_A^2 \left\{ 2 \frac{[z_p s_{23} - (1-z_p)s_{13}]^2}{s_{12} \theta_a^2 \bar{\theta}_{12}^2} + \frac{s_{123}}{s_{13}} (z_p r - 1)(2 - z_p) \right. \\ \left. + \frac{s_{123}}{s_{23}} [(1-z_p)r - 1](1+z_p) + r [1 - 8z_p(1-z_p)] + \frac{4s_{123}^2}{s_{13}s_{23}} \right\} \quad (\text{B.7})$$

We note that since we have made the explicit choice to take $z \equiv z_3 \rightarrow 1$, the symmetry factor associated with this contribution is $1/2$ and not $1/3!$.

The NDL subtraction term is a bit more involved than in the previous cases. On top of the contribution where the first soft gluon undergoes a hard-collinear splitting, we need to account for the case in which the two soft gluons are emitted off the hard one. This contribution is more naturally first written in terms of the θ_{13} and θ_{23} angles, followed by a change in variables to θ_a and $\bar{\theta}_{12}$ by using

$$\left(\frac{2\alpha_s C_A}{\pi} \right)^2 \frac{dz_1}{z_1} \frac{dz_2}{z_2} \frac{d\theta_{13}^2}{\theta_{13}^2} \frac{d\theta_{23}^2}{\theta_{23}^2} \frac{d\phi}{2\pi} = \left(\frac{2C_A \alpha_s}{\pi} \right)^2 \frac{dz}{1-z} dz_p \frac{d\theta_q^2}{\theta_g^2} \frac{d\bar{\theta}_{12}^2}{\bar{\theta}_{12}^2} \frac{d\phi}{2\pi} \frac{\bar{\theta}_{12}^2}{[1+z_p(1-z_p)\bar{\theta}_{12}^2]^2} \frac{s_{123}^2}{s_{13}s_{23}}. \quad (\text{B.8})$$

These steps yield the following NDL subtraction term:

$$\mathcal{P} = \left(\frac{2\alpha_s C_A}{\pi} \right)^2 \left[P_{g \rightarrow gg}(1-z_p) + \frac{s_{123}^2}{s_{13}s_{23}} \frac{\bar{\theta}_{12}^2}{[1+z_p(1-z_p)\bar{\theta}_{12}^2]^2} \right]. \quad (\text{B.9})$$

It is interesting to note that the presence of the right-most term in Eq. (B.9) cancels exactly the last term in Eq. (B.7), so that, up to the overall colour factor, the remaining part is the same as for the emission of two soft gluons from a hard quark, Eq. (B.2), explaining the equality between $D_{\text{pair}}^{g \rightarrow ggg}$ and $D_{\text{pair}}^{q \rightarrow ggg}$ in (4.27b).

References

- [1] PLUTO collaboration, C. Berger et al., *Multiplicity Distributions in e^+e^- Annihilations at PETRA Energies*, *Phys. Lett. B* **95** (1980) 313–317.
- [2] OPAL collaboration, M. Z. Akrawy et al., *A Measurement of Global Event Shape Distributions in the Hadronic Decays of the Z^0* , *Z. Phys. C* **47** (1990) 505–522.
- [3] L3 collaboration, B. Adeva et al., *Studies of hadronic event structure and comparisons with QCD models at the Z^0 resonance*, *Z. Phys. C* **55** (1992) 39–62.
- [4] ALEPH collaboration, R. Barate et al., *Studies of quantum chromodynamics with the ALEPH detector*, *Phys. Rept.* **294** (1998) 1–165.
- [5] S. Gieseke, C. Rohr and A. Siodmok, *Colour reconnections in Herwig++*, *Eur. Phys. J. C* **72** (2012) 2225, [[1206.0041](#)].
- [6] P. Skands, S. Carrazza and J. Rojo, *Tuning PYTHIA 8.1: the Monash 2013 Tune*, *Eur. Phys. J. C* **74** (2014) 3024, [[1404.5630](#)].
- [7] SHERPA collaboration, E. Bothmann et al., *Event Generation with Sherpa 2.2*, *SciPost Phys.* **7** (2019) 034, [[1905.09127](#)].

- [8] J. Gallicchio and M. D. Schwartz, *Quark and Gluon Tagging at the LHC*, *Phys. Rev. Lett.* **107** (2011) 172001, [[1106.3076](#)].
- [9] ATLAS collaboration, G. Aad et al., *Light-quark and gluon jet discrimination in pp collisions at $\sqrt{s} = 7$ TeV with the ATLAS detector*, *Eur. Phys. J. C* **74** (2014) 3023, [[1405.6583](#)].
- [10] C. Frye, A. J. Larkoski, J. Thaler and K. Zhou, *Casimir Meets Poisson: Improved Quark/Gluon Discrimination with Counting Observables*, *JHEP* **09** (2017) 083, [[1704.06266](#)].
- [11] ALICE collaboration, K. Aamodt et al., *First proton-proton collisions at the LHC as observed with the ALICE detector: Measurement of the charged particle pseudorapidity density at $s^{*}(1/2) = 900$ -GeV*, *Eur. Phys. J. C* **65** (2010) 111–125, [[0911.5430](#)].
- [12] A. Bassetto, M. Ciafaloni and G. Marchesini, *Inelastic Distributions and Color Structure in Perturbative QCD*, *Nucl. Phys. B* **163** (1980) 477–518.
- [13] W. Furmanski, R. Petronzio and S. Pokorski, *Heavy Flavor Multiplicities at Very High-Energies*, *Nucl. Phys. B* **155** (1979) 253–268.
- [14] A. H. Mueller, *On the Multiplicity of Hadrons in QCD Jets*, *Phys. Lett. B* **104** (1981) 161–164.
- [15] B. R. Webber, *Average Multiplicities in Jets*, *Phys. Lett. B* **143** (1984) 501–504.
- [16] E. D. Malaza and B. R. Webber, *QCD CORRECTIONS TO JET MULTIPLICITY MOMENTS*, *Phys. Lett. B* **149** (1984) 501–503.
- [17] E. D. Malaza and B. R. Webber, *Multiplicity Distributions in Quark and Gluon Jets*, *Nucl. Phys. B* **267** (1986) 702–713.
- [18] I. M. Dremin and R. C. Hwa, *Average multiplicities in gluon and quark jets as exact solution of QCD equations*, *Phys. Lett. B* **324** (1994) 477–481.
- [19] K. Konishi, A. Ukawa and G. Veneziano, *Jet Calculus: A Simple Algorithm for Resolving QCD Jets*, *Nucl. Phys. B* **157** (1979) 45–107.
- [20] Y. L. Dokshitzer, V. A. Khoze, A. H. Mueller and S. I. Troian, *Basics of perturbative QCD*. Editions frontières, 1991.
- [21] R. Perez-Ramos and D. d’Enterria, *Energy evolution of the moments of the hadron distribution in QCD jets including NNLL resummation and NLO running-coupling corrections*, *JHEP* **08** (2014) 068, [[1310.8534](#)].
- [22] I. M. Dremin and J. W. Gary, *Hadron multiplicities*, *Phys. Rept.* **349** (2001) 301–393, [[hep-ph/0004215](#)].
- [23] OPAL collaboration, K. Ackerstaff et al., *Multiplicity distributions of gluon and quark jets and tests of QCD analytic predictions*, *Eur. Phys. J. C* **1** (1998) 479–494, [[hep-ex/9708029](#)].
- [24] S. Catani, Y. L. Dokshitzer, F. Fiorani and B. Webber, *Average number of jets in e^+e^- annihilation*, *Nucl. Phys. B* **377** (1992) 445–460.
- [25] S. Catani, B. Webber, Y. L. Dokshitzer and F. Fiorani, *Average multiplicities in two and three jet e^+e^- annihilation events*, *Nucl. Phys. B* **383** (1992) 419–441.
- [26] K. Hamilton, R. Medves, G. P. Salam, L. Scyboz and G. Soyez, *Colour and logarithmic accuracy in final-state parton showers*, *JHEP* **03** (2021) 041, [[2011.10054](#)].
- [27] S. Catani, Y. L. Dokshitzer, M. Olsson, G. Turnock and B. Webber, *New clustering algorithm for multi-jet cross-sections in e^+e^- annihilation*, *Phys.Lett.B* **269** (1991) 432–438.

- [28] E. Gerwick, S. Schumann, B. Gripaios and B. Webber, *QCD Jet Rates with the Inclusive Generalized kt Algorithms*, *JHEP* **04** (2013) 089, [[1212.5235](#)].
- [29] OPAL collaboration, P. D. Acton et al., *A Determination of $\alpha_s(M(Z0))$ at LEP using resummed QCD calculations*, *Z. Phys. C* **59** (1993) 1–20.
- [30] Y. L. Dokshitzer, G. D. Leder, S. Moretti and B. R. Webber, *Better jet clustering algorithms*, *JHEP* **08** (1997) 001, [[hep-ph/9707323](#)].
- [31] S. Catani, B. Webber and Y. Dokshitzer, *The $K(T)$ clustering algorithm for jets in deep inelastic scattering*, *Nucl. Phys. B Proc. Suppl.* **29** (1992) 136–143.
- [32] S. Catani, Y. L. Dokshitzer and B. Webber, *Average number of jets in deep inelastic scattering*, *Phys. Lett. B* **322** (1994) 263–269.
- [33] M. H. Seymour, *The Subjet multiplicity in quark and gluon jets*, *Phys. Lett. B* **378** (1996) 279–286, [[hep-ph/9603281](#)].
- [34] J. R. Forshaw and M. H. Seymour, *Subjet rates in hadron collider jets*, *JHEP* **09** (1999) 009, [[hep-ph/9908307](#)].
- [35] D0 collaboration, V. M. Abazov et al., *Subjet Multiplicity of Gluon and Quark Jets Reconstructed with the k_T Algorithm in $p\bar{p}$ Collisions*, *Phys. Rev. D* **65** (2002) 052008, [[hep-ex/0108054](#)].
- [36] F. A. Dreyer, G. P. Salam and G. Soyez, *The Lund Jet Plane*, *JHEP* **12** (2018) 064, [[1807.04758](#)].
- [37] M. Wobisch and T. Wengler, *Hadronization corrections to jet cross-sections in deep inelastic scattering*, in *Workshop on Monte Carlo Generators for HERA Physics (Plenary Starting Meeting)*, pp. 270–279, 4, 1998. [[hep-ph/9907280](#)].
- [38] B. Andersson, G. Gustafson, L. Lonnblad and U. Pettersson, *Coherence Effects in Deep Inelastic Scattering*, *Z. Phys. C* **43** (1989) 625.
- [39] A. Lifson, G. P. Salam and G. Soyez, *Calculating the primary Lund Jet Plane density*, *JHEP* **10** (2020) 170, [[2007.06578](#)].
- [40] ATLAS collaboration, G. Aad et al., *Measurement of the Lund Jet Plane Using Charged Particles in 13 TeV Proton-Proton Collisions with the ATLAS Detector*, *Phys. Rev. Lett.* **124** (2020) 222002, [[2004.03540](#)].
- [41] F. A. Dreyer and H. Qu, *Jet tagging in the Lund plane with graph networks*, *JHEP* **03** (2021) 052, [[2012.08526](#)].
- [42] O. Fedkevych, C. K. Khosa, S. Marzani and F. Sforza, *Identification of b -jets using QCD-inspired observables*, [2202.05082](#).
- [43] F. Dreyer, G. Soyez and A. Takacs, *Quarks and gluons in the Lund plane*, [2112.09140](#).
- [44] M. Dasgupta, F. A. Dreyer, K. Hamilton, P. F. Monni, G. P. Salam and G. Soyez, *Parton showers beyond leading logarithmic accuracy*, *Phys. Rev. Lett.* **125** (2020) 052002, [[2002.11114](#)].
- [45] JADE, OPAL collaboration, P. Pfeifenschneider et al., *QCD analyses and determinations of $\alpha_s(s)$ in e^+e^- annihilation at energies between 35-GeV and 189-GeV*, *Eur. Phys. J. C* **17** (2000) 19–51, [[hep-ex/0001055](#)].
- [46] S. Catani and M. H. Seymour, *The Dipole formalism for the calculation of QCD jet cross-sections at next-to-leading order*, *Phys. Lett. B* **378** (1996) 287–301, [[hep-ph/9602277](#)].
- [47] S. Catani and M. H. Seymour, *A General algorithm for calculating jet cross-sections in NLO QCD*, *Nucl. Phys. B* **485** (1997) 291–419, [[hep-ph/9605323](#)].

- [48] B. Andersson, P. Dahlkvist and G. Gustafson, *AN INFRARED STABLE MULTIPLICITY MEASURE ON QCD PARTON STATES*, *Phys. Lett. B* **214** (1988) 604–608.
- [49] M. Cacciari, G. P. Salam and G. Soyez, *FastJet User Manual*, *Eur. Phys. J. C* **72** (2012) 1896, [[1111.6097](#)].
- [50] A. J. Larkoski, S. Marzani, G. Soyez and J. Thaler, *Soft Drop*, *JHEP* **05** (2014) 146, [[1402.2657](#)].
- [51] A. J. Larkoski, D. Neill and J. Thaler, *Jet Shapes with the Broadening Axis*, *JHEP* **04** (2014) 017, [[1401.2158](#)].
- [52] G. Altarelli and G. Parisi, *Asymptotic Freedom in Parton Language*, *Nucl. Phys. B* **126** (1977) 298–318.
- [53] R. K. Ellis, W. J. Stirling and B. R. Webber, *QCD and Collider Physics*. Cambridge Monographs on Particle Physics, Nuclear Physics and Cosmology. Cambridge University Press, 1996. 10.1017/CBO9780511628788.
- [54] A. Banfi, G. P. Salam and G. Zanderighi, *Principles of general final-state resummation and automated implementation*, *JHEP* **03** (2005) 073, [[hep-ph/0407286](#)].
- [55] S. D. Badger, E. W. N. Glover and V. V. Khoze, *MHV rules for Higgs plus multi-parton amplitudes*, *JHEP* **03** (2005) 023, [[hep-th/0412275](#)].
- [56] JADE collaboration, W. Bartel et al., *Experimental Studies on Multi-Jet Production in e^+e^- Annihilation at PETRA Energies*, *Z. Phys. C* **33** (1986) 23.
- [57] S. Catani, B. R. Webber and G. Marchesini, *QCD coherent branching and semiinclusive processes at large x* , *Nucl. Phys. B* **349** (1991) 635–654.
- [58] M. Dasgupta and B. K. El-Menoufi, *Dissecting the collinear structure of quark splitting at NNLL*, *JHEP* **12** (2021) 158, [[2109.07496](#)].
- [59] Y. L. Dokshitzer, G. Marchesini and G. Orian, *Measuring color flows in hard processes: Beyond leading order*, *Nucl. Phys. B* **387** (1992) 675–714.
- [60] S. Catani and M. Grazzini, *Infrared factorization of tree level QCD amplitudes at the next-to-next-to-leading order and beyond*, *Nucl. Phys. B* **570** (2000) 287–325, [[hep-ph/9908523](#)].
- [61] K. Hamilton, A. Karlberg, G. P. Salam, L. Scyboz and R. Verheyen, *Soft spin correlations in final-state parton showers*, *JHEP* **03** (2022) 193, [[2111.01161](#)].
- [62] M. Dasgupta, F. Dreyer, G. P. Salam and G. Soyez, *Small-radius jets to all orders in QCD*, *JHEP* **04** (2015) 039, [[1411.5182](#)].
- [63] S. Catani, L. Trentadue, G. Turnock and B. R. Webber, *Resummation of large logarithms in e^+e^- event shape distributions*, *Nucl. Phys. B* **407** (1993) 3–42.
- [64] C. Bierlich et al., *A comprehensive guide to the physics and usage of PYTHIA 8.3*, [2203.11601](#).
- [65] M. Bahr et al., *Herwig++ Physics and Manual*, *Eur. Phys. J. C* **58** (2008) 639–707, [[0803.0883](#)].
- [66] J. Bellm et al., *Herwig 7.0/Herwig++ 3.0 release note*, *Eur. Phys. J. C* **76** (2016) 196, [[1512.01178](#)].
- [67] E. Gerwick, S. Hoeche, S. Marzani and S. Schumann, *Soft evolution of multi-jet final states*, *JHEP* **02** (2015) 106, [[1411.7325](#)].
- [68] Y. Chen et al., *Jet energy spectrum and substructure in e^+e^- collisions at 91.2 GeV with ALEPH Archived Data*, [2111.09914](#).

- [69] A. Badea, A. Baty, P. Chang, G. M. Innocenti, M. Maggi, C. McGinn et al., *Measurements of two-particle correlations in e^+e^- collisions at 91 GeV with ALEPH archived data*, *Phys. Rev. Lett.* **123** (2019) 212002, [[1906.00489](#)].
- [70] P. Caucal, A. Soto-Ontoso and A. Takacs, *Dynamical Grooming meets LHC data*, *JHEP* **07** (2021) 020, [[2103.06566](#)].
- [71] OPAL collaboration, G. Abbiendi et al., *Determination of $\alpha(s)$ using jet rates at LEP with the OPAL detector*, *Eur. Phys. J. C* **45** (2006) 547–568, [[hep-ex/0507047](#)].
- [72] A. Gehrmann-De Ridder, T. Gehrmann, E. W. N. Glover and G. Heinrich, *EERAD3: Event shapes and jet rates in electron-positron annihilation at order α_s^3* , *Comput. Phys. Commun.* **185** (2014) 3331, [[1402.4140](#)].
- [73] V. Del Duca, C. Duhr, A. Kardos, G. Somogyi, Z. Ször, Z. Trócsányi et al., *Jet production in the CoLoRFulNNLO method: event shapes in electron-positron collisions*, *Phys. Rev. D* **94** (2016) 074019, [[1606.03453](#)].
- [74] V. Del Duca, C. Duhr, A. Kardos, G. Somogyi and Z. Trócsányi, *Three-Jet Production in Electron-Positron Collisions at Next-to-Next-to-Leading Order Accuracy*, *Phys. Rev. Lett.* **117** (2016) 152004, [[1603.08927](#)].
- [75] T. Gehrmann, E. W. N. Glover, A. Huss, J. Niehues and H. Zhang, *NNLO QCD corrections to event orientation in e^+e^- annihilation*, *Phys. Lett. B* **775** (2017) 185–189, [[1709.01097](#)].
- [76] F. Caola, S. Ferrario Ravasio, G. Limatola, K. Melnikov and P. Nason, *On linear power corrections in certain collider observables*, *JHEP* **01** (2022) 093, [[2108.08897](#)].
- [77] D. Reichelt, S. Caletti, O. Fedkevych, S. Marzani, S. Schumann and G. Soyez, *Phenomenology of jet angularities at the LHC*, *JHEP* **03** (2022) 131, [[2112.09545](#)].
- [78] A. Ghosh, X. Ju, B. Nachman and A. Siodmok, *Towards a Deep Learning Model for Hadronization*, [2203.12660](#).
- [79] B. Bhattacharjee, S. Mukhopadhyay, M. M. Nojiri, Y. Sakaki and B. R. Webber, *Associated jet and subjet rates in light-quark and gluon jet discrimination*, *JHEP* **04** (2015) 131, [[1501.04794](#)].
- [80] CMS collaboration, V. Khachatryan et al., *Jet energy scale and resolution in the CMS experiment in pp collisions at 8 TeV*, *JINST* **12** (2017) P02014, [[1607.03663](#)].
- [81] ATLAS collaboration, M. Aaboud et al., *Jet energy scale measurements and their systematic uncertainties in proton-proton collisions at $\sqrt{s} = 13$ TeV with the ATLAS detector*, *Phys. Rev. D* **96** (2017) 072002, [[1703.09665](#)].
- [82] D. Bertolini, T. Chan and J. Thaler, *Jet Observables Without Jet Algorithms*, *JHEP* **04** (2014) 013, [[1310.7584](#)].
- [83] T. Sjöstrand, S. Ask, J. R. Christiansen, R. Corke, N. Desai, P. Ilten et al., *An introduction to PYTHIA 8.2*, *Comput. Phys. Commun.* **191** (2015) 159–177, [[1410.3012](#)].